

NATIONAL AERONAUTICS AND SPACE ADMINISTRATION

Technical Memorandum No. 33-278

Revision 1

Mariner Mars 1964 Flight Dynamic Data

J. E. Randolph

GPO PRICE \$ _____

CFSTI PRICE(S) \$ _____

Hard copy (HC) 2.50

Microfiche (MF) 1.75

ff 653 July 65

jpl

JET PROPULSION LABORATORY
CALIFORNIA INSTITUTE OF TECHNOLOGY
PASADENA, CALIFORNIA

September 15, 1966

N66 36858

(ACCESSION NUMBER)

86

(PAGES)

CR-78054

(NASA CR OR TMX OR AD NUMBER)

(THRU)

1

(CODE)

31

(CATEGORY)

FACILITY FORM 602

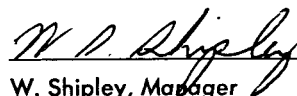
NATIONAL AERONAUTICS AND SPACE ADMINISTRATION

Technical Memorandum No. 33-278

Revision 1

Mariner Mars 1964 Flight Dynamic Data

J. E. Randolph

A handwritten signature in dark ink, appearing to read "W. Shipley", is written over a horizontal line.

W. Shipley, Manager
Environmental Requirements Section

JET PROPULSION LABORATORY
CALIFORNIA INSTITUTE OF TECHNOLOGY
PASADENA, CALIFORNIA

September 15, 1966

Copyright © 1966
Jet Propulsion Laboratory
California Institute of Technology
Prepared Under Contract No. NAS 7-100
National Aeronautics & Space Administration

CONTENTS

| | |
|--|----|
| I. Introduction and Summary | 1 |
| II. Instrumentation | 3 |
| A. Flight Telemetry and Coverage | 3 |
| B. Launch Pad Acoustic Telemetry | 9 |
| III. Analysis Techniques | 14 |
| A. Oscillograms | 14 |
| B. Band Pass | 14 |
| C. Power Spectra | 14 |
| D. Shock Spectra | 16 |
| E. Data Compression Techniques | 17 |
| IV. Analysis Results and Discussions | 18 |
| A. Oscillograms | 18 |
| B. Band Pass | 18 |
| C. Power Spectra | 19 |
| D. Shock Spectra | 20 |
| E. Data Compression | 21 |
| V. Data | 22 |
| VI. Conclusions | 77 |
| References | 77 |
| Table 1. Agena telemetry channel descriptions | 8 |

FIGURES

| | |
|--|----|
| 1. Adapter instrumentation | 2 |
| 2. Adapter instrumentation (detail) | 3 |
| 3. Spacecraft flight accelerometer | 6 |
| 4. Spacecraft bus configuration showing instrumentation locations | 7 |
| 5. Telemetry frequency response—high frequency channels | 8 |
| 6. Tracking station telemetry coverage and events | 9 |
| 7. Mariner III launch pad—acoustic instrumentation | 10 |
| 8. Mariner III acoustic instrumentation (detail) | 11 |

FIGURES (Cont'd)

| | |
|--|----|
| 9. <i>Mariner IV</i> launch pad—acoustic instrumentation | 12 |
| 10. <i>Mariner IV</i> acoustic instrumentation (detail) | 13 |
| 11. Power spectra analysis schematic | 15 |
| 12. Typical shock spectrum plots | 17 |
| 13. Wide band levels vs. time (<i>Mariner IV</i>), umbilical tower microphone M7, and spacecraft accelerometer B3 | 19 |
| 14. Oscillogram, <i>Mariner III</i> liftoff, all channels | 23 |
| 15. Band pass, <i>Mariner III</i> liftoff and transonic, B3 low frequency | 25 |
| 16. Band pass, <i>Mariner III</i> liftoff and transonic, B3 high frequency | 26 |
| 17. Band pass, <i>Mariner III</i> liftoff and transonic, F4 low frequency | 27 |
| 18. Band pass, <i>Mariner III</i> liftoff and transonic, F4 high frequency | 28 |
| 19. Acceleration spectral density, <i>Mariner III</i> liftoff, F1 | 29 |
| 20. Acceleration spectral density, <i>Mariner III</i> liftoff, F3 | 29 |
| 21. Acceleration spectral density, <i>Mariner III</i> liftoff, F2 | 29 |
| 22. Acceleration spectral density, <i>Mariner III</i> liftoff, B3 | 29 |
| 23. Acceleration spectral density, <i>Mariner III</i> liftoff, F4 | 29 |
| 24. Spectra ratio, <i>Mariner III</i> liftoff, B3/F4 | 29 |
| 25. Sound pressure spectrum level, <i>Mariner III</i> liftoff, M1, M2 | 30 |
| 26. Sound pressure spectrum level, <i>Mariner III</i> liftoff, M3, M4 | 30 |
| 27. Acoustic acceptance, <i>Mariner III</i> liftoff, B3/M3, M4 | 30 |
| 28. Acoustic acceptance, <i>Mariner III</i> liftoff, F4/M3, M4 | 30 |
| 29. Oscillogram, <i>Mariner IV</i> liftoff, all channels | 31 |
| 30. Band pass, <i>Mariner IV</i> liftoff and transonic, B3 low frequency | 33 |
| 31. Band pass, <i>Mariner IV</i> liftoff and transonic, B3 high frequency | 34 |
| 32. Band pass, <i>Mariner IV</i> liftoff and transonic, F4 low frequency | 35 |
| 33. Band pass, <i>Mariner IV</i> liftoff and transonic, F4 high frequency | 36 |
| 34. Acceleration spectral density, <i>Mariner IV</i> liftoff, F1 | 37 |
| 35. Acceleration spectral density, <i>Mariner IV</i> liftoff, F3 | 37 |
| 36. Acceleration spectral density, <i>Mariner IV</i> liftoff, F2 | 37 |
| 37. Acceleration spectral density, <i>Mariner IV</i> liftoff, B3 | 37 |
| 38. Acceleration spectral density, <i>Mariner IV</i> liftoff, F4 | 37 |
| 39. Spectra ratio, <i>Mariner IV</i> liftoff, B3/F4 | 37 |
| 40. Sound pressure spectrum level, <i>Mariner IV</i> liftoff, M5, M6 | 38 |

FIGURES (Cont'd)

| | |
|---|----|
| 41. Sound pressure spectrum level, <i>Mariner IV</i> liftoff, M7, M8 | 38 |
| 42. Acoustic acceptance, <i>Mariner IV</i> liftoff, B3/M7, M8 | 38 |
| 43. Acoustic acceptance, <i>Mariner IV</i> liftoff, F4/M7, M8 | 38 |
| 44. Oscillogram, <i>Mariner III</i> transonic, all channels | 39 |
| 45. Acceleration spectral density, <i>Mariner III</i> transonic, F1 | 40 |
| 46. Acceleration spectral density, <i>Mariner III</i> transonic, F3 | 40 |
| 47. Acceleration spectral density, <i>Mariner III</i> transonic, F2 | 40 |
| 48. Acceleration spectral density, <i>Mariner III</i> transonic, B3 | 40 |
| 49. Acceleration spectral density, <i>Mariner III</i> transonic, F4 | 40 |
| 50. Spectra ratio, <i>Mariner III</i> transonic, B3/F4 | 40 |
| 51. Oscillogram, <i>Mariner IV</i> transonic, all channels | 41 |
| 52. Acceleration spectral density, <i>Mariner IV</i> transonic, F1 | 42 |
| 53. Acceleration spectral density, <i>Mariner IV</i> transonic, F3 | 42 |
| 54. Acceleration spectral density, <i>Mariner IV</i> transonic, F2 | 42 |
| 55. Acceleration spectral density, <i>Mariner IV</i> transonic, B3 | 42 |
| 56. Acceleration spectral density, <i>Mariner IV</i> transonic, F4 | 42 |
| 57. Spectra ratio, <i>Mariner IV</i> transonic, B3/F4 | 42 |
| 58. Acceleration spectral density, <i>Mariner IV</i> transonic, F4 (analog) | 43 |
| 59. Oscillogram, <i>Mariner III</i> , BECO, all channels | 44 |
| 60. Oscillogram, <i>Mariner IV</i> , BECO, all channels | 46 |
| 61. Shock spectra, <i>Mariner III</i> , IV, BECO, B3 | 48 |
| 62. Shock spectra, <i>Mariner III</i> , IV, BECO, F1 | 48 |
| 63. Shock spectra, <i>Mariner III</i> , IV, BECO, F3 | 48 |
| 64. Oscillogram, <i>Mariner III</i> , SECO, all channels | 49 |
| 65. Oscillogram, <i>Mariner IV</i> , SECO, all channels | 50 |
| 66. Shock spectra, <i>Mariner III</i> , IV, SECO, B3 | 51 |
| 67. Shock spectra, <i>Mariner III</i> , IV, SECO, F1 | 51 |
| 68. Shock spectra, <i>Mariner III</i> , IV, SECO, F3 | 51 |
| 69. Oscillogram, <i>Mariner III</i> , H/S fairing jettison, all channels | 52 |
| 70. Oscillogram, <i>Mariner IV</i> , H/S fairing jettison, all channels | 53 |
| 71. Shock spectra, <i>Mariner III</i> , IV, H/S fairing jettison, B3 | 54 |
| 72. Shock spectra, <i>Mariner III</i> , IV, H/S fairing jettison, F1 | 54 |
| 73. Shock spectra, <i>Mariner III</i> , IV, H/S fairing jettison, F3 | 54 |

FIGURES (Cont'd)

| | |
|---|----|
| 74. Oscillogram, <i>Mariner III</i> , shroud ejection, all channels | 55 |
| 75. Oscillogram, <i>Mariner IV</i> , shroud ejection, all channels | 56 |
| 76. Transient, <i>Mariner III</i> , shroud ejection, B3 | 57 |
| 77. Shock spectra, <i>Mariner III</i> , shroud ejection, B3 | 57 |
| 78. Oscillogram, <i>Mariner III</i> , Atlas—Agena separation, all channels | 58 |
| 79. Oscillogram, <i>Mariner IV</i> , Atlas—Agena separation, all channels | 59 |
| 80. Transient, <i>Mariner III</i> , Atlas—Agena Separation, B3 | 60 |
| 81. Shock spectra, <i>Mariner III, IV</i> , Atlas—Agena separation, B3 | 60 |
| 82. Oscillogram, <i>Mariner III</i> , Agena first ignition, all channels | 61 |
| 83. Oscillogram, <i>Mariner IV</i> , Agena first ignition, all channels | 62 |
| 84. Shock spectra, <i>Mariner III, IV</i> , Agena first ignition, B3 | 63 |
| 85. Shock spectra, <i>Mariner III, IV</i> , Agena first ignition, F4 | 63 |
| 86. Oscillogram, <i>Mariner III</i> , typical Agena first burn, all channels | 64 |
| 87. Acceleration spectral density, <i>Mariner III</i> , Agena first burn, F4 | 65 |
| 88. Acceleration spectral density, <i>Mariner IV</i> , Agena first burn, F4 | 65 |
| 89. Oscillogram, <i>Mariner III</i> , Agena first cutoff, all channels | 66 |
| 90. Oscillogram, <i>Mariner IV</i> , Agena first cutoff, all channels | 67 |
| 91. Oscillogram, <i>Mariner III</i> , Agena pyro events, all channels | 68 |
| 92. Oscillogram, <i>Mariner IV</i> , Agena pyro events, all channels | 69 |
| 93. Oscillogram, <i>Mariner III</i> , Agena second ignition, all channels | 70 |
| 94. Oscillogram, <i>Mariner III</i> , Agena second burn, all channels | 71 |
| 95. Acceleration spectral density, <i>Mariner III</i> , Agena second burn, F4 | 72 |
| 96. Acceleration spectral density, <i>Mariner IV</i> , Agena second burn, F4 | 72 |
| 97. Oscillogram, <i>Mariner III</i> , Agena second cutoff, all channels | 73 |
| 98. Oscillogram, <i>Mariner IV</i> , Agena second cutoff, all channels | 74 |
| 99. Oscillogram, <i>Mariner III</i> , spacecraft separation, all channels | 75 |
| 100. Oscillogram, <i>Mariner IV</i> , spacecraft separation, all channels | 76 |
| 101. Shock spectra, <i>Mariner III, IV</i> , maxima, minima, B3 | 76 |

N66-36858

ABSTRACT

This Memorandum presents an analysis of the dynamic flight environment of the *Mariner* Mars 1964 spacecraft. The reduced data from *Mariner III* and *Mariner IV* are presented and compared. Nine environmental measurements were taken for each spacecraft. These consisted of five vibration transducers within the payload area of each launch vehicle and four microphones mounted outside the vehicle on the launch complex umbilical tower. These telemetered and recorded data have been analyzed using the following techniques: oscillograms, bandpass, power spectra, shock spectra, and data compression. The reduced data are discussed with reference to each appropriate analysis technique. No comparison with ground test data is made. *Author*

I. INTRODUCTION AND SUMMARY

This Memorandum summarizes the dynamic data acquired during the preinjection phase of the *Mariner* Mars 1964 missions. It includes only those data acquired by certain telemetry measurements in and around the spacecraft area of the launch vehicles. The response of the spacecraft to various forms of excitation environments was measured by accelerometers and telemetered by the transmitter systems aboard the *Atlas-Agena* vehicles.

Emphasis is placed on the instrumentation and analysis techniques utilized to obtain the reduced data. Included are detailed discussions and illustrations of the instrumentation on the spacecraft, *Agena* adapter, and launch pad. The limitations of these systems are presented and

discussed. The analysis techniques are also discussed in the chronological order of utilization and the particular use of each technique in defining the total measured environment.

The data are discussed with reference to the analysis techniques utilized in its reduction. Comments that have been made about the causes of particular response vibrations are included in the discussion section (IV).

All of the reduced data are presented in a single section (V) using oscillogram records of specific events as a chronological index of the data as they occurred during the flight.

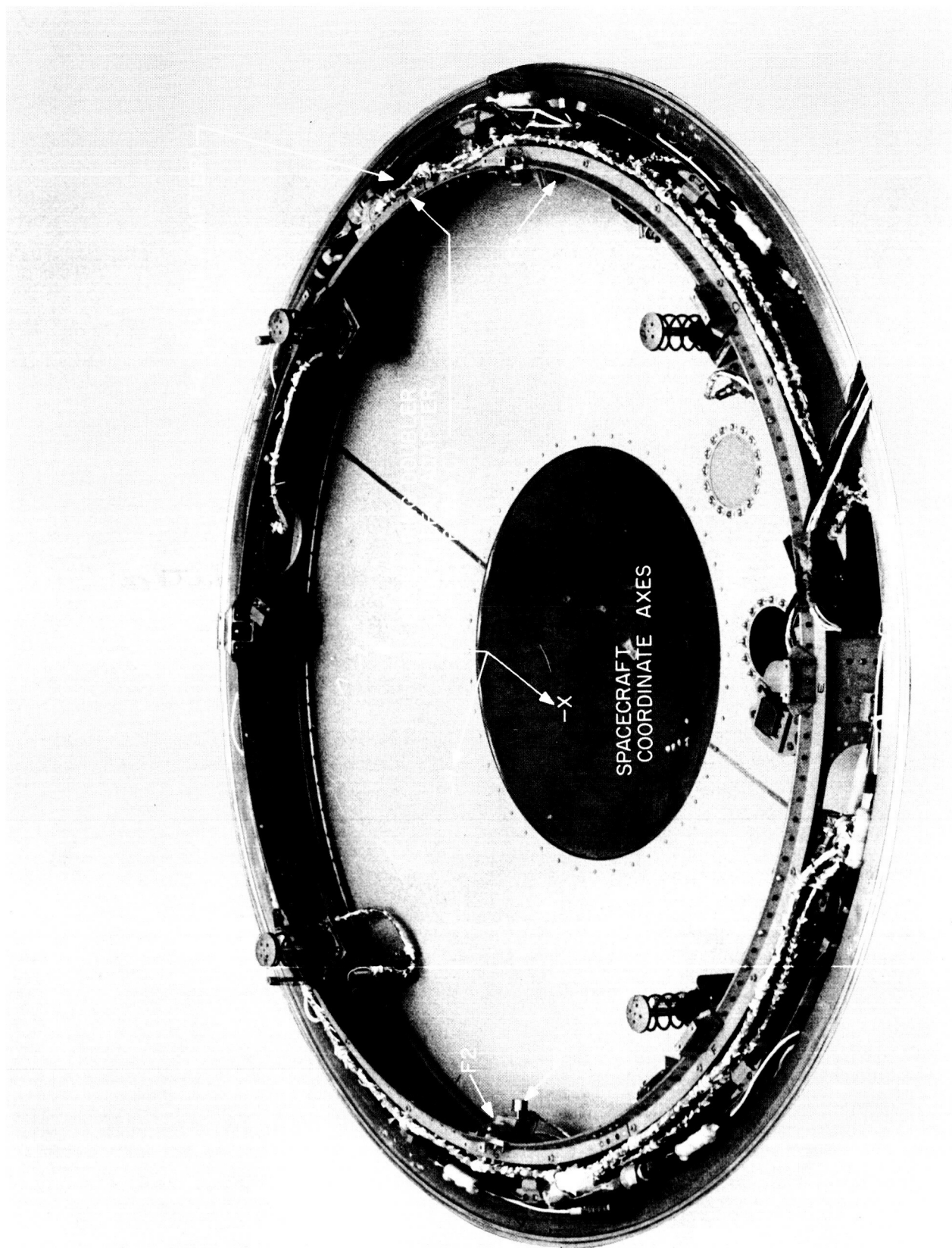


Fig. 1. Adapter instrumentation

II. INSTRUMENTATION

A. Flight Telemetry System

The flight instrumentation, for the *Mariner III* and *IV* vehicles, was chosen by agreement between NASA Lewis Research Center and JPL as reported in Reference 1. The final instrumentation was located as follows:

1. The general locations of the four adapter accelerometers are shown in Fig. 1. Figure 2 shows the three Satham (model A69TC) low frequency and the Endevco (model 2217) high frequency accelerometers in detail as well as the spacecraft coordinate

axes. The Satham transducers (F1, F2, and F3) were of the low frequency strain-gage type, whereas the Endevco (F4) was a wide band piezoelectric type.

2. One spacecraft high frequency accelerometer (B3) (Endevco model 2217) was used on the main structure to define the response of the bus during the launch phase. Its rigid mounting near spacecraft leg B is shown in Fig. 3 with the spacecraft Z axis (booster axis) displayed. An external reference to its location is the solar panel monoball support shown in Figs. 3 and 4.

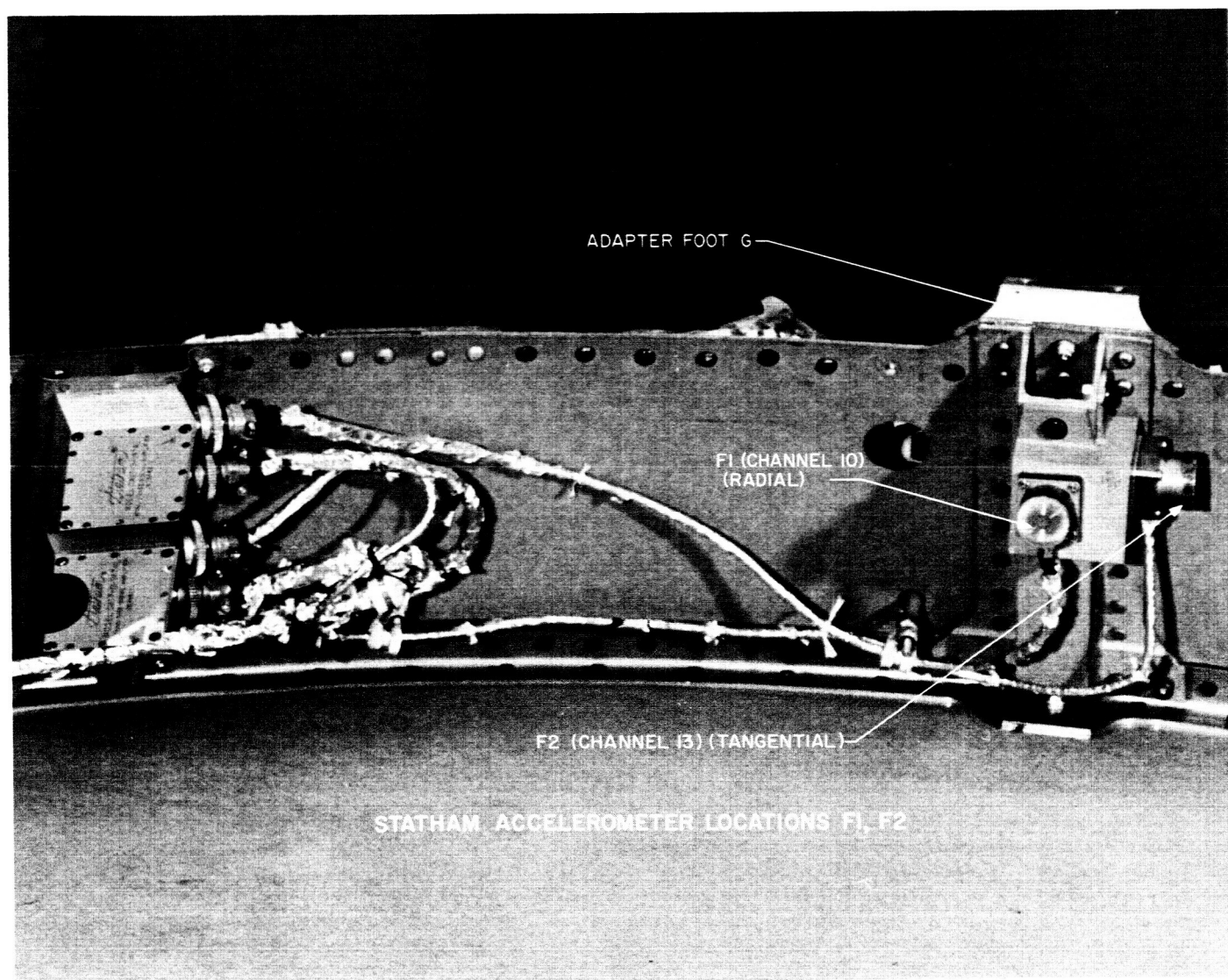


Fig. 2a. Adapter instrumentation (detail)

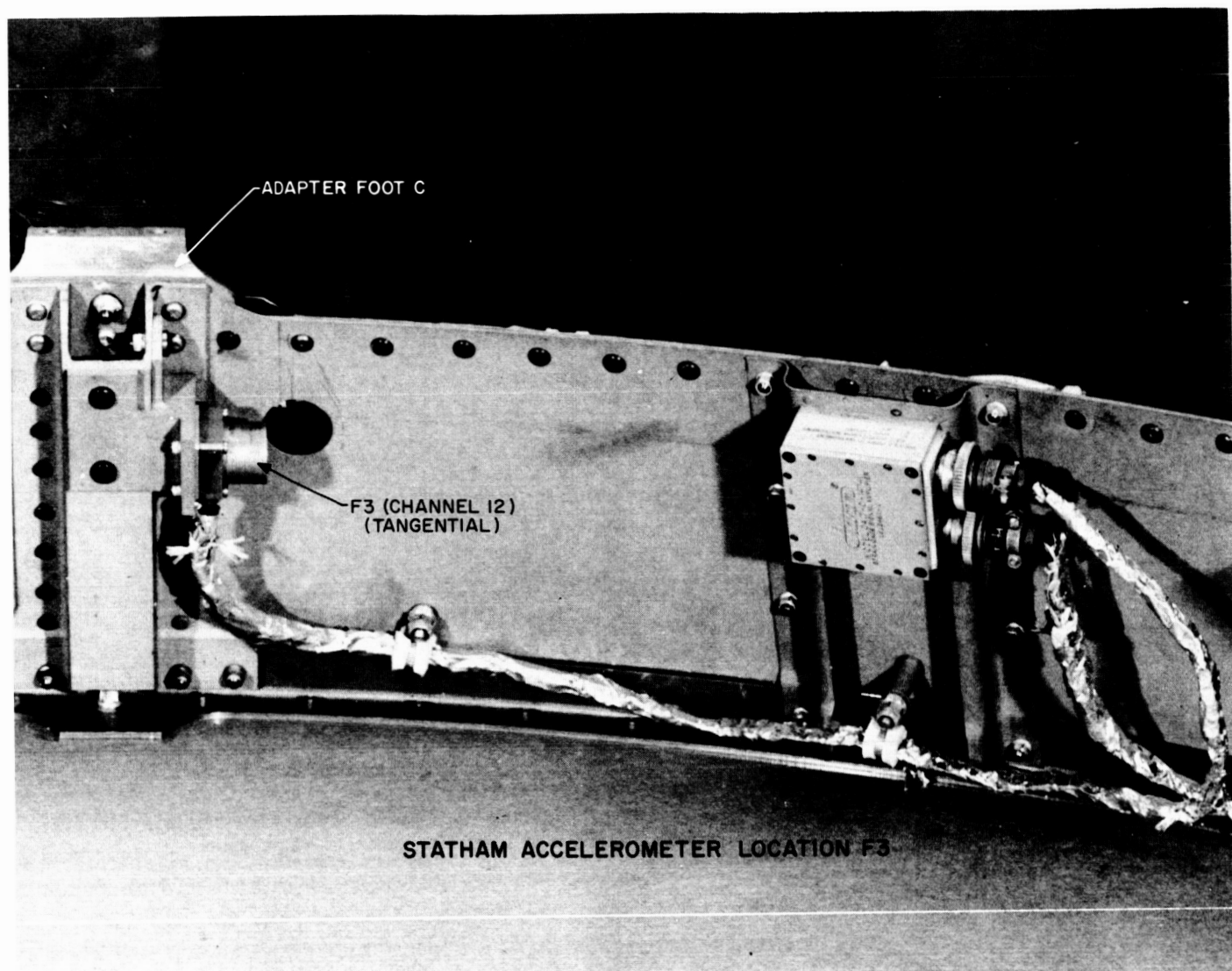


Fig. 2 b. Adapter instrumentation (detail)

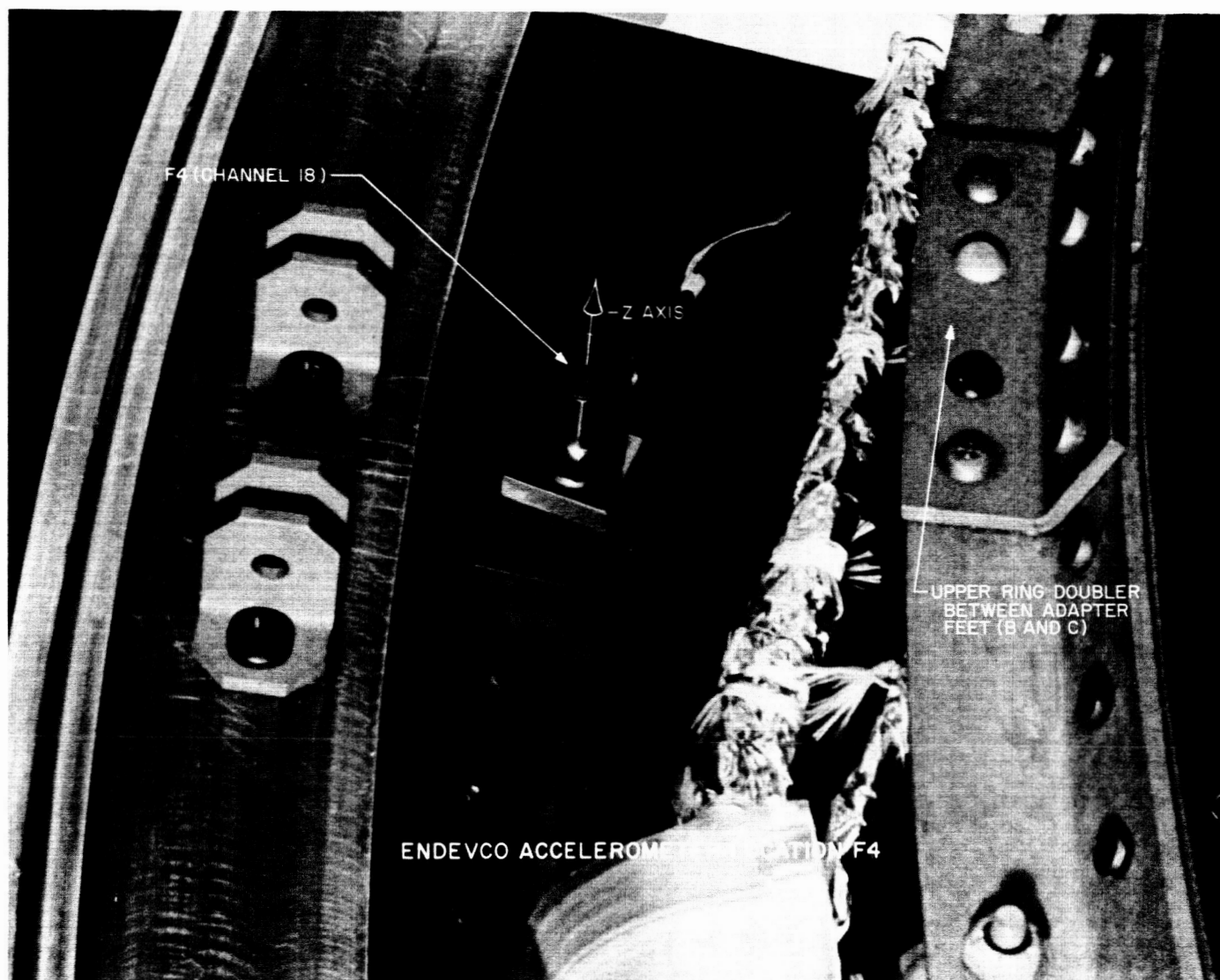


Fig. 2c. Adapter instrumentation (detail)

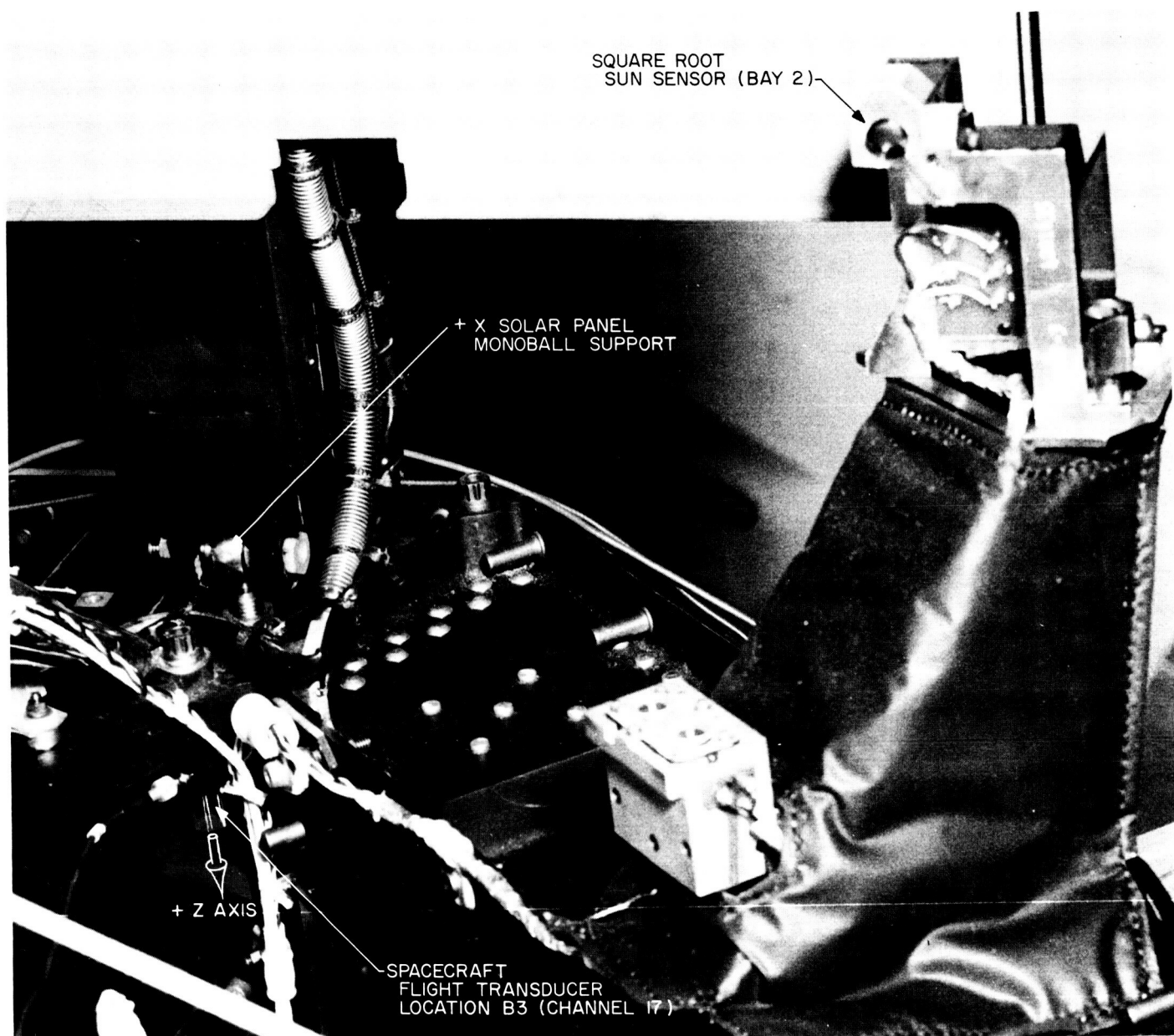


Fig. 3. Spacecraft flight accelerometer

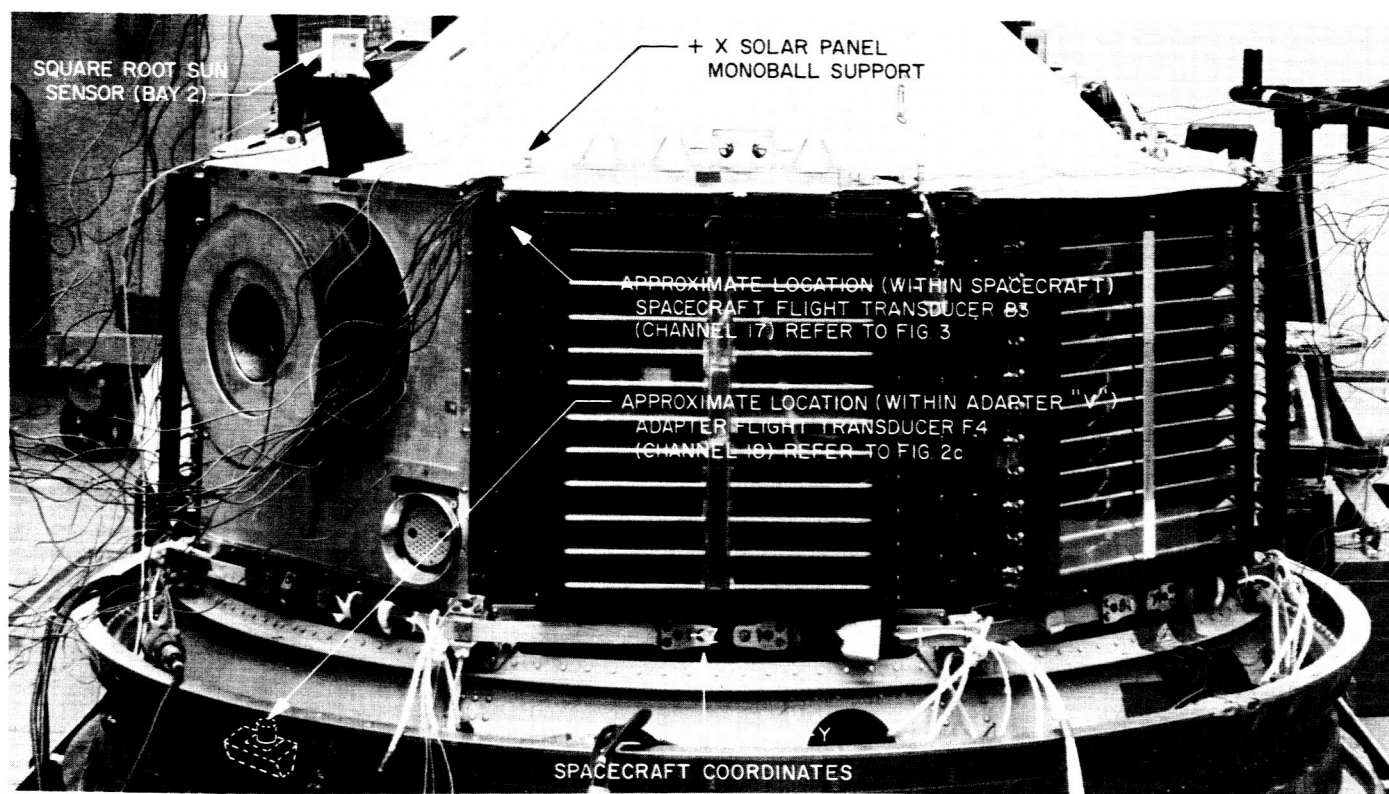


Fig. 4. Spacecraft bus configuration showing instrumentation locations

A typical test configuration is shown in Fig. 4, illustrating the approximate position of both of the high frequency flight transducers within the spacecraft and adapter.

Table 1 displays the *Mariner-Agena* telemetry channels on the 244.3 mc FM/FM carrier. Included are the calibration and frequency response of each flight accelerometer channel. Due to the limitations of the telemetry system, higher frequency data, sensed by the accelerometers, are not relayed above the frequency limitations of the telemetry channels.

The *Agena* telemetry system used on the *Mariner* Mars flight was a standard Inter Range Instrumentation Group (IRIG) system using 18 channels. The 244.3 mc FM/FM carrier contains subcarriers for each FM channel of data. Each transducer signal or commutated set of signals is used to deviate a Voltage Controlled Oscillator (VCO) from its specific subcarrier center frequency to a maximum of 7.5% deviation from that frequency. The summed subcarriers are transmitted on the 244.3 mc modulated main carrier to the tracking stations where the carrier is demodulated and the subcarrier information is recorded directly. To play back the original data signal, it is neces-

sary to discriminate this recorded signal using IRIG discriminator filters.

There are specified limits on the frequency response of each telemetry channel in the IRIG system. These limits are imposed by the necessary deviation (7.5%) of each subcarrier frequency and the signal to noise ratio or modulation index required to ensure a significant level of data. Table 1 displays the limited frequency response of the standard IRIG flight telemetry channels. These standard IRIG frequency cutoff limits have proven to be very conservative.

The *Agena* telemetry systems used with the *Mariner* spacecraft were not calibrated "end-to-end"; however, this test was performed on the *Agena* systems of *Ranger VIII* and *IX*. Assuming the telemetry systems were similar, some conclusions can be made regarding the frequency response limits of each channel.

Figure 5 was derived from the *Ranger VIII* end-to-end calibration (Ref. 2) and displays the overall frequency of the total transmission link under noise excitation of channels 17 and 18. Clearly, these channels are capable

Table 1. Agena telemetry channel descriptions

| Channel No. | Measurement | LMSC I.D. No. | JPL I.D. No. | Frequency response | | Nominal calibration |
|-------------|--|---------------|--------------|--------------------|--|---------------------|
| | | | | Std. IRIG | Extended range (2 × IRIG) + Error | |
| 3 | Shroud V-Band tension No. 1 | A101 | | 11 | | 0-4000 μ strain |
| 4 | Shroud V-Band tension No. 2 | A102 | | 14 | | 0-4000 μ strain |
| 5 | Spacecraft adapter V-Band tension No. 1 | A105 | | 20 | | 0-3600 lb |
| 6 | Spacecraft adapter V-Band tension No. 2 | A106 | | 25 | | 0-3600 lb |
| 7 | Agena gas valve currents 1-6 | D149 | | 35 | | |
| 8 | Spacecraft separation monitor No. 1 Y axis accel. (Agena) | A007 D8 | | 45 | | ± 1.5 g |
| 9 | Spacecraft separation monitor No. 2 Z axis accel. (Agena) | A008 D9 | | 59 | | ± 1.5 g |
| 10 | Adapter radial accel. | PL 37 | F1 | 81 | 162 $\left\{ \begin{array}{l} +0\text{db} \\ -0.3\text{db} \end{array} \right.$ | ± 3.7 g/7.5% |
| 11 | Spacecraft separation monitor No. 3 X axis accel. (Agena) | A009 D7 | | 110 | | -4 to +12 g |
| 12 | Adapter tangential accel. | PL 31 | F3 | 160 | 320 $\left\{ \begin{array}{l} +0.3\text{db} \\ -0.1\text{db} \end{array} \right.$ | ± 5.5 g/7.5% |
| 13 | Adapter tangential accel. | PL 33 | F2 | 220 | 440 $\left\{ \begin{array}{l} +0.3\text{db} \\ -0.1\text{db} \end{array} \right.$ | ± 5.5 g/7.5% |
| 14 | Velocity meter and F/MA | D88/D83 | | 330 | | 0-50/0-300 pps |
| 15 | Comm 1B | | | 450 | | 5 rps, 60 points |
| 16 | Comm 1A | | | 600 | | 5 rps, 60 points |
| 17 | Spacecraft separation rate monitor No. 79 | A010 | | | | ± 2.5 deg/sec |
| | Spacecraft bus axial accel. | PL 25 | B3 | 790 | 1580 $\left\{ \begin{array}{l} +1.5\text{db} \\ -0\text{db} \end{array} \right.$ | ± 23 g/7.5% |
| 18 | Spacecraft separation rate monitor No. 89 | A011 | | | | ± 2.5 deg/sec |
| | Adapter axial accel. | PL 6 | F4 | 1050 | 2100 $\left\{ \begin{array}{l} +1.5\text{db} \\ -1.5\text{db} \end{array} \right.$ | ± 22 g/7.5% |

NOTE: Channels 8, 9, 11, 12, 17, and 18 were dual purpose channels switched prior to Spacecraft separation.

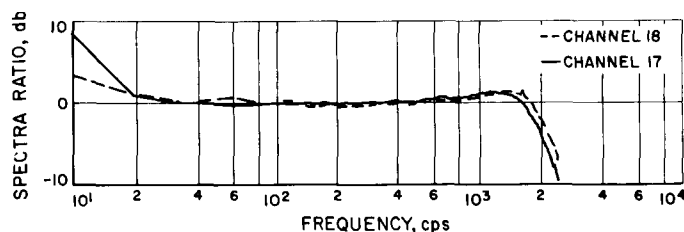


Fig. 5. Telemetry frequency response—high-frequency channels

of transmitting higher frequency information than the standard IRIG cutoff of 750 cps and 1050 cps respectively. The frequency response of these channels can be extended to at least twice the standard IRIG cutoff. Most of the data in this Memorandum have been played back with a $3 \times$ IRIG low pass filter. Examination of the *Ranger* calibration curves indicates the channels to be accurate to ± 1.5 db up to twice the IRIG cutoff frequency when analyzed with a $3 \times$ IRIG discriminator low pass filter. Table 1 shows this extended range in frequency response for the five flight transducers (F1, F2,

F3, F4, and B3) that are analyzed in this Memorandum with the probable error associated with each measurement.

A brief discussion of telemetry coverage during the launch phase follows. Figure 6 shows the *Agena* telemetry coverage and event sequence for *Mariner III* and *IV* respectively. In general, the coverage was adequate and good data were acquired. The spacecraft separation event was not recovered. This event produced the highest level shock response experienced during spacecraft level ground tests; and flight telemetry data would have been very useful. The tracking coverage was adequate here, but it was necessary to switch out the high frequency channels in the telemetry system before this event.

Channel calibrations were decided upon which allowed for the range of expected data to be recorded. It is necessary to set the peak calibration values at a low enough level for a significant signal to noise ratio for the lower level random data at the liftoff and transonic periods.

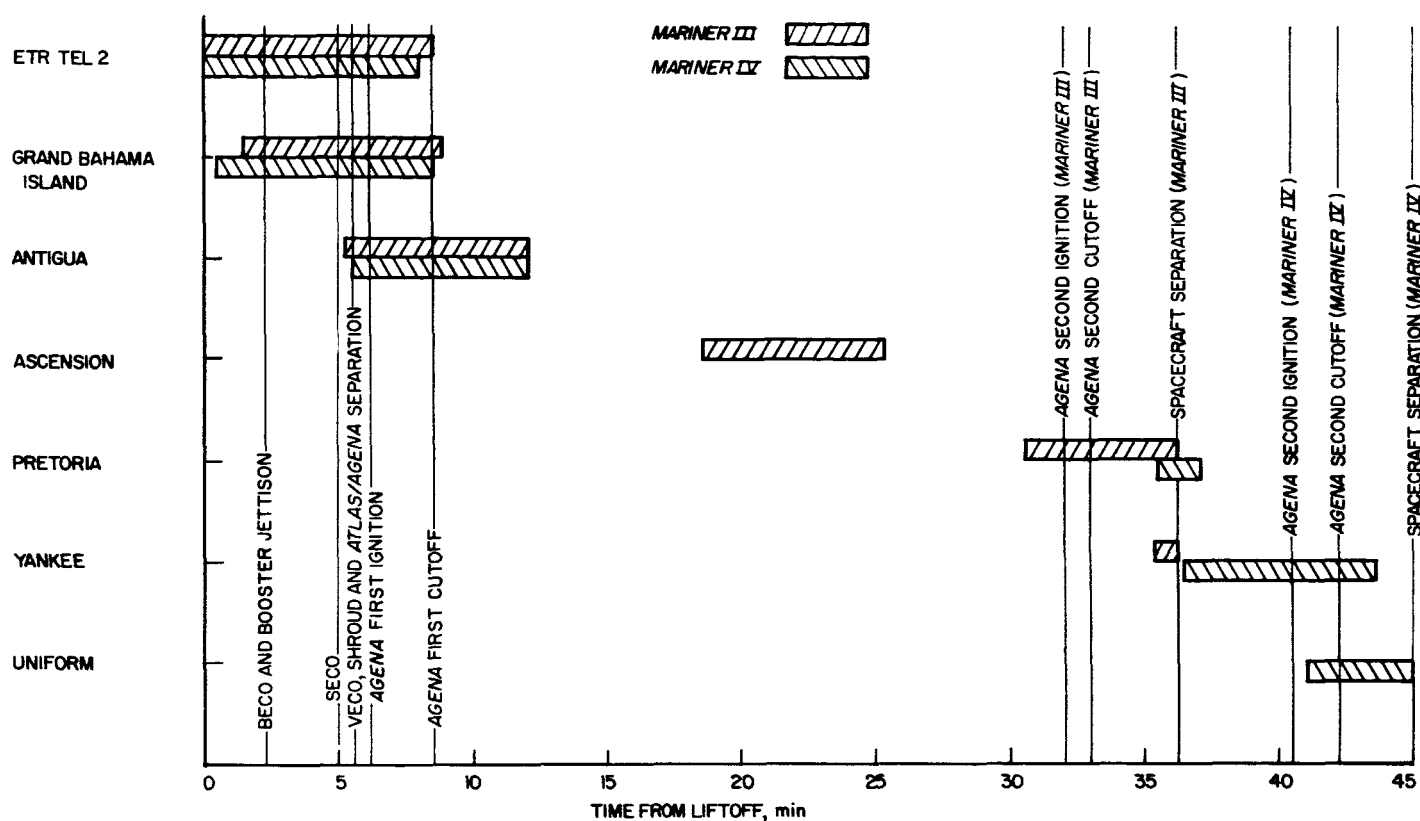


Fig. 6. Tracking station telemetry coverage and events

However, with a low peak calibration, the high level pyrotechnic events that occur usually exceed the channel sensitivity and cause a "loss of lock" or amplifier overload signal in the channel. In general on both *Mariner* flights, the calibration levels were such that total loss of lock occurred on only the highest level shocks. (The shock levels were high enough at times that the accelerometer amplifiers were saturated also.)

B. Launch Pad Acoustic Instrumentation

Both *Mariner* Mars 1964-*Atlas* launch pads were equipped with similar instrumentation to record the acoustic field around the booster during the liftoff period. Two sets of microphones were utilized. Figures 7 and 9 show the approximate locations of these microphones for both pads. More detailed schematics of their locations are shown in Figs. 8 and 10.

One set of two microphones was mounted on an out-board structure near the top of the umbilical tower facing the spacecraft. These microphones were chosen to measure the near acoustic field around the spacecraft as closely as possible during the ignition and liftoff phase.

The other set of two microphones was located on a lamppost just above ground level in a direction toward the flame bucket. This location was chosen to measure the far field from the booster, to possibly correlate with the tower microphones.

This instrumentation system was flat to at least 10 kc but the range utilized in this Memorandum was less than 3 kc to be comparable with flight telemetry measurements. The microphones were B & K model NM 125 with Endevco 2609 amplifiers. The signal was recorded on a double band Ampex FR 1300 tape recorder at 60 ips.



Fig. 7. Mariner III launch pad—acoustic instrumentation

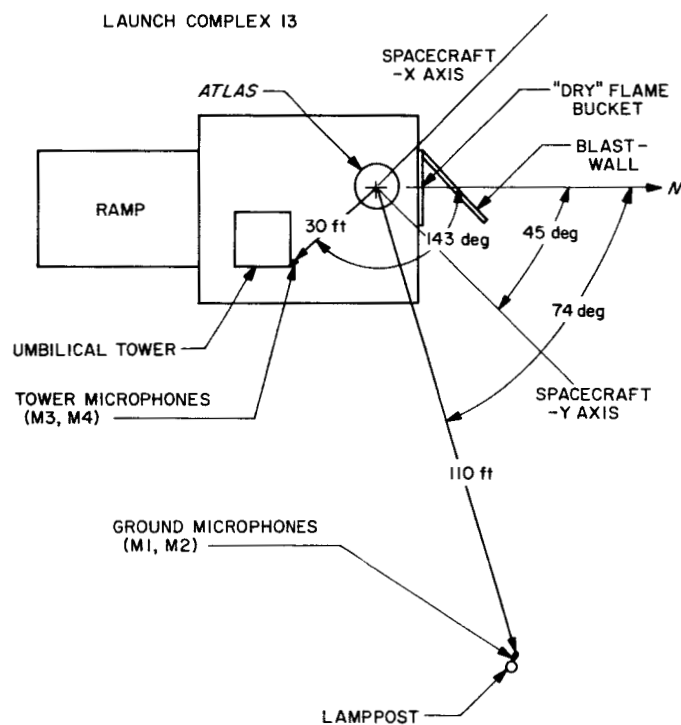


Fig. 8. Mariner III acoustic instrumentation (detail)

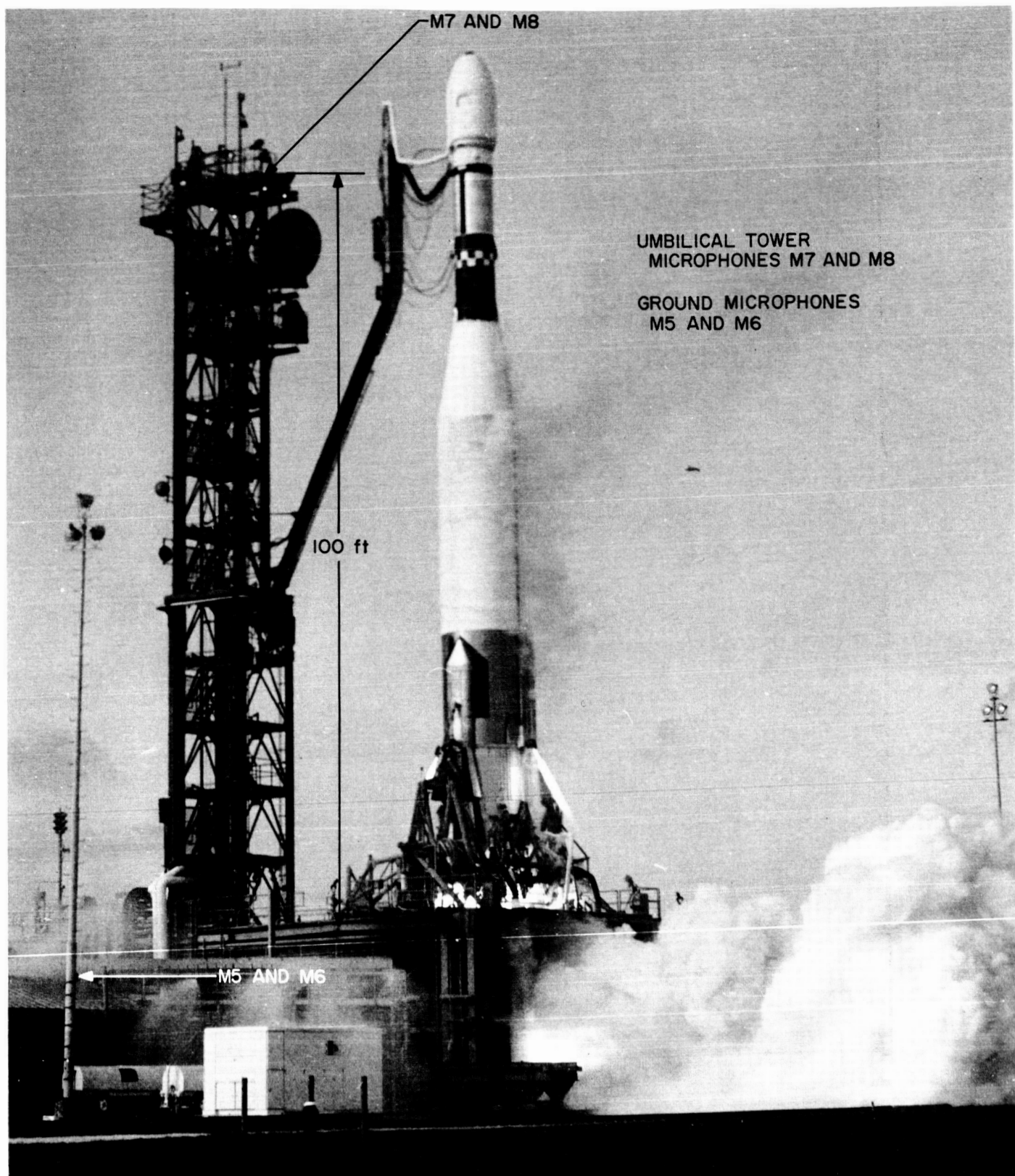


Fig. 9. Mariner IV launch pad—acoustic instrumentation

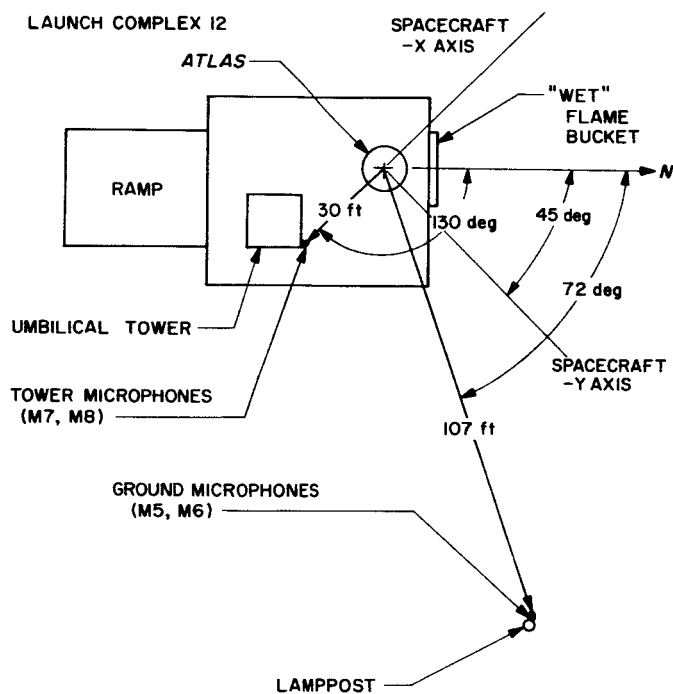


Fig. 10. Mariner IV acoustic instrumentation (detail)

III. ANALYSIS TECHNIQUES

The techniques utilized in the data reduction are summarized in this section. Included are limitations and possible error sources. The order of the five techniques in this section proceeds logically from the general to the specific.

A. Oscillograms

A direct playback of the data is displayed on these records. The only limits on the data are the $3\times$ IRIG low pass filter and the *Agena* telemetry band edge of each channel.

Figure 14 is an example of five *Agena* telemetry channels on a single oscillogram. Included are the AMR-D5 time code, and "loss of lock" records.

B. Band Pass Analysis

Two banks of band pass filters are used for this sequence of data analysis. Mainly 100 cps bandwidths are used, along with other ranges as defined below. When raw flight data are passed through this "Comb" filter bank, frequency discrimination results.

The first bank contains twelve low frequency band pass filters in the order as follows:

- 10-50 cps (1)
- 10-100 cps (1)
- 100 cps band pass filters with center frequencies from 150 cps through 950 cps (9)
- 10-1000 cps (1)

Figure 15 is a resulting plot from this low frequency bank.

The second bank contains twelve high frequency band pass filters as follows:

- 100 cps band pass filters with center frequencies from 1050 cps through 1950 cps (10)
- 1000-2000 cps (1)
- 10-2000 cps (1)

Figure 16 is an example of the analysis from these filters with the same telemetry channel as the first bank.

Each filter in the system has associated with it a signal averaging device. The output from this averager is plotted as a function of time simultaneously for each band in

the bank. Therefore, magnitudes equal to average g level are recorded as a record on the vertical scaling. The calibration is given in several locations shown on the final plots as vertical arrows to the left of the frequency axis.

Horizontal scaling is provided by the apparatus in the form of timing lines every second.

Errors in the system are dependent on the skill of the operator. As in any electronic playback system, the calibration procedures are most critical.

C. Power Spectral Density Analyses

The two types of analyses used in this data reduction consist of an analog analysis with a purely electronic system in the frequency domain, and a digital process using numerical sampling within the time domain.

Analog Power Spectral Density (PSD) plots are obtained by the following procedure. The flight data tape, which has a signal amplitude proportional to acceleration in g 's, is first played back and monitored to find the required time sample. (This selection is explained in Section IV-B of the Memorandum). A tape loop of this exact time sample is recorded for use in the remainder of the analysis.

A continuous data signal for the selected time increment results when the tape loop is played repeatedly. Passing the signal through a band pass filter of fixed width and variable center frequency results in discrimination of the data within the frequency band. Squaring and averaging the filter output produces a narrow band mean square signal which is then divided by the filter bandwidth. Applying this signal to the vertical axis pen of an X-Y plotter produces the required analog PSD plot with logarithmic vertical scaling displaying g^2/cps . Horizontal scaling of the plot utilizes the signal representing the variable center frequency of the band pass filter as it sweeps along the frequency axis using linear scaling. The units of the plot, g^2/cps versus cps, define the Acceleration Spectral Density (ASD). Figure 58 is an example of an analog ASD.

All averaging, squaring, and division are done electronically in the frequency domain using this system as illustrated in the schematic diagram, Figure 11. The errors inherent to this system can usually be traced to human origin. Recording the tape loop and displaying the

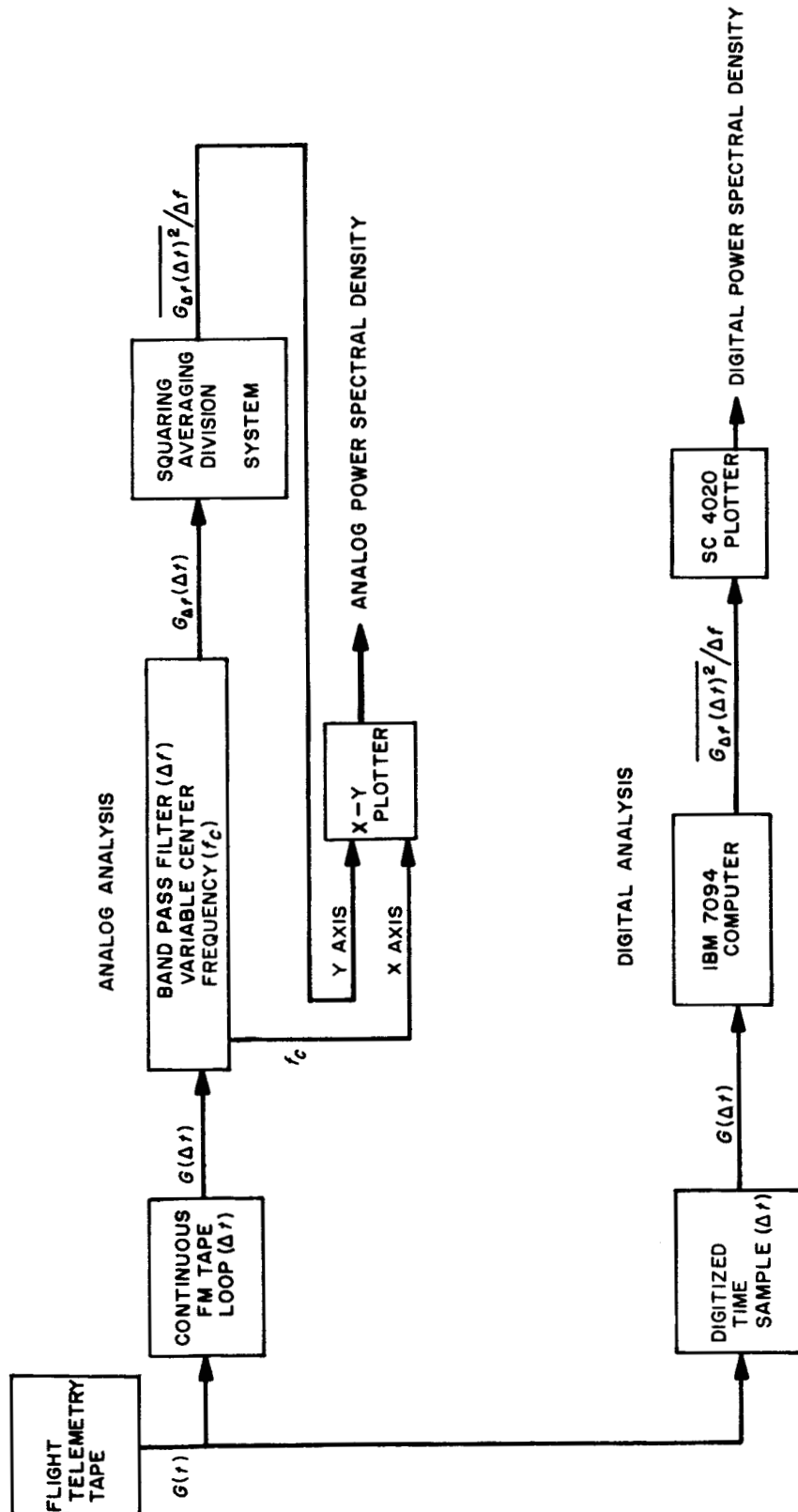


Fig. 11. Power spectra analysis schematic

final plot on the X-Y plotter are both areas that must be carefully calibrated and executed.

In contrast to the analog or purely electronic system, there exists the larger production PSD capability using high speed digital computers. Little similarity exists between the analog and digital techniques; however, the results are very similar. The latter analysis will be described in the following paragraphs.

A time sample is chosen from the flight tape. Playing the tape at this time increment through an analog to digital converter (in conjunction with a PDP-4 computer) produces a "digital" tape to be processed further. The "digitized" data are an accurate set of numbers proportional to the data signal on the original flight tape.

Processing the "digital" tape on the IBM 7094 computer proceeds with the use of JPL program number 5470. Although there are some highly complex modes of calculation within the program, a brief description of its general operation and limitations is in order.

The autocorrelation function of the data is used as a basis for the program. Computing the Fourier transform of the autocorrelation function defines the PSD of the data sample. Reference 3 contains all the information used to program this analysis for the 7094. Practical use of these methods implies certain necessary assumptions. Data stationarity is assumed, and is only approximated using short time increments. Proper data sampling requires a sample size 10 times the number of lag products (autocorrelation products). Also, the highest frequency desired on the PSD must be no more than one half the digitizing sample rate because of aliasing (folding of higher frequency data over to be confused with lower frequency levels). To further eliminate the possibility of aliasing, the data are passed through a low pass filter set just below the maximum frequency desired. The roll-off noted on Fig. 5 past 2 kc is due to this low pass filter. Presently, we are limited to one bandwidth resolution per plot, which may affect the accuracy of the data in certain regions. The most economically feasible resolution at this time seems to be 20 cps. The definition of data at low frequencies (less the 150 cps) is questionable because of this problem. Decibel scale units are used on the ordinate of all plots whether acceleration or sound pressure data. The acceleration data reference is $1 \text{ g}^2/\text{cps}$ and the sound pressure data reference is $2 \times 10^{-4} \text{ } \mu\text{bar (rms)}/\text{cps}$, or $4 \times 10^{-8} \text{ } \mu\text{bar (rms)}^2/\text{cps}$. Figure 22 is an example of a digital ASD plot. In addition to the plot out-

put, punched cards are produced containing acceleration spectrum level and sound pressure spectrum level values. Subsequent analyses and comparisons can be performed using these cards.

The possibility of errors in this system is greatly reduced because of minimum human contact with the data. Only in the digitizing process could human error affect it.

D. Shock Spectra

Flight transients consist mainly of pyrotechnic shocks which are inherently very erratic pulses. Because of the highly nonstationary aspects of the transients, no statistical methods of frequency analysis are applicable. To attempt an analysis of these shocks in the time domain is of questionable value. It appears at this time that it is more meaningful to analyze transients in the frequency domain, which leads to the present utilization of shock spectra analyses.

The maximum response of a tuned simple resonator, excited by the transient, defines a single ordinate at one resonant frequency (abscissa) of a shock spectrum. By varying the tuned frequency of the resonator and plotting the maximum response for each frequency, the entire shock spectrum is generated.

The result is a plot of frequency content of the transient pulse input. The units of the ordinate are peak g 's response, while the abscissa is plotted as tuned or resonant frequency in cycles per second. Another parameter associated with each spectrum is the percent of critical damping of the resonator (zeta). The effect of increasing the damping is to smooth and lower the spectrum. A zeta value of 2.5% has been used in this Memorandum for all shock analyses.

A digital processing program was used to calculate the shock spectra and to display the transient in a convenient form. The approximate time increment of the shock is used to trigger the analog to digital converter as it accepts the flight tape data. Using a high sample rate ($10 \times$ maximum frequency) very accurate definition of the shock is produced and recorded on digital tape. JPL program number 5352 is used to process the tape on the IBM 7094 computer. The program produces plots of the transient-time history and shock spectra. Figure 12 is an example of this plot format.

Because of the concept used to obtain shock spectra, the units of the ordinate are not comparable with power spectra or bandpass analysis. The practical value of a

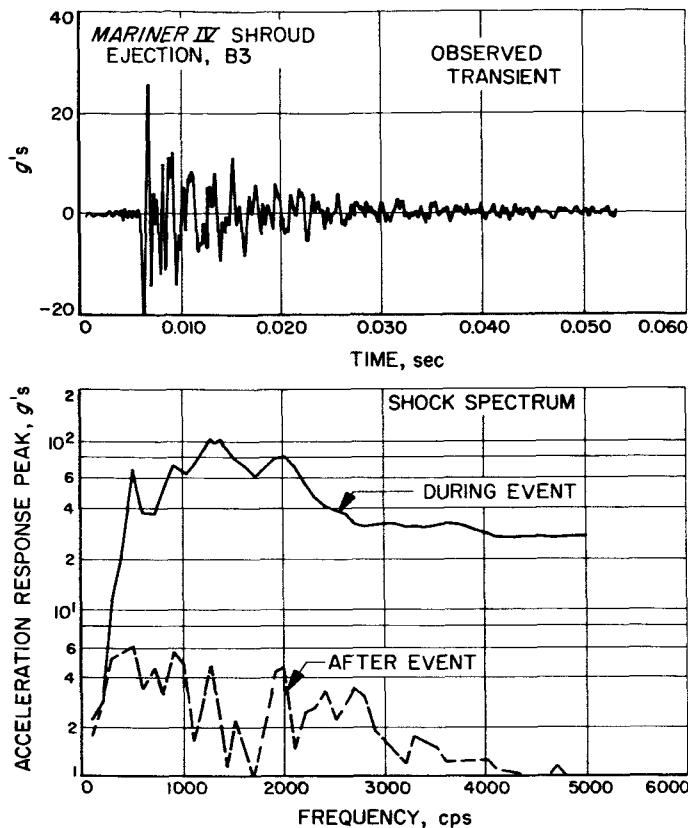


Fig. 12. Typical shock spectrum plots

shock spectrum used in analyzing transients is not primarily in its absolute units but its usefulness as a comparative tool for two or more shocks. As long as shocks are analyzed in exactly the same manner, their spectra form a reasonable basis of describing their relative severity.

Errors associated with this type of analysis are small because of the almost completely digital methods utilized. A question may exist about the precise definition of a shock above the "quiet" level of the data. It has been assumed here that the shock ends when its level drops to approximately 10% of its peak.

E. Data Compression Techniques

An additional advantage of digital processing is the convenient format of the output which lends itself to further comparison and compression of the data. Both the PSD and Shock Spectra programs have punched IBM card outputs of all the frequency spectra. Simple calculations may be performed using these cards as input data. Comparison and manipulation of these vibration, acoustic, and shock data are possible using the IBM 7094 computer.

Two programs may be used for these purposes. Both vibration and acoustic data can be analyzed by the program "GAME" (JPL number 5524). The Shock Spectra program can be further processed using the program "SHOCK SPECTRA GAME" (JPL number 5574). Inputs to both programs are IBM punched cards. Outputs are either digital plots, IBM cards or both.

There are eight manipulation operations available in the programs as follows: Mean, Percentile Levels (Normal), Percentile Levels (Log-Normal), Maximum Envelope, Minimum Envelope, Product, Ratio, $\frac{1}{3}$ Octave Conversion (used only with GAME program), and a composite plot capability. Figure 101 is an example of three of these operations used simultaneously (i.e., maximum, minimum envelopes and composite plot capability).

IV. ANALYSIS RESULTS AND DISCUSSIONS

Each of the techniques previously described has a specific and necessary purpose in defining the total flight environment. This section includes all of these techniques. The approximate chronological order of the usage of these techniques is retained here.

A. Oscillograms

As an initial "quick-look" type of analysis, the oscillogram displays all of the data on the tape in detail in the time domain. The actual wave form is presented with the approximate peak levels that can be read directly. Shocks are the most significant data recovered from these traces. Approximate magnitudes and exact time increments of the shocks are displayed in a convenient form that can be utilized for more detailed shock spectra analyses. The maximum random vibration response can be estimated and time correlated approximately, but this is more clearly defined in the band pass analysis. Oscillograms proved to be very valuable in the initial analysis of the flight shock anomalies that occurred on *Mariner III*.

Any principal periodic frequency that exists in a signal can be read approximately from the trace. This is true particularly in the BECO and SECO transients as indicated in Figs. 59 and 64 which contain relatively low frequency "ringing" caused by booster modes.

The validity of some of the shocks could be estimated by the "loss of lock" signal displayed simultaneously for each channel. This "loss of lock" occurred frequently with the high level shocks caused by pyrotechnics. A preliminary examination of the wave form can also detect invalid data caused by other defects such as connections, amplifier problems, etc.

High frequency transients could not be analyzed for an estimate of principal frequencies using the oscillograms in this Memorandum because the paper speed was not high enough. Any high frequencies in the shocks are displayed with the shock spectra that follow.

Some time transients are included in this Memorandum as oscillograms only, with no corresponding shock spectra. These were either insignificant shocks or anomalies which are discussed briefly in the following paragraph.

Figures 89 and 90 show the time traces of the first *Agena* engine cutoff. Other than the shock anomalies of the *Mariner III* trace, the levels of this event were con-

sidered low enough to neglect shock spectrum analyses. Figures 91 and 92 are time traces of two *Agena* events typical of other high frequency pyrotechnic shocks. Figure 93 is a trace of the *Mariner III*-*Agena* second ignition. This is again a low level event except for the shock anomaly shown. Good *Mariner IV* data do not exist for this event because of the poor quality of the Yankee telemetry tape. Figures 97 and 98 display the second *Agena* engine cutoff. The *Mariner III* data show the nominal dc shift of the axial accelerometers. The Channel 13 trace from *Mariner IV* shows definite erratic disturbances not seen on the other spacecraft. Figures 99 and 100 are the traces of the spacecraft separation event showing the channels switched to other monitors and the out of lock conditions existing on the other channels.

B. Band Pass

This more detailed analysis displays a concise record of the quasi-stationary data over a large time period. The various frequency bands allow interpretation of the data initially in lieu of frequency spectra which are usually to follow. Each band plotted as a function of time gives an estimate of the spacecraft response energy within this band. The maximum random vibration time samples can be determined with reasonable accuracy using this method. These time increments can then be analyzed in more detail using PSD methods.

The relationship between the band pass analysis and PSD analysis with the same time sample is clearly shown in Figs. 32 and 38. In the former, the levels of data within the frequency bands are related closely to the latter spectrum levels for these same frequencies. (These are relative comparisons ignoring the obvious difference in units.) The value of the band pass can be seen from this example showing that approximate frequency analysis can be made as a function of time in areas that may not have been analyzed previously by PSD's.

A correlation between the acoustic field and the liftoff vibration of *Mariner IV* is shown in Fig. 13. The wide band filter output of B3 (10-2000 cps) has been plotted on the same time scale as the tower microphones for the same period. Near 1.6 sec after liftoff there seems to be a lower level in both traces than existed previously. This could possibly be explained by uncorrelated noise sources as the booster altitude changes.

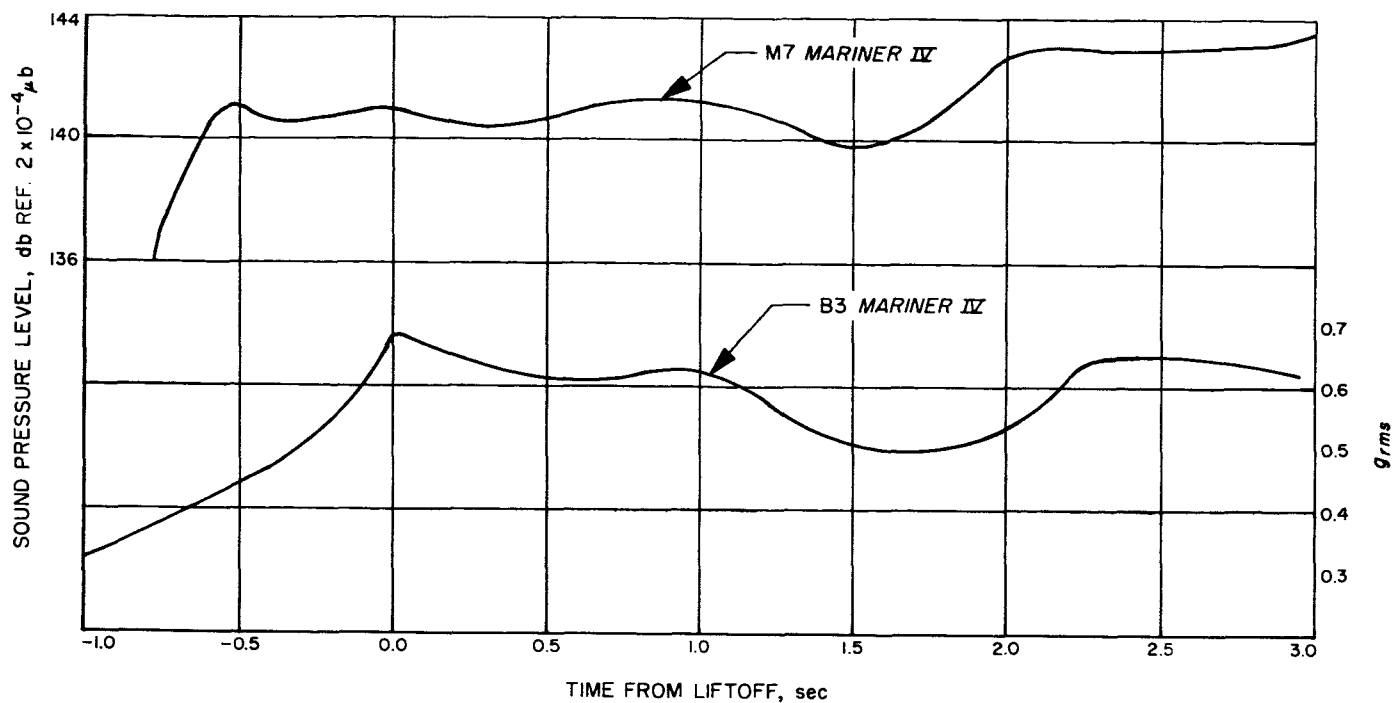


Fig. 13. Wide band levels vs. time (*Mariner IV*), umbilical tower microphone M7, and spacecraft accelerometer B3

Shortly before the maximum transonic excitation, there seems to be a characteristic notch in the wide band (10–2000 cps) signal of Figs. 18 and 33. This corresponds approximately to 51 sec after liftoff for both flights, which is nearly the theoretical time of Mach 1. There are probably localized disturbances which are supersonic previous to this time but this abrupt change in level seems to have significant correlation with supersonic velocity. *Mariner IV* shows the most abrupt change. Also, the theoretical maximum dynamic pressure was not associated with the maximum spacecraft response as recorded by B3 or F4.

The relationship between the overall wide band levels for the principal random excitation periods (liftoff and transonic) is shown in Figs. 16 and 31. Included are the wide band (10–2000 cps) data levels for the spacecraft accelerometer B3 during these periods. The liftoff levels of *Mariner III* are higher than the transonic levels but the reverse is true for *Mariner IV*. This difference will be discussed and correlated in the following section.

C. Power Spectra

The most detailed analysis of stationary random data available at this time is the PSD data reduction. The quasi-stationary data are considered stationary for the

small time increments taken in the analysis. These reduced data are in a form that can be compared directly with test or other flight data, or utilized as a basis for future test environments. Generally, only digital analysis results are presented here.

The power spectra displays the response of the spacecraft to various portions of the launch phase excitation. Structural responses that occur near the spacecraft instrumentation can be defined in detail. The locations of instrumentation were carefully chosen to describe, most generally, the response of the spacecraft.

The maximum random excitations of both the liftoff and transonic periods are analyzed using this method. Comparing the liftoff plots of B3 (Figs. 22 and 37) the level of the *Mariner III* data is seen to be significantly higher than that of *Mariner IV*. The *Mariner III* experienced the highest overall noise level measured on the spacecraft for both flights. The frequency content of the data is comparable only at some very specific frequencies. The data above 1 kc are similar and are probably the localized response of the spacecraft bus at these frequencies. The liftoff plots of F4 (Figs. 23 and 38) again show the large difference in the liftoff levels. In particular, the response above 800 cps is reasonably similar although the *Mariner III* data are at much higher levels.

The following is an attempt to explain the higher level data on *Mariner III*. If it is assumed that the spacecraft is excited by acoustic sources as discussed in Sec. IV-B, the response levels reflect the excitation levels. The launch pad microphone spectra tend to correlate this difference in excitation levels. The tower microphone spectra (Figs. 26 and 41) show an overall level 6 db higher for *Mariner III*. Ground microphones correlate this also. The "dry" flame bucket and blast wall of launch complex 13 (Fig. 7) could explain the higher excitation noted. This is compared to the "wet" flame bucket of launch complex 12 (Fig. 9) used for *Mariner IV* with the natural attenuation of the water and the direction of the field away from the pad.

Although the response at liftoff was the highest level on *Mariner III*, the maximum overall level of transonic vibration occurred on *Mariner IV*. Figures 48 and 55 show the spectra from B3 at the maximum transonic response. In the range of 700 to 1500 cps, the data are reasonably correlated. Overall excitation of the adapter accelerometer F4 is higher than B3 as shown in Figs. 49 and 56. Between 350 and 1100 cps the F4 spectra are reasonably comparable in shape. In this region the *Mariner III* spectrum level is higher than that of *Mariner IV*. Above 1.5 kc, the *Mariner IV* data become predominant. Transonic excitation is assumed to be transmitted through the adapter. The shroud and the *Agena* vehicle are excitation sources of the adapter. The vibration attenuation of the fiberglass shroud at the higher frequencies may account for the lower levels of *Mariner III* as compared to the magnesium-thorium shroud of *Mariner IV*. The higher levels at these frequencies raise the overall level of transonic vibration much higher for *Mariner IV*.

The vibration induced by the *Agena* engine operation has been analyzed for both down range firing periods. Although the level of the data is significantly lower than any of the previous vibration, some discussion of the constituents in the data seems appropriate. The low levels recorded at location B3 were highly saturated with channel noise and are not presented here. Data exists at location F4 on the adapter for the first burn as shown in Figs. 87 and 88 for both flights. There exist some pronounced quasi-periodic high frequency signals in these plots that are very similar for both flights and are of uncertain origin. They may possibly be in the telemetry system, but nothing at these frequencies is shown in quiet time analyses of these channels. High speed turbo-pumps on the engine could possibly be a mechanical source. The data below 400 cps are invalid because of system noise.

The *Agena* second burn period consists of the same type of periodic signal. For this time period, F4 is shown in Figs. 95 and 96 for both spacecraft. Periodic signals occur again at approximately 950, 1700, and 1900 cps with levels that are lower than the first burn.

D. Shock Spectra

Most transient signals (less than 1 sec in length) were analyzed for frequency content by using shock spectra. The peak values of the transients as well as the frequency peaks were displayed much more accurately than on the oscillogram by using the digital output (Fig. 76 compared with Channel 17 trace in Fig. 74).

Included within this data section are most of the principal staging and other shocks associated with the launch vehicle operation. These excitations form the largest number of flight data observations recorded during the pre-injection phase of the flights. The interest in these data is in the definition of the effective response of the spacecraft due to these vehicle transients. Analysis of the peak frequency content can be useful for test generation or comparison.

The locations presented here are considered sufficient to define the spacecraft response. Data from three positions are presented with a discussion of each. Only those data which had comparable events on both flights are included here as shock spectra. The three positions will be the spacecraft axial measurement (B3), the adapter radial measurement (F1), and one of the adapter torsional measurements (F3). Transducer F4 is not presented here because the shock data from this channel were usually out of lock during these events. Transducer F2 was not included because, in general, this response was very similar to F3.

The booster engine cutoff (BECO) transient was the first significant shock to be analyzed. Figures 59a and 60a display the transient signal from each of the flight transducers. The axial spacecraft measurement B3 is shown as a shock spectrum for both flights in Fig. 61. The low frequency peak that occurs at approximately 70 cps is a known frequency associated with a booster torsional mode. A 120 cps peak is also shown in the figure. The same peaks are evident in Fig. 62 of the radial measurement F1 with the 120 cps showing a higher level. These peaks can be seen in Fig. 63 of the typical tangential accelerometer F3; however the relative difference between the two peaks is diminished. In fact, the *Mariner IV* measurement is a higher level at 70 cps. Also, the F3 measurement seems to indicate a high level peak at a higher frequency (220 cps).

These BECO spectra suggest that the axial and radial excitation seem to be principally a 120 to 130 cps phenomenon whereas the torsional excitation may contain both of the predominant frequencies (70 and 120 cps) as well as a higher mode.

Figures 64 and 65 show the time histories of the sustainer engine cutoff (SECO) shocks. Position B3 shock spectra (Fig. 66) have a frequency peak at approximately 90 cps which may be a mode of the sustainer vehicle. Other peaks are not as clearly defined. The radial and tangential measurements (Figs. 67 and 68) show nearly the same frequency (80 cps) at the highest level. However, secondary frequency peaks seem to exist in these directions at approximately 10 and 250 cps in both measurement directions.

To summarize the SECO spectra, the recorded excitation seems to be more omnidirectional than the BECO shock with a 90 cps peak predominating. Other secondary frequency peaks were measured at the adapter locations in the tangential and radial directions, but the levels were much lower than the 90 cps peak.

The first high frequency pyrotechnic event that was clearly transmitted to the spacecraft was the jettison of the horizon sensor-fairings (VECO occurs simultaneously). A close look at the time traces (Figs. 69 and 70) indicates that these are wide band phenomena. This is confirmed by Fig. 71 of B3 spectra. Both spacecraft measurements seem to have a high level excitation in the 800 to 900 cps range. Figures 72 and 73 show F1 and F3 respectively. These display typical responses of low frequency accelerometers to high frequency excitation. The shock spectra of F1 show a reasonably high level in the 200 cps range for both spacecraft; otherwise the peaks are not clearly defined. The shock spectra of F3 indicate little correspondence between the spacecraft.

The oscillograms of the shroud ejection event are shown in Figs. 74 and 75. It is apparent from these traces that unstable phenomena existed in both channels 10 and 18 (F1 and F4), invalidating these data. The other low frequency channels show a loss of lock indication, making these data questionable also. However, B3 recorded the spacecraft response to this excitation. This is also a wide band event as shown in Fig. 77 including the inherent telemetry system roll-off at higher frequencies. There seems to be a corresponding peak near 2 kc for both spacecraft.

The *Atlas-Agena* separation events are displayed in Figs. 78 and 79. All channels except B3 were questionable

for reasons similar to the previous discussion. Response of B3 to this excitation (Fig. 81) seems to be similar in level to the previous shock with the exception of a more clearly defined peak near 900 cps for both spacecraft.

The responses due to the squib firing associated with the first *Agena* engine ignition are shown in Figs. 82 and 83. Figure 82 contains some of the shock anomalies in the *Mariner III* flight. These will not be discussed here. The only shock comparable with *Mariner IV* occurred at GMT 1928: 19.89 (shown on the oscillogram time code). Only the shock spectra from B3 and F4 are presented here. In Fig. 84 the B3 spectra are shown with a reasonably comparable peak at about 1 kc. This is a lower level than the previous two pyrotechnically induced shocks. In Fig. 85 the F4 spectra are shown to compare the spectra levels with B3, which has similar frequency content.

E. Data Compression

The principal use of data compression programs is to reorganize the data into a concise and usable form for direct comparison or application.

The ratio of B3/F4 is a typically useful result of this program. This ratio presents the difference in (db) levels between the high frequency transducers on the spacecraft and the adapter. The interest in these data is in the interpretation of the source of excitation. Figures 24 and 39 display this ratio for the maximum *liftoff* excitation of both spacecraft. The frequency content under 1 kc is reasonably similar with a much larger variance in the *Mariner III* data. In this range the overall level of the *Mariner III* is higher than that of the other spacecraft. Above 1 kc the average level of the *Mariner IV* data seems to be higher, which could be explained by an assumption of higher transmissibility of the metal shroud in this range. The frequency content in this range is not very similar. Figures 50 and 57 show this ratio for the *transonic* periods of *Mariner III* and *IV* respectively. There is a much closer correlation of these levels above 700 cps. This suggests that the transonic sources of excitation may be very similar in these ranges even though the ASD levels of each transducer may be very different between spacecraft. Below 700 cps a larger difference in the levels and frequency content develops with little correlation suggested.

Another ratio that is very descriptive of a specific phenomenon is a high frequency accelerometer relative to the launch pad microphones. This ("acoustic acceptance") describes a relationship between the acoustic excitation

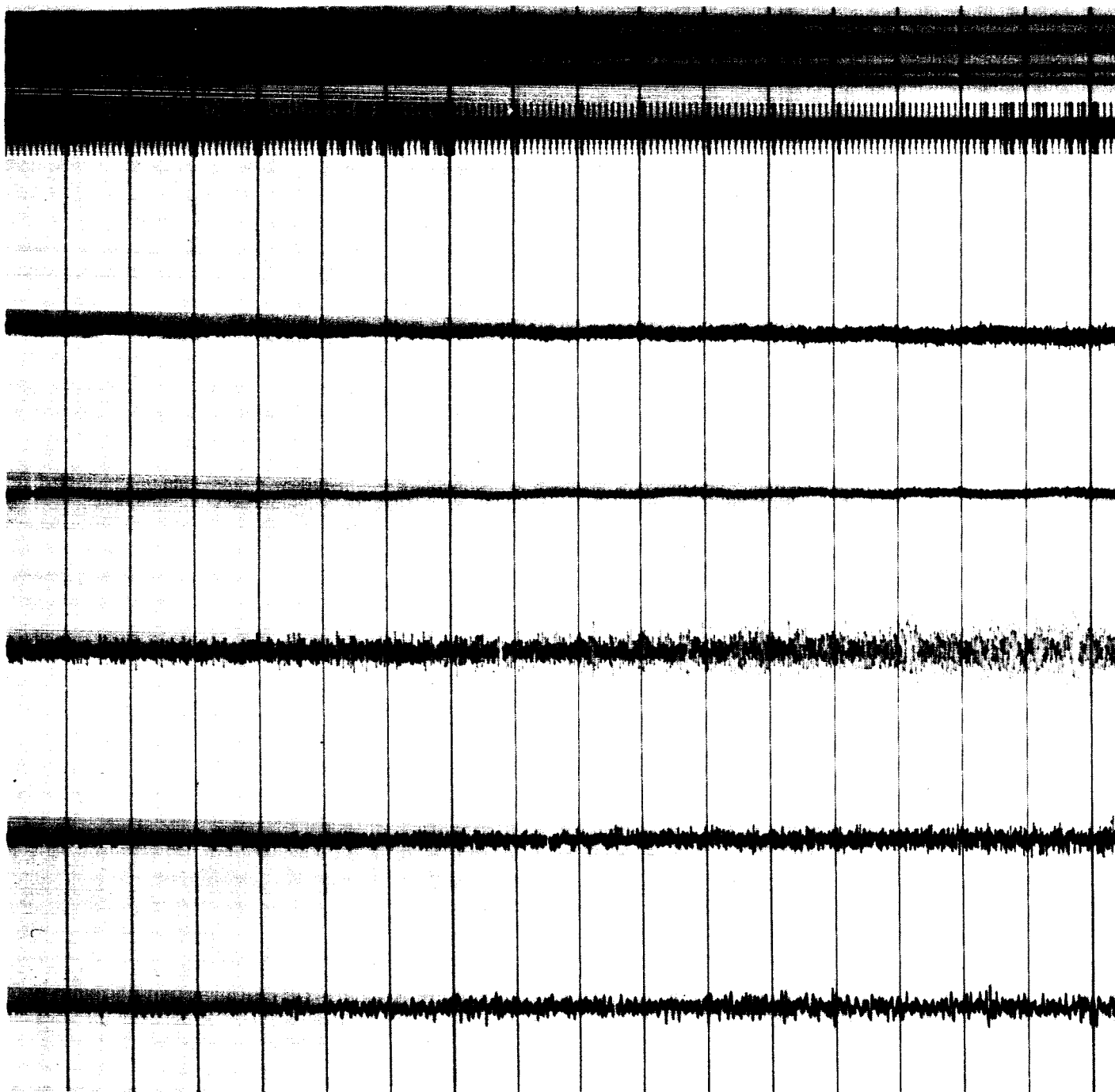
and the spacecraft response as a function of frequency. Figures 27 and 42 show the ratio between B3 and the mean of the umbilical tower microphones for each flight. The frequency content of the data above 1 kc is reasonably correlated but the level of the *Mariner IV* data is much higher. This level difference could be explained by the assumed high transmissibility of the metal shroud at these higher frequencies. This same discussion applies to Figs. 28 and 43 displaying the ratio between F4 and the same microphones.

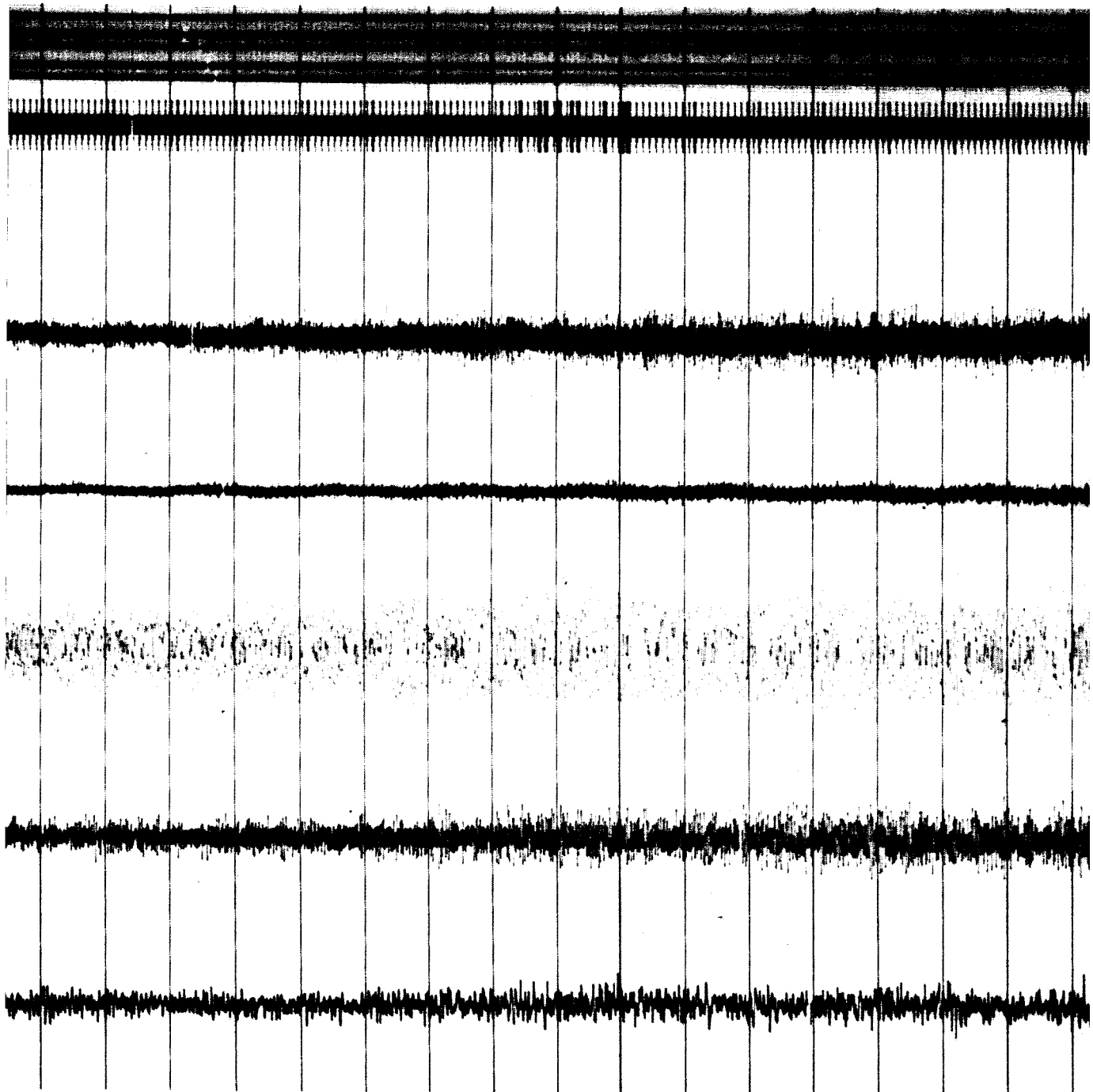
The composite plot capability of the program has been utilized to show comparisons between the principal shock spectra that have been presented. In each case the shock spectra from both flights have been plotted on the same plot for direct comparison as in Fig. 62.

Maximum and minimum envelopes were calculated for all the shocks of both flights. This shows the maximum variance of the shock data. The composite plot of these envelopes is shown in Fig. 101.

V. DATA

This section is arranged in the chronological sequence in which the events occurred in the launch phase. The oscillograms exhibit the real time signals of each event. Immediately following each oscillogram can be found a more detailed analysis of that event utilizing the appropriate analysis techniques. The plots have been ordered on each page to simplify comparison of *Mariner III* and *IV* data as much as possible. Flight data are compared with ground test data in Ref. 4.

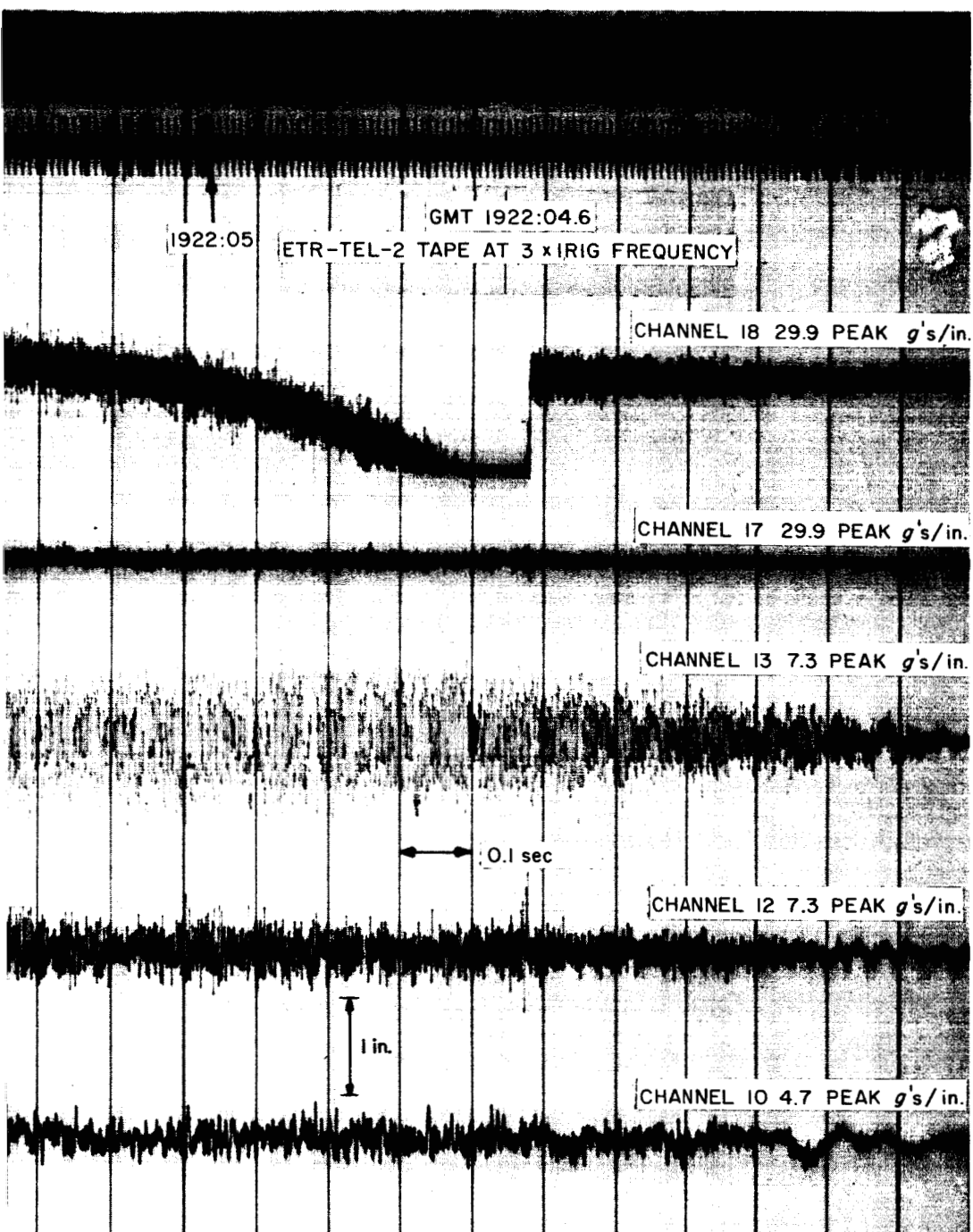


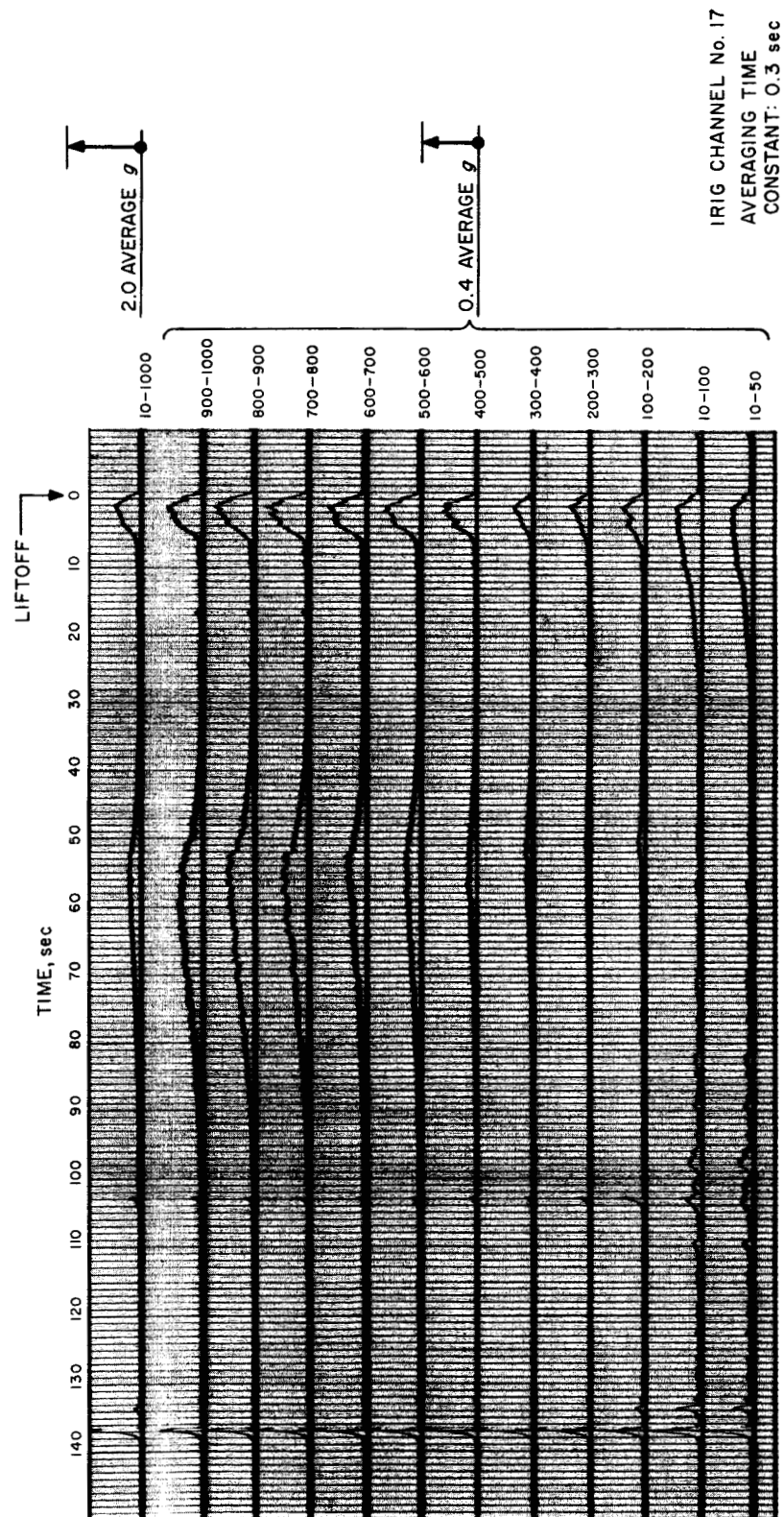


1922:08

1922:06

24-1

Fig. 14. Oscillogram, *Mariner III* liftoff, all channels

Fig. 15. Band pass, *Mariner III* liftoff and transonic, B3 low frequency

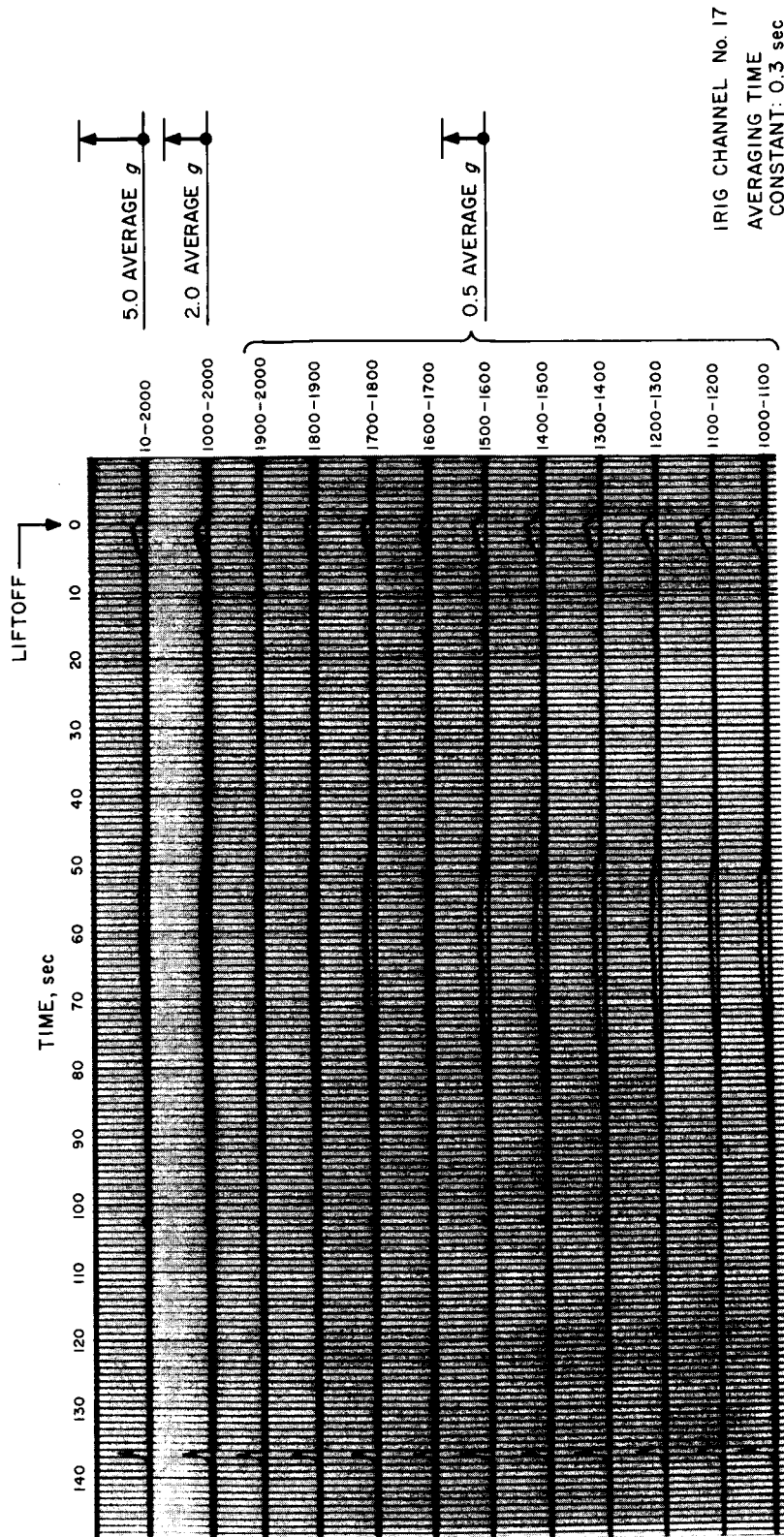


Fig. 16. Band pass, Mariner III liftoff and transonic, B3 high frequency

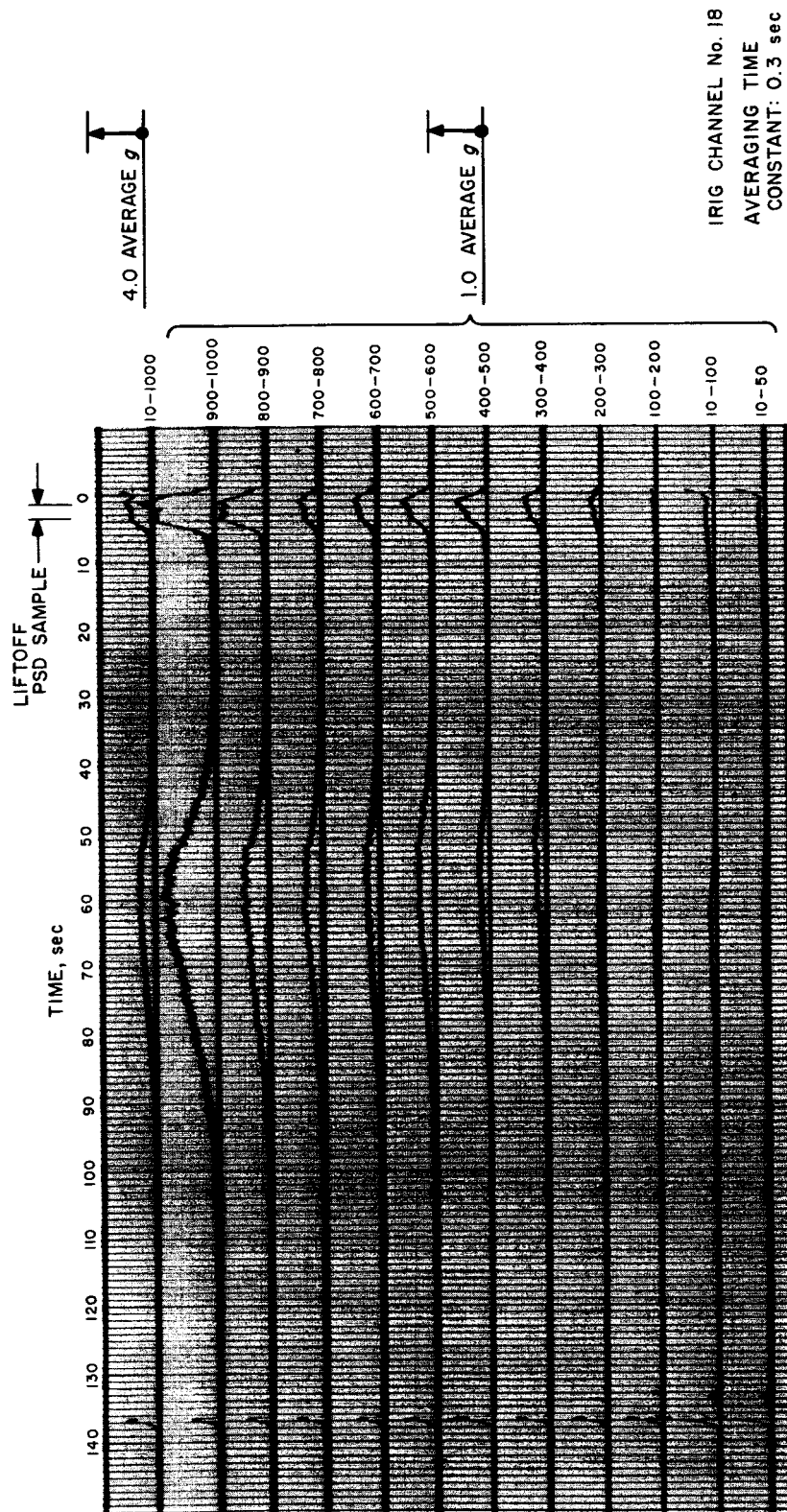


Fig. 17. Band pass, *Mariner III* lift-off and transonic, F4 low frequency

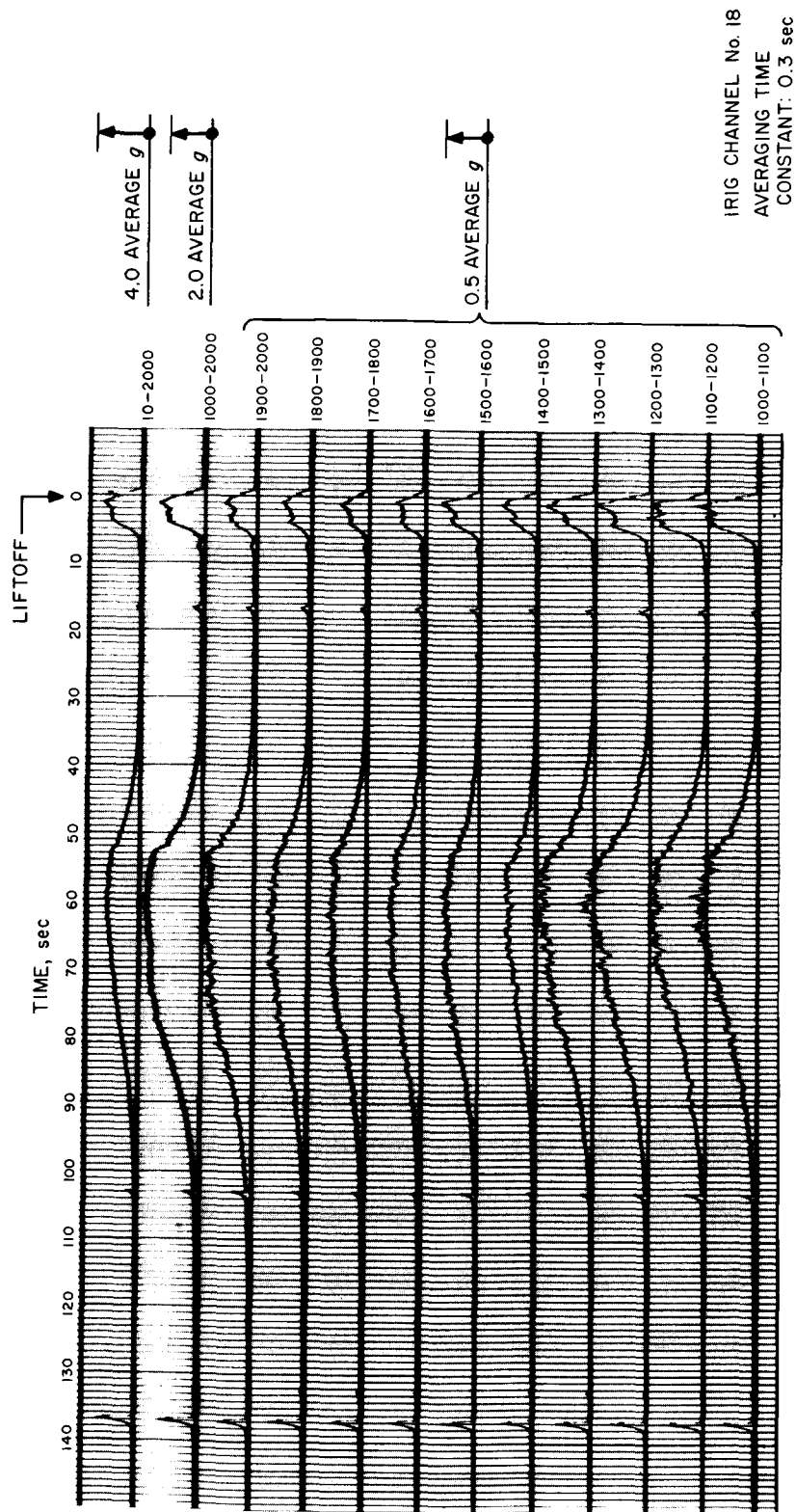


Fig. 18. Band pass, Mariner III liftoff and transonic, F4 high frequency

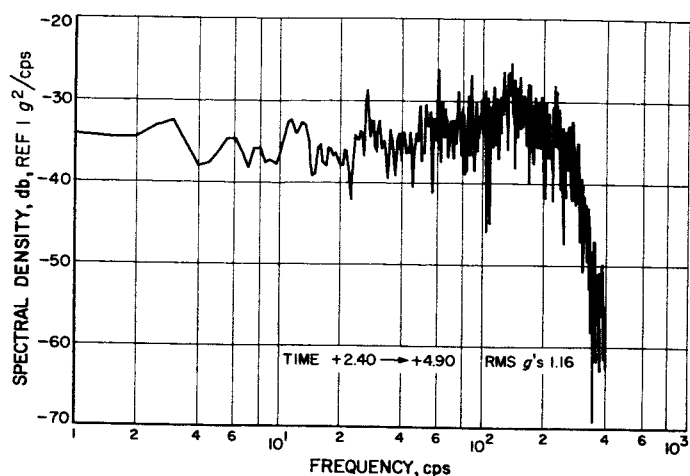


Fig. 19. Acceleration spectral density, Mariner III liftoff, F1

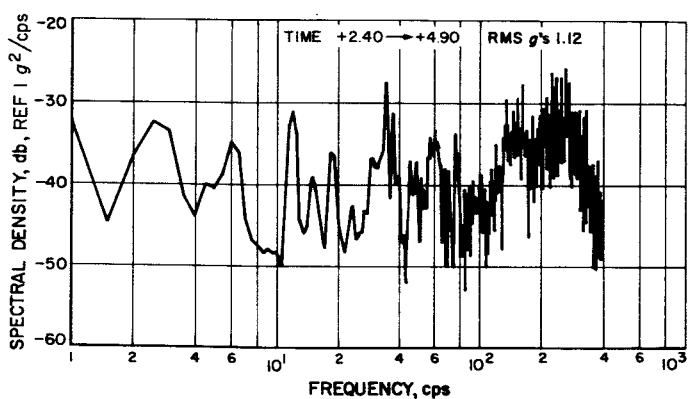


Fig. 20. Acceleration spectral density, Mariner III liftoff, F3

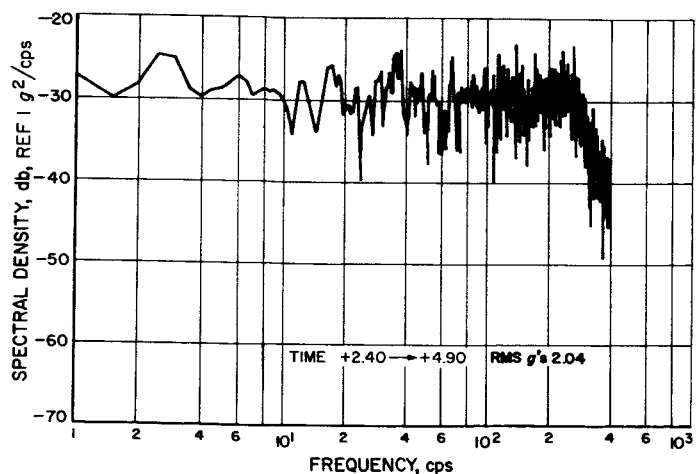


Fig. 21. Acceleration spectral density, Mariner III liftoff, F2

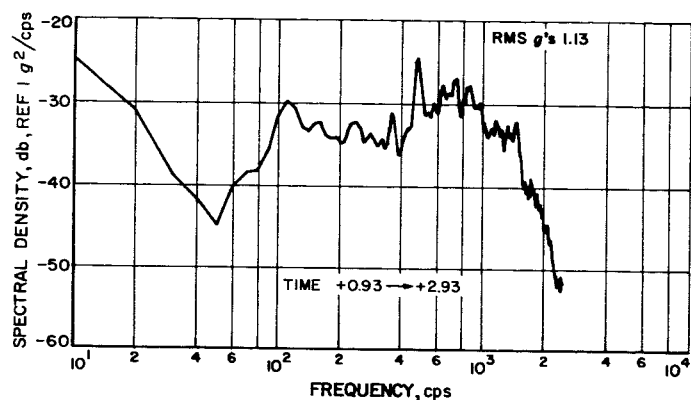


Fig. 22. Acceleration spectral density, Mariner III liftoff, B3

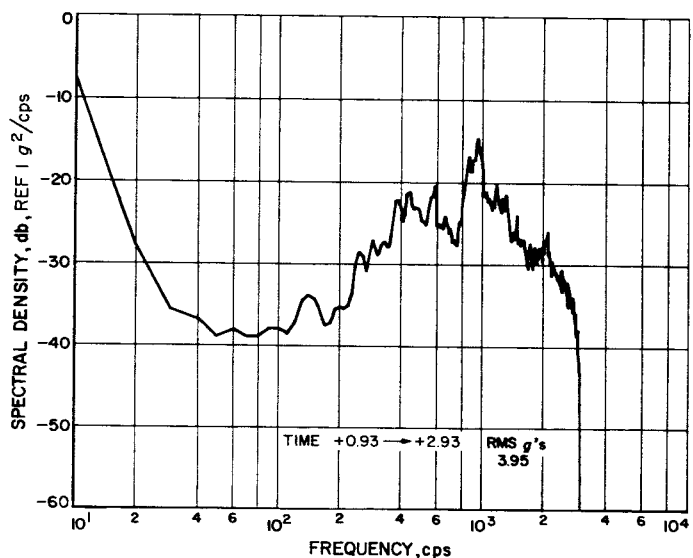


Fig. 23. Acceleration spectral density, Mariner III liftoff, F4

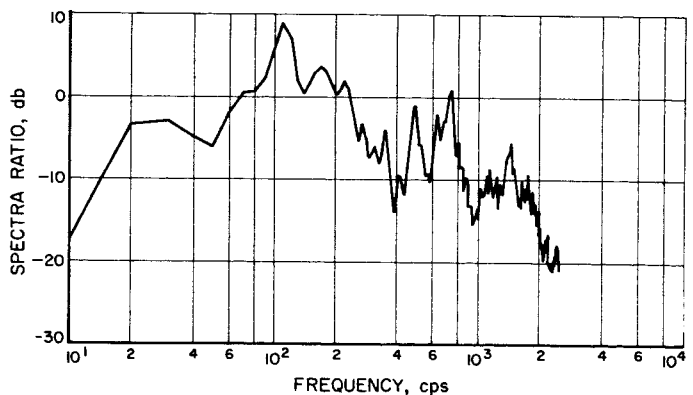


Fig. 24. Spectra ratio, Mariner III liftoff, B3/F4

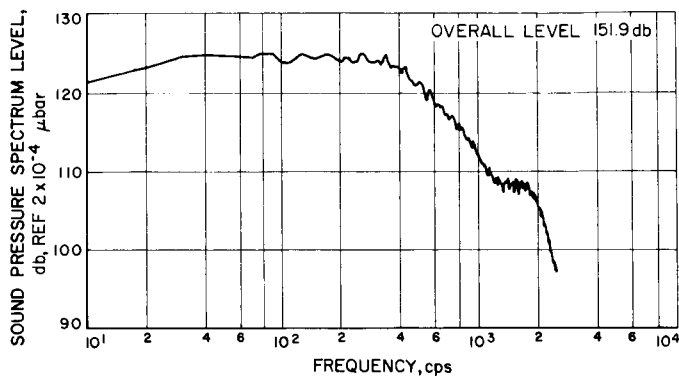


Fig. 25. Sound pressure spectrum level, *Mariner III* liftoff, M1, M2

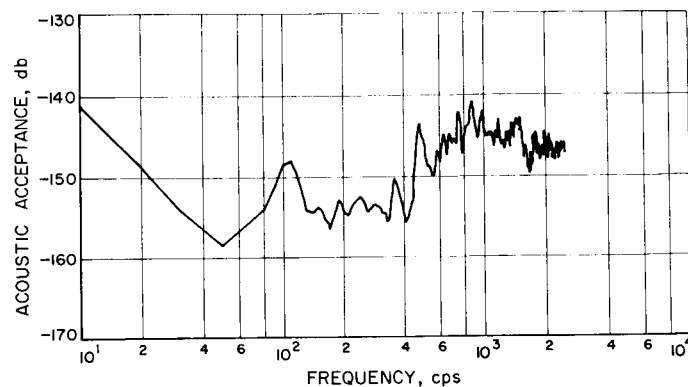


Fig. 27. Acoustic acceptance, *Mariner III* liftoff, B3/M3, M4

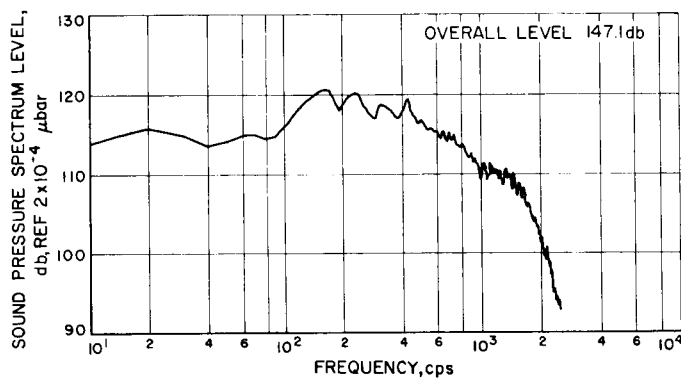


Fig. 26. Sound pressure spectrum level, *Mariner III* liftoff, M3, M4

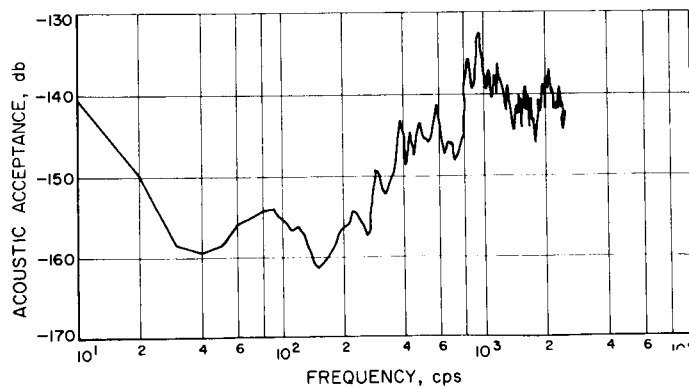
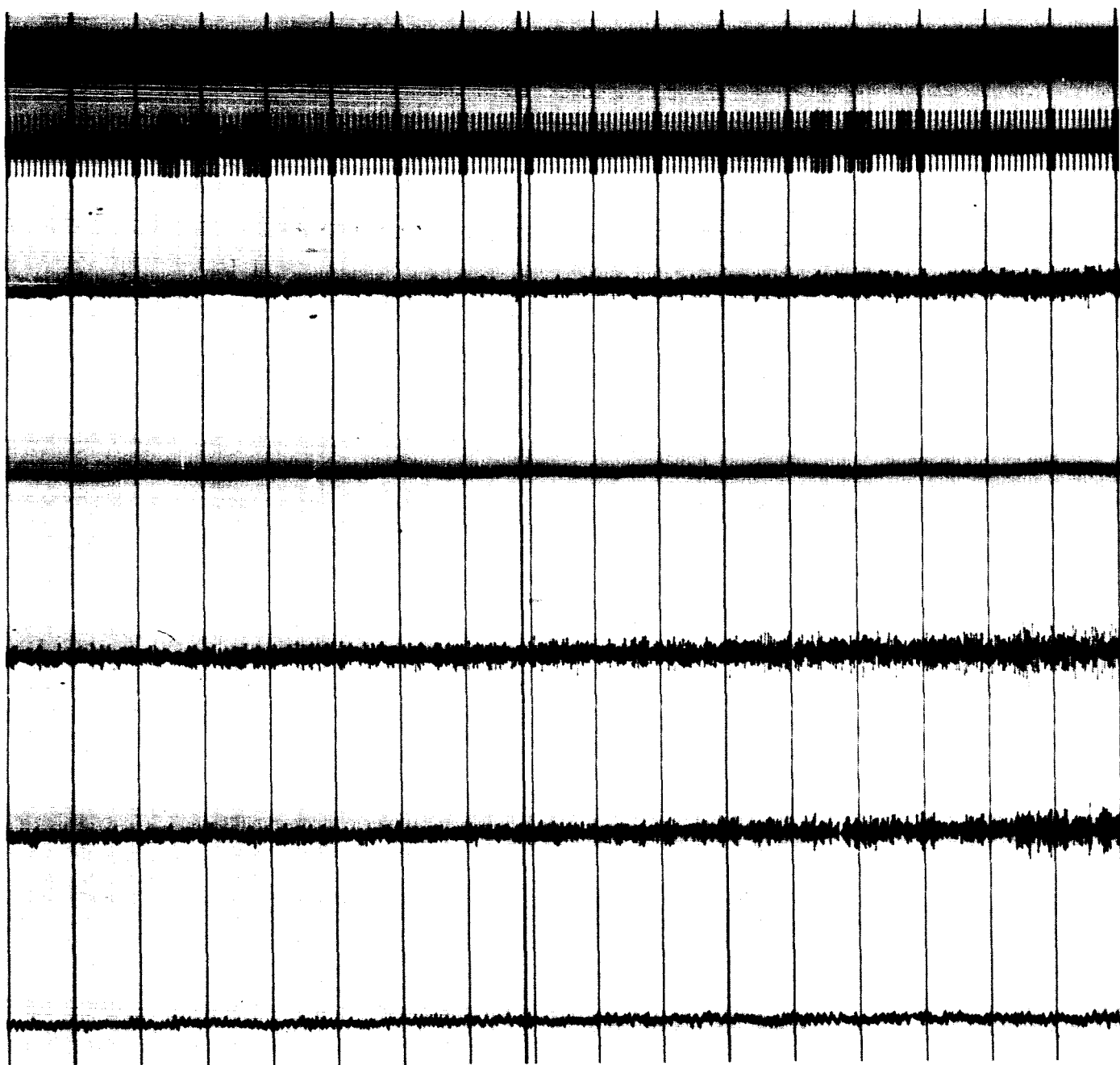
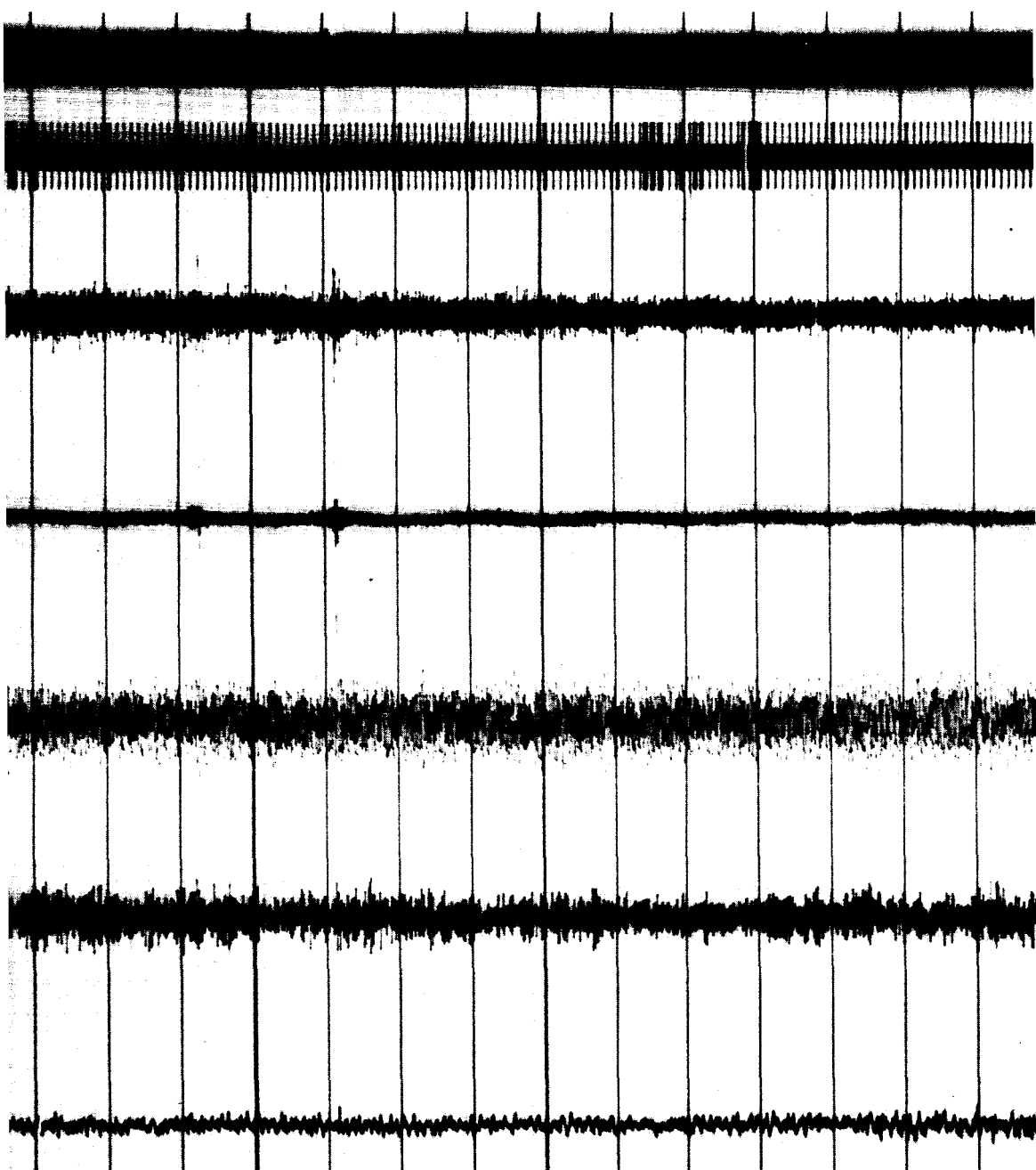


Fig. 28. Acoustic acceptance, *Mariner III* liftoff, F4/M3, M4

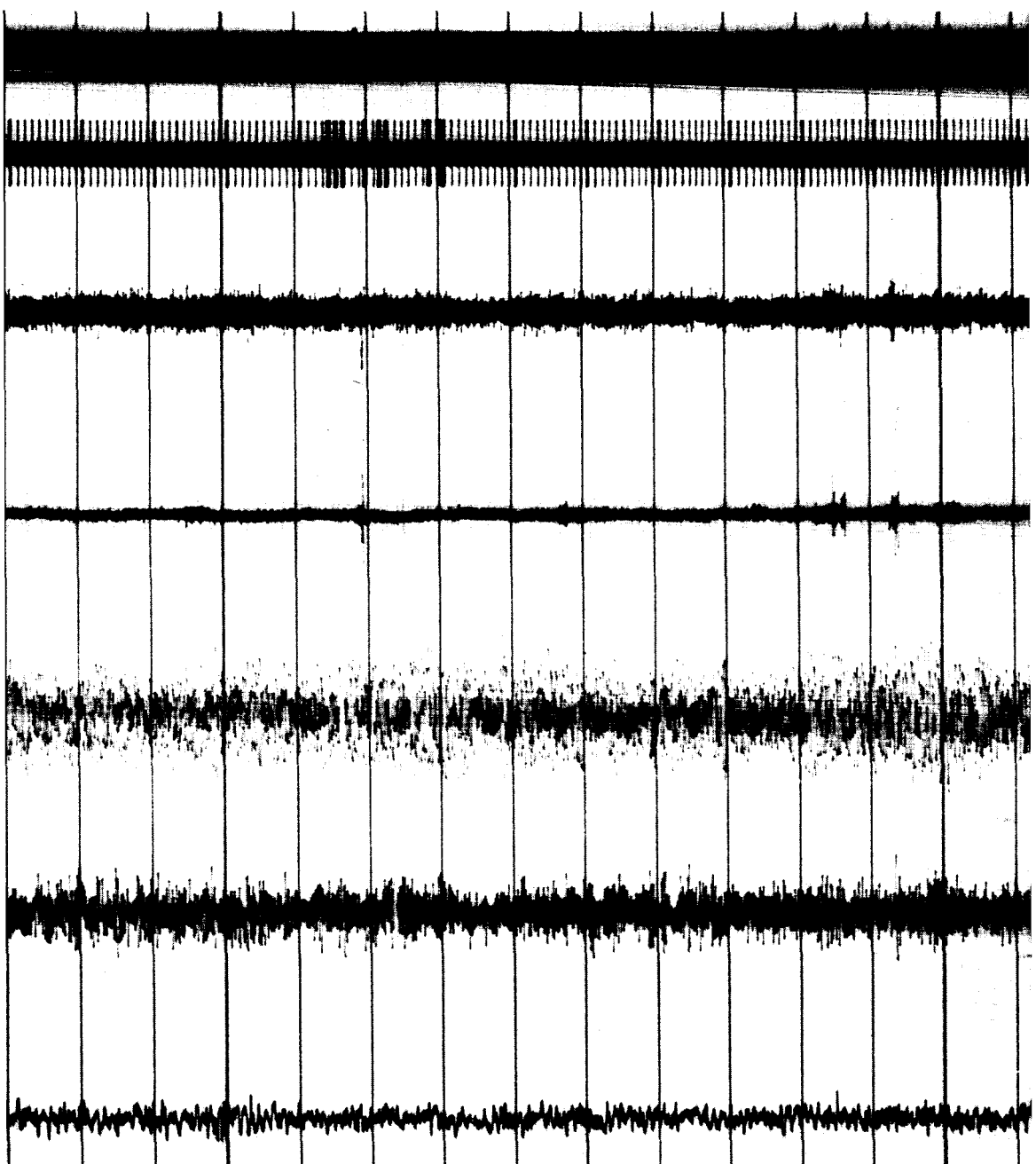


31-1

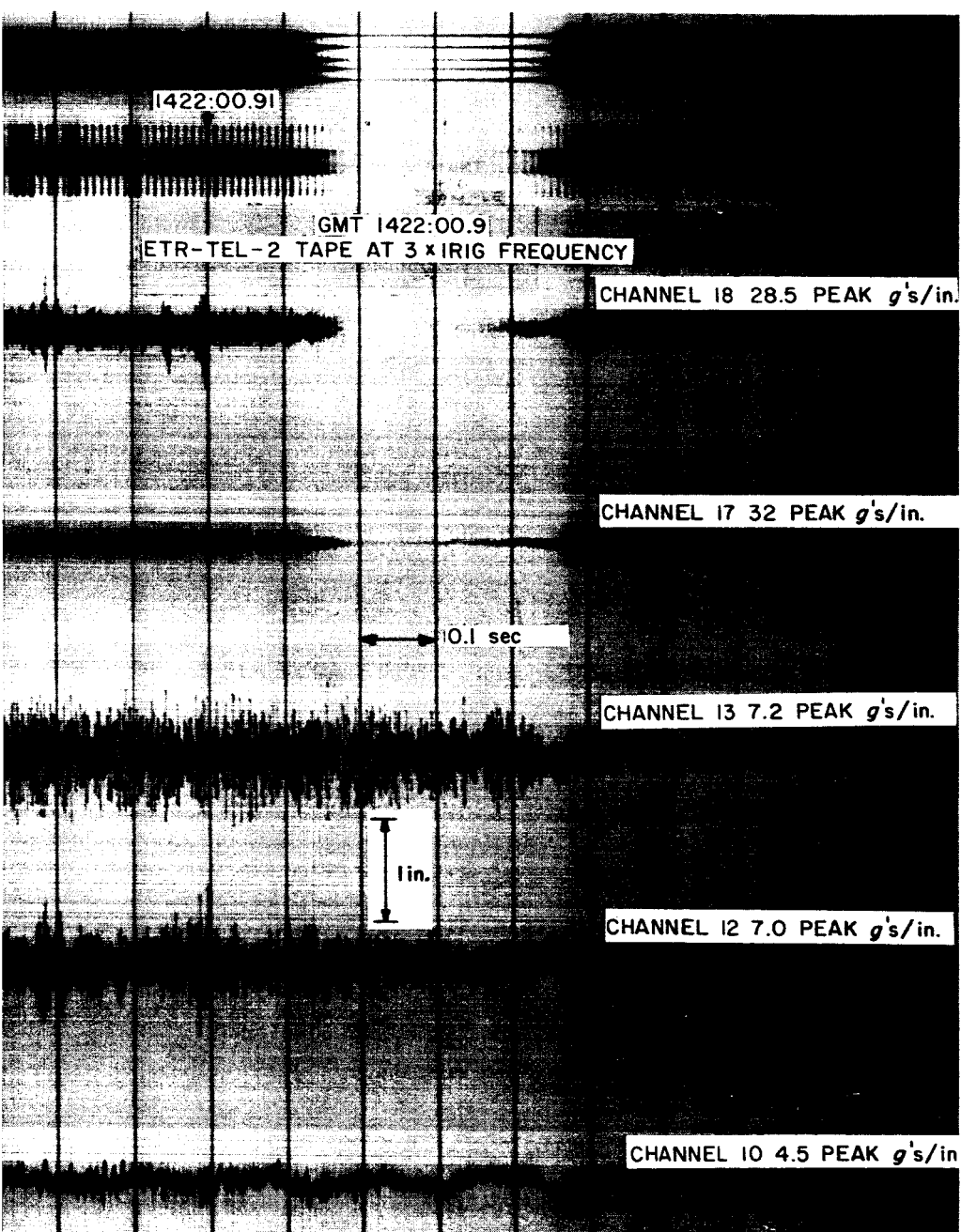
1422:05.0



32-1



32-2

Fig. 29. Oscillogram, *Mariner IV* liftoff, all channels

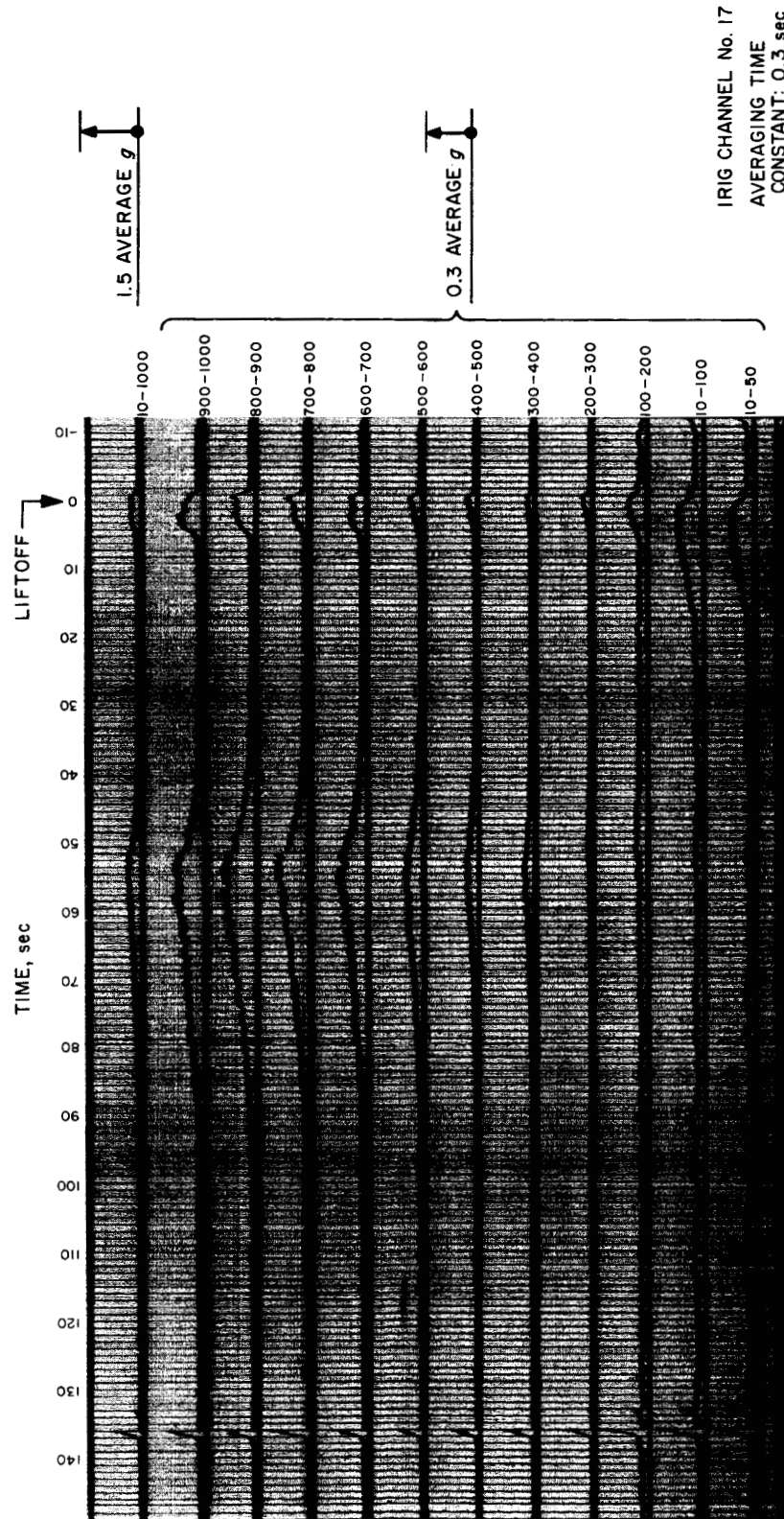


Fig. 30. Band pass, Mariner IV liftoff and transonic, B3 low frequency

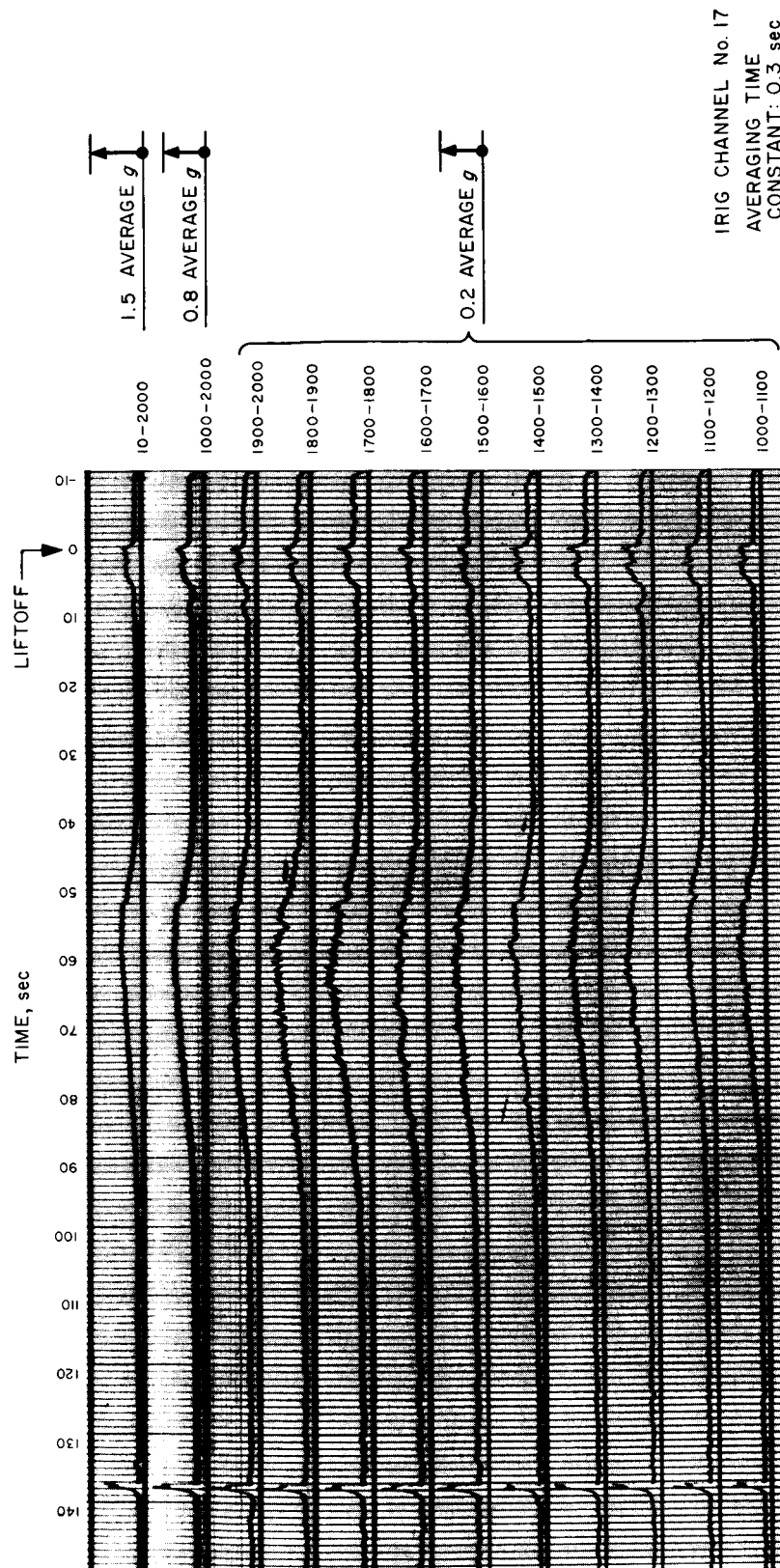


Fig. 31. Band pass, Mariner IV liftoff and transonic, B3 high frequency

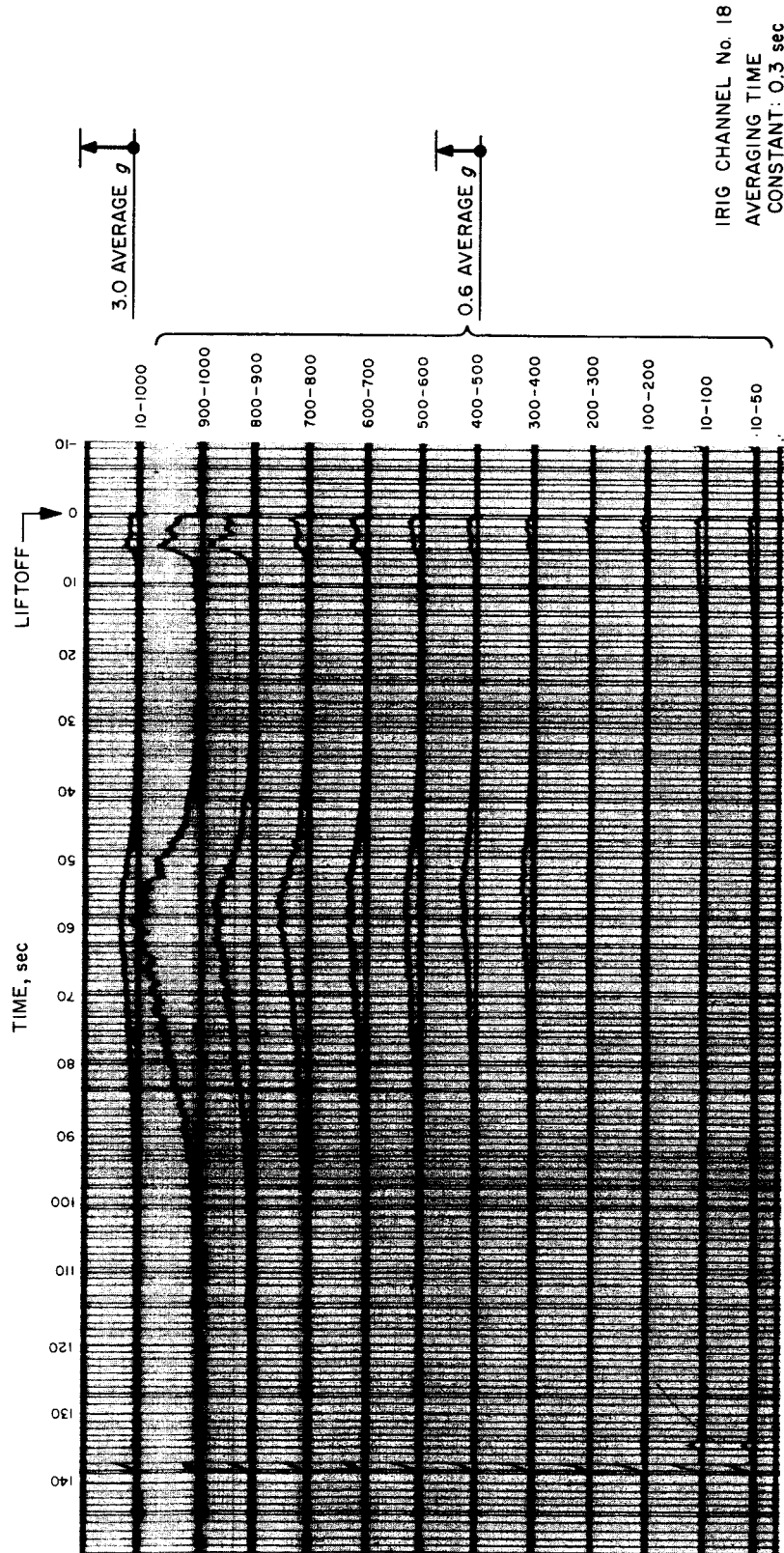


Fig. 32. Band pass, Mariner IV lift-off and transonic, F4 low frequency

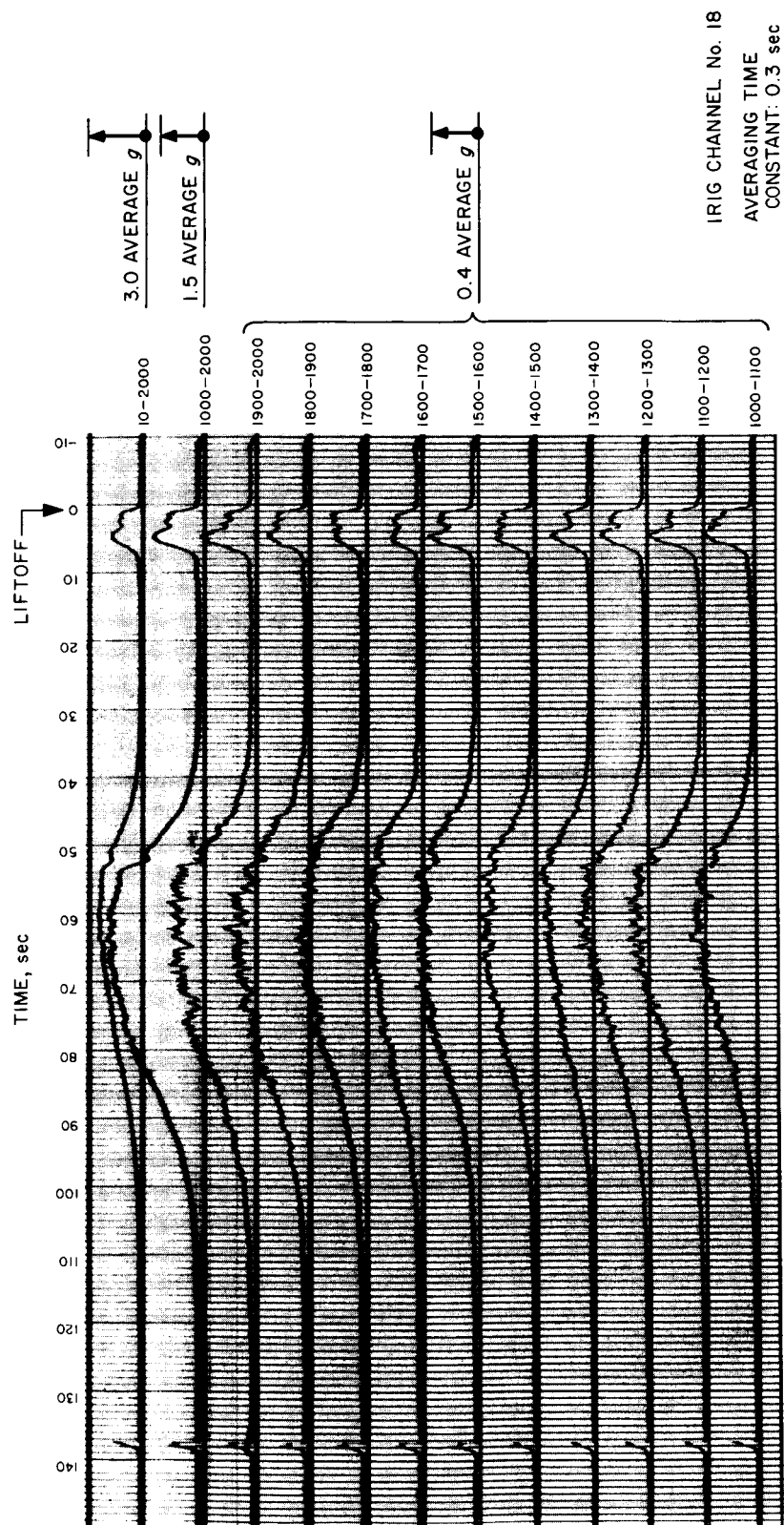


Fig. 33. Band pass, Mariner IV lift-off and transonic, F4 high frequency

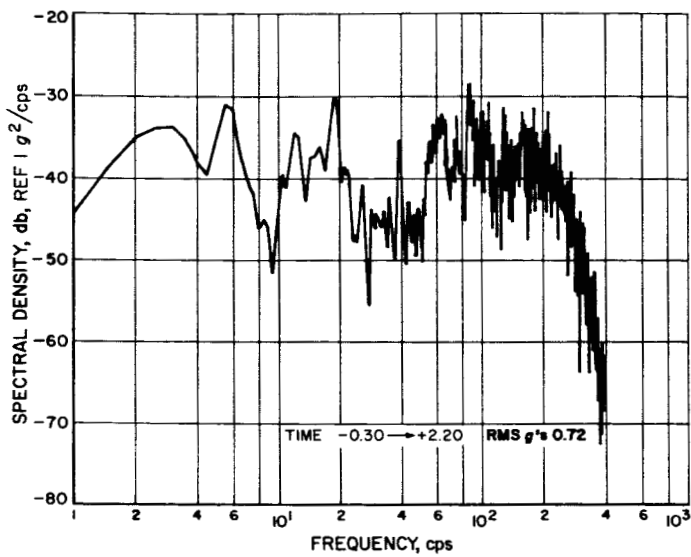


Fig. 34. Acceleration spectral density, Mariner IV liftoff, F1

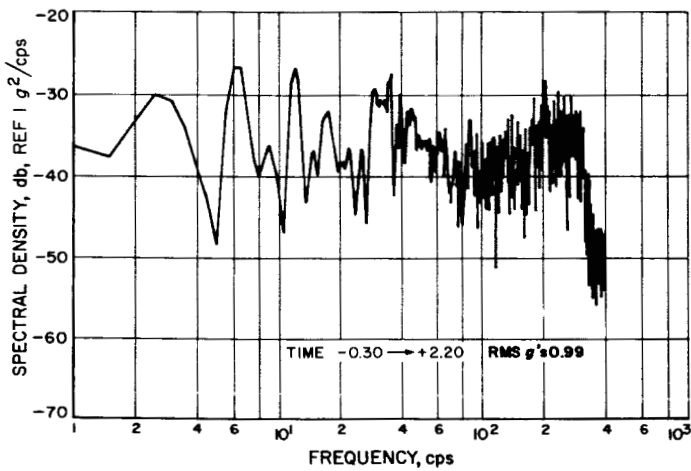


Fig. 35. Acceleration spectral density, Mariner IV liftoff, F3

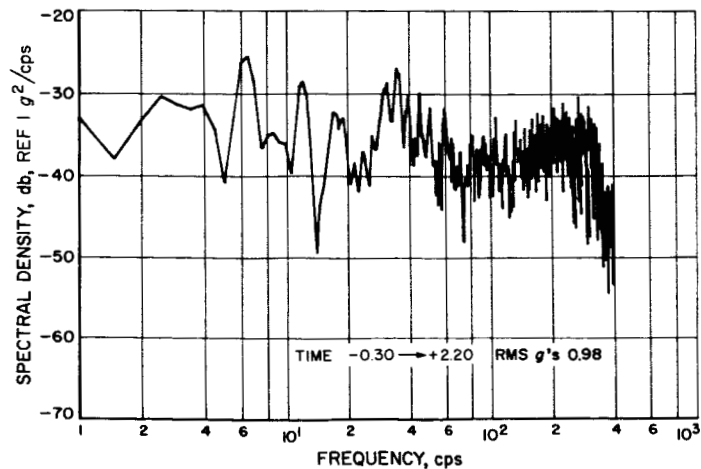


Fig. 36. Acceleration spectral density, Mariner IV liftoff, F2

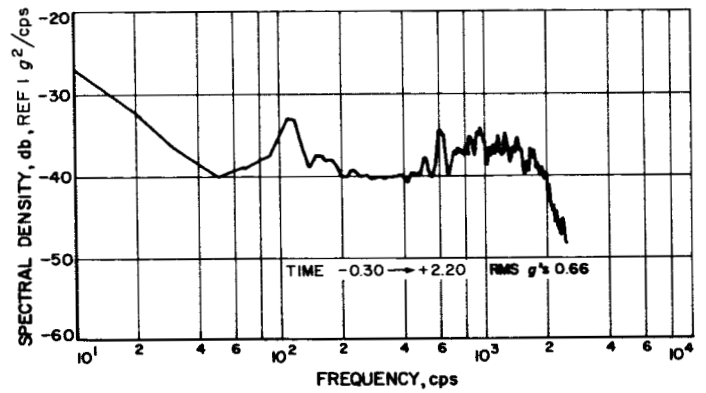


Fig. 37. Acceleration spectral density, Mariner IV liftoff, B3

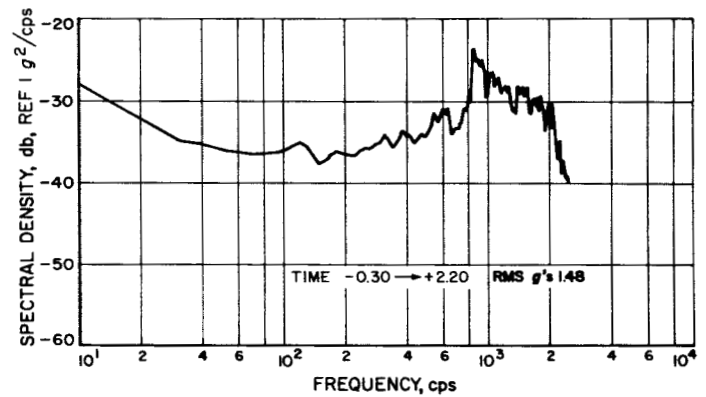


Fig. 38. Acceleration spectral density, Mariner IV liftoff, F4

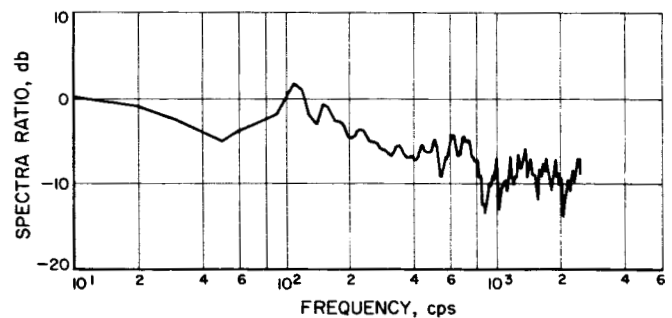


Fig. 39. Spectra ratio, Mariner IV liftoff, B3/F4

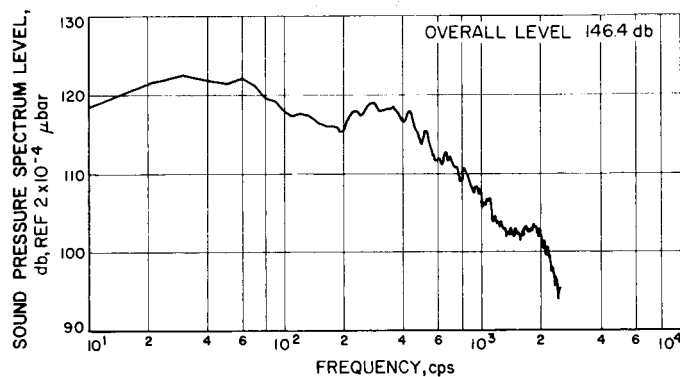


Fig. 40. Sound pressure spectrum level, Mariner IV liftoff, M5, M6

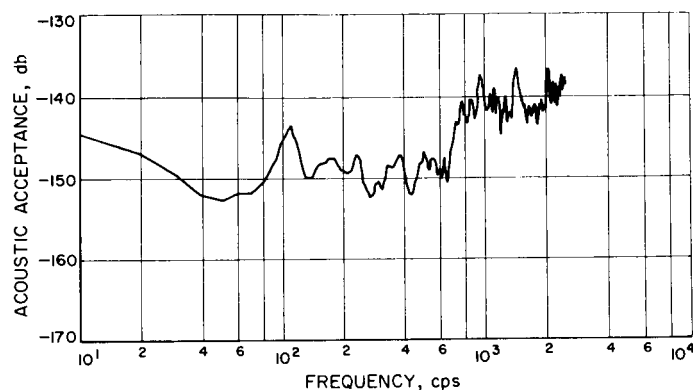


Fig. 42. Acoustic acceptance, Mariner IV liftoff, B3/M7, M8

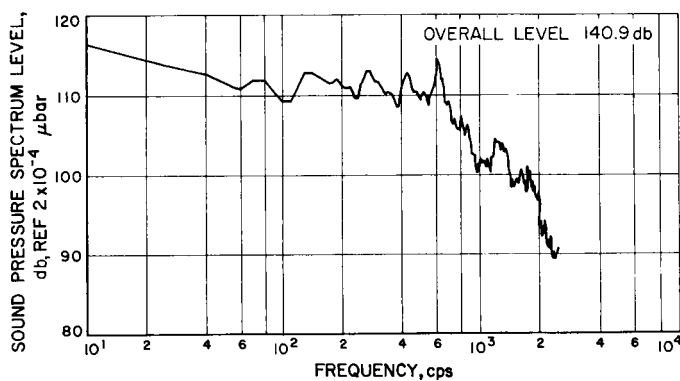


Fig. 41. Sound pressure spectrum level, Mariner IV liftoff, M7, M8

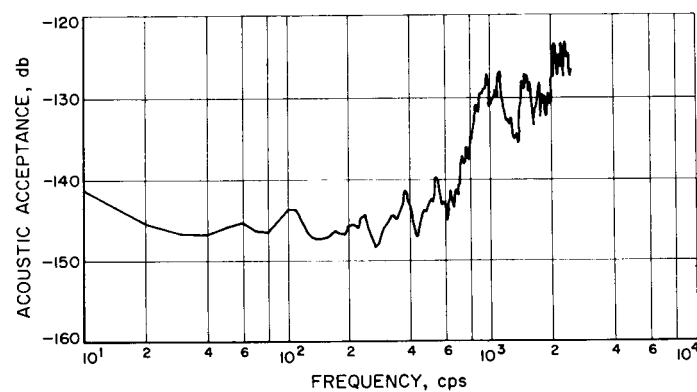


Fig. 43. Acoustic acceptance, Mariner IV liftoff, F4/M7, M8

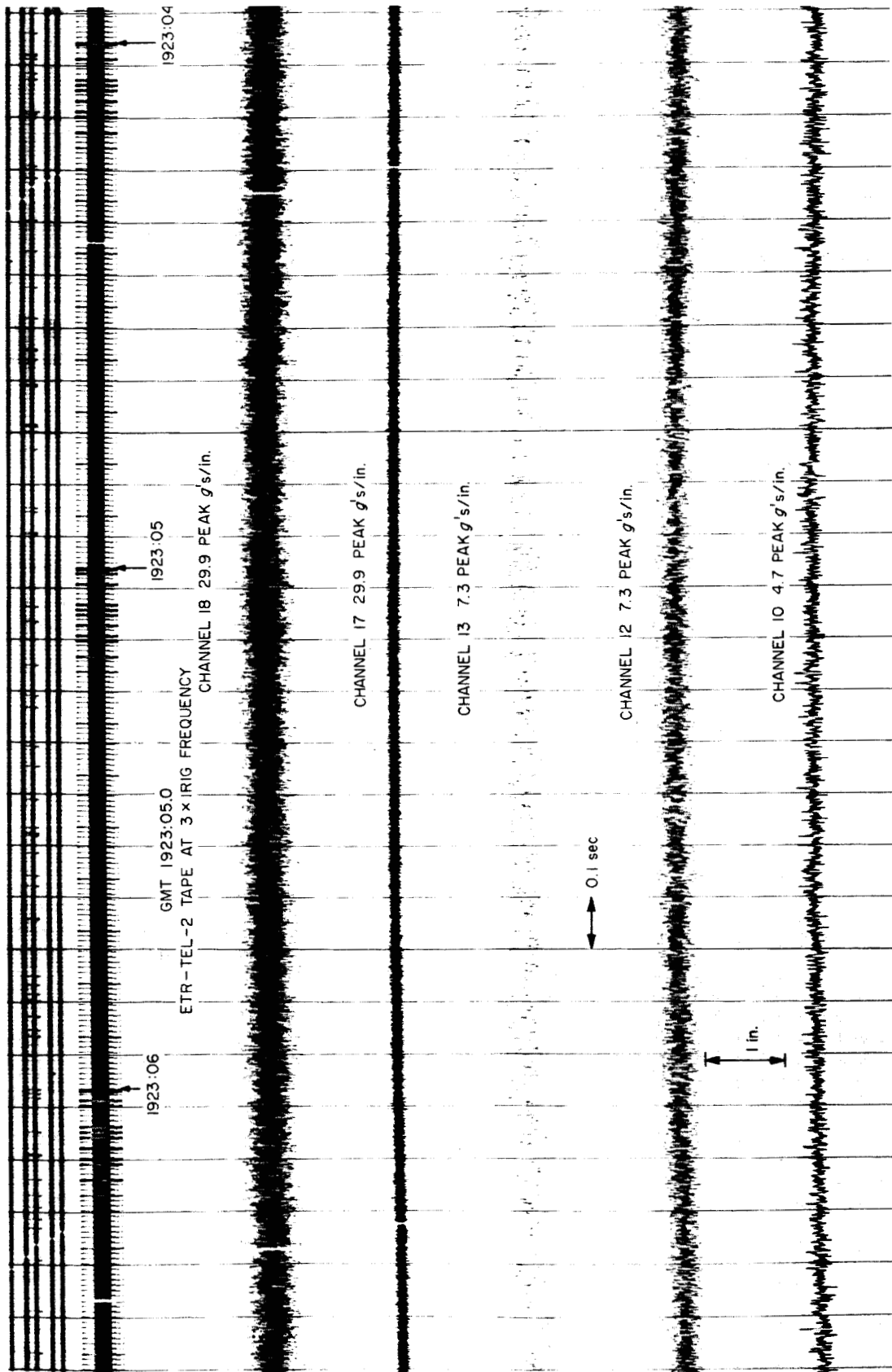


Fig. 44. Oscillogram, Mariner III transonic, all channels

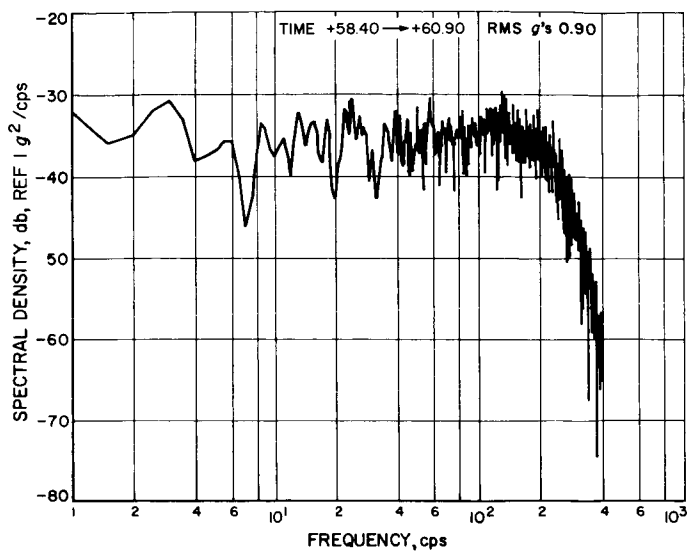


Fig. 45. Acceleration spectral density, Mariner III transonic, F1

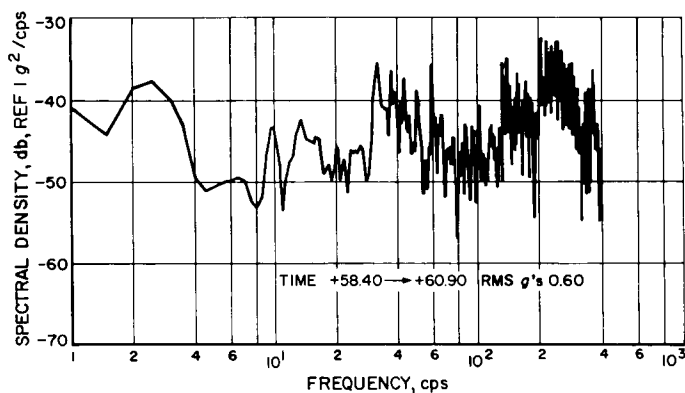


Fig. 46. Acceleration spectral density, Mariner III transonic, F3

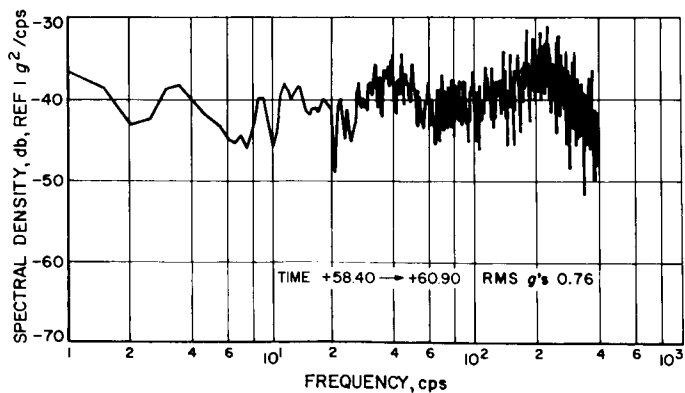


Fig. 47. Acceleration spectral density, Mariner III transonic, F2

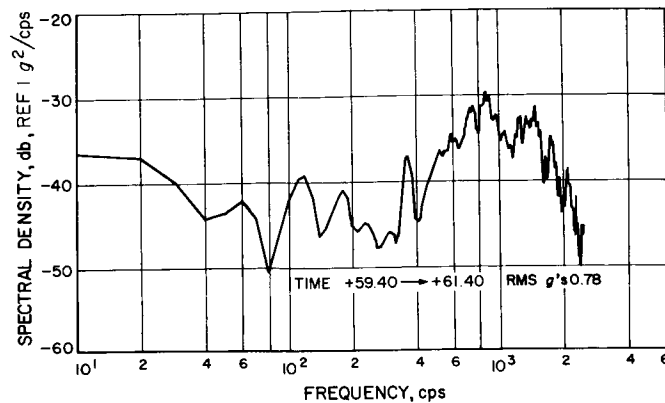


Fig. 48. Acceleration spectral density, Mariner III transonic, B3

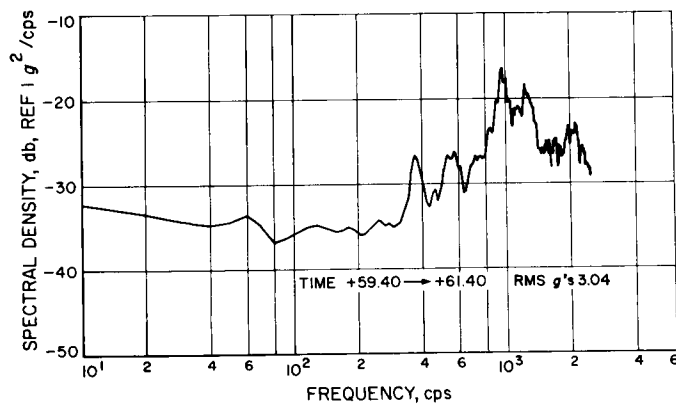


Fig. 49. Acceleration spectral density, Mariner III transonic, F4

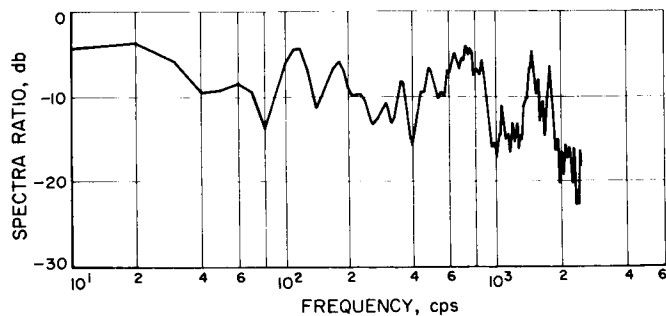


Fig. 50. Spectra ratio, Mariner III transonic, B3/F4

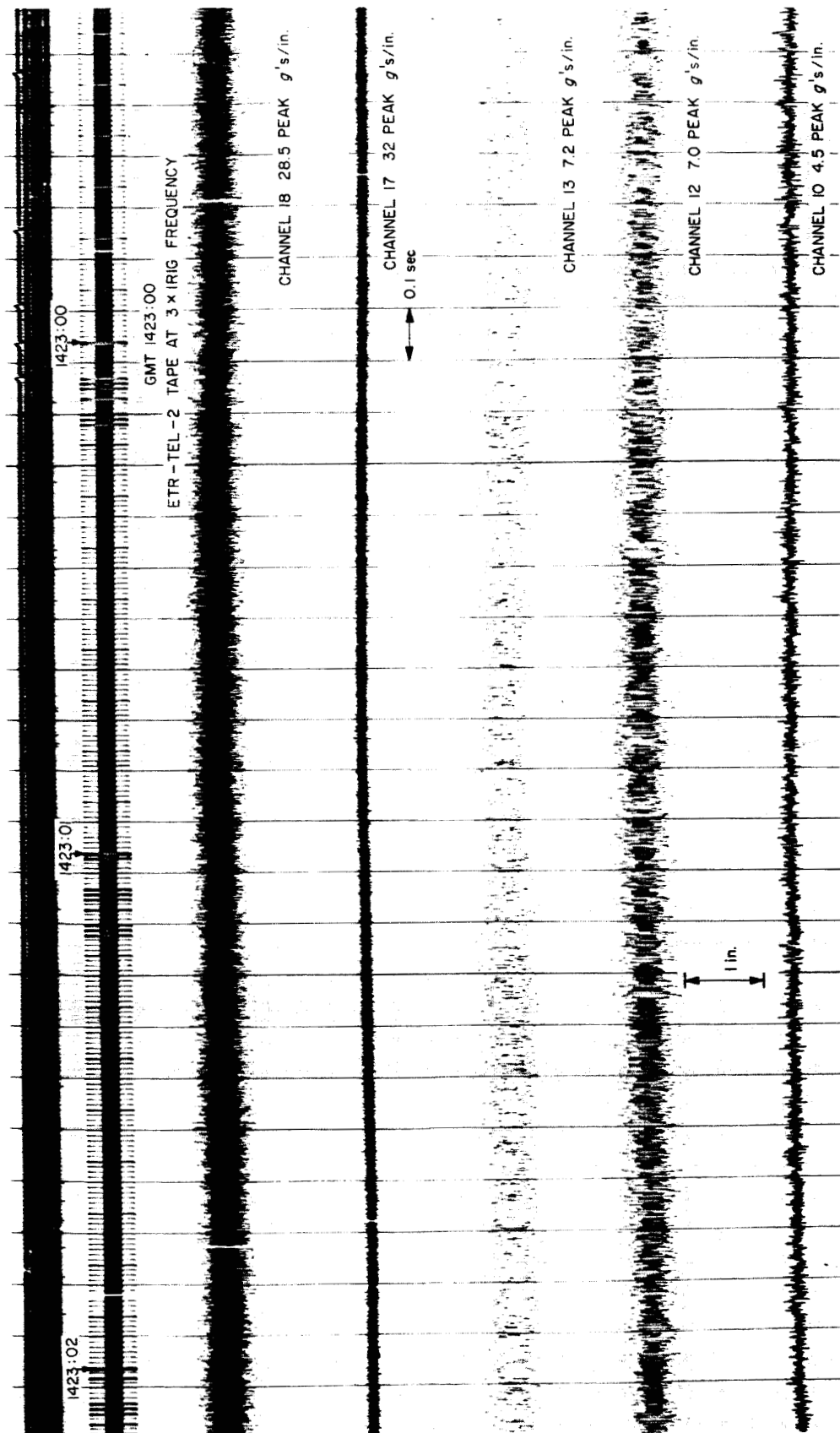


Fig. 51. Oscillogram, Mariner IV transonic, all channels

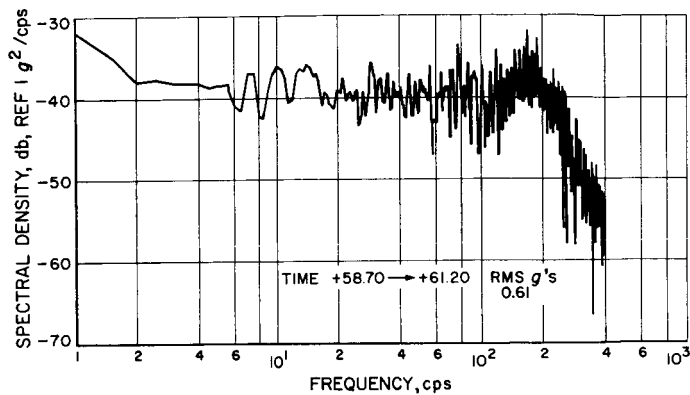


Fig. 52. Acceleration spectral density, Mariner IV transonic, F1

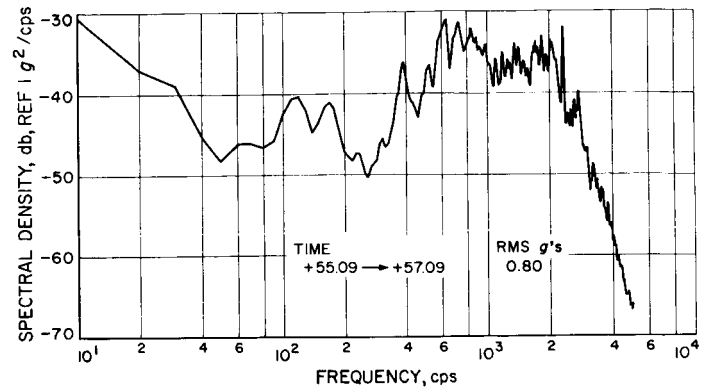


Fig. 55. Acceleration spectral density, Mariner IV transonic, B3

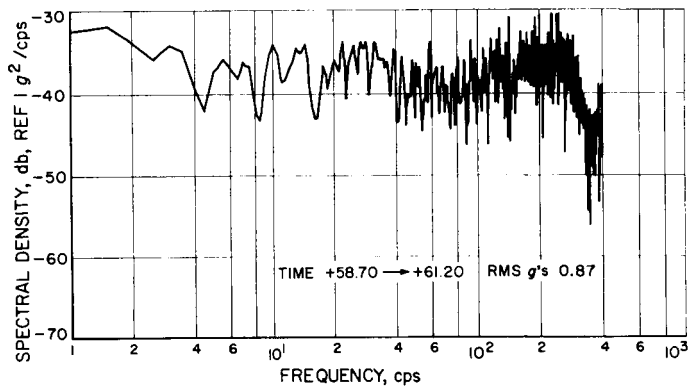


Fig. 53. Acceleration spectral density, Mariner IV transonic, F3

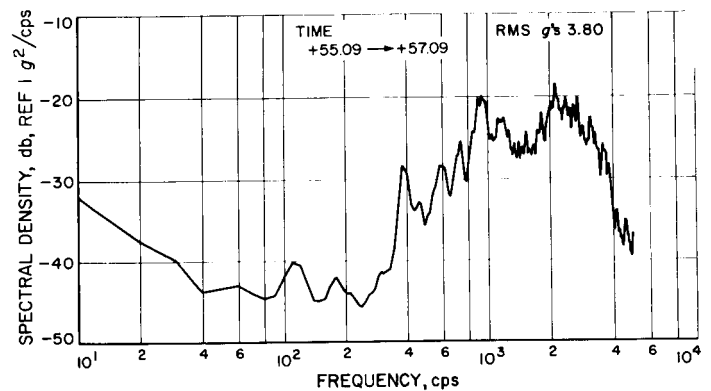


Fig. 56. Acceleration spectral density, Mariner IV transonic, F4

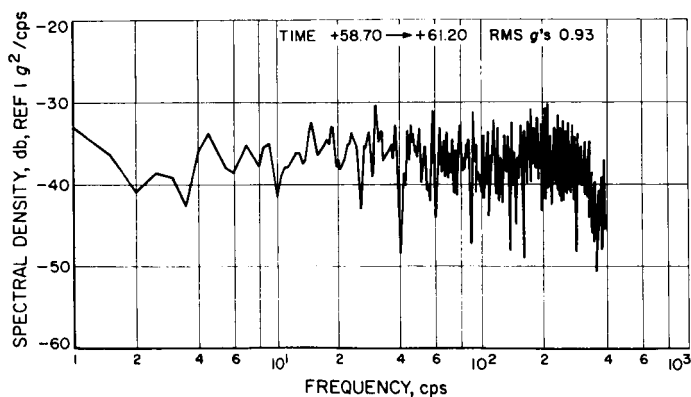


Fig. 54. Acceleration spectral density, Mariner IV transonic, F2

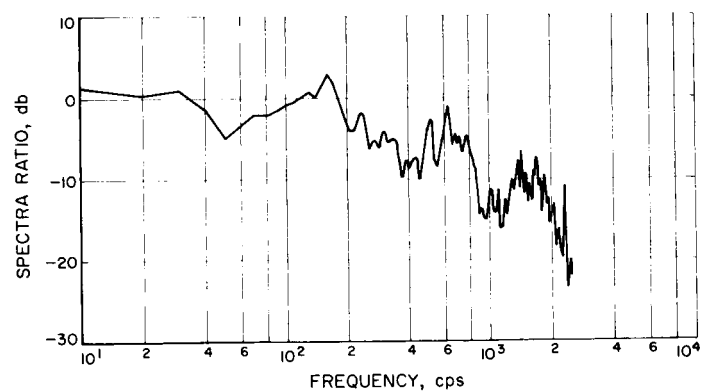


Fig. 57. Spectra ratio, Mariner IV transonic, B3/F4

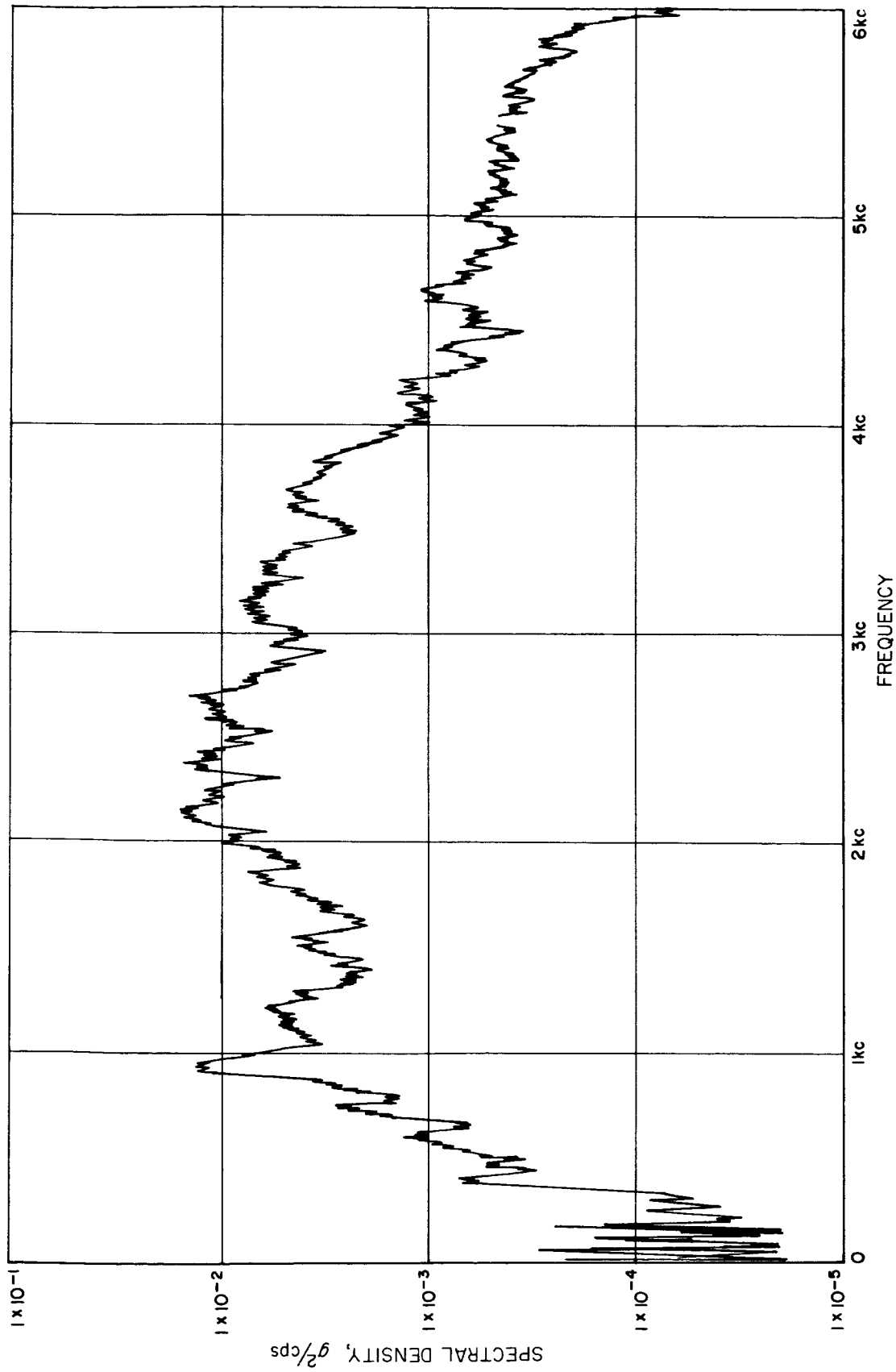


Fig. 58. Acceleration spectral density, Mariner IV transonic, F4 (analog)

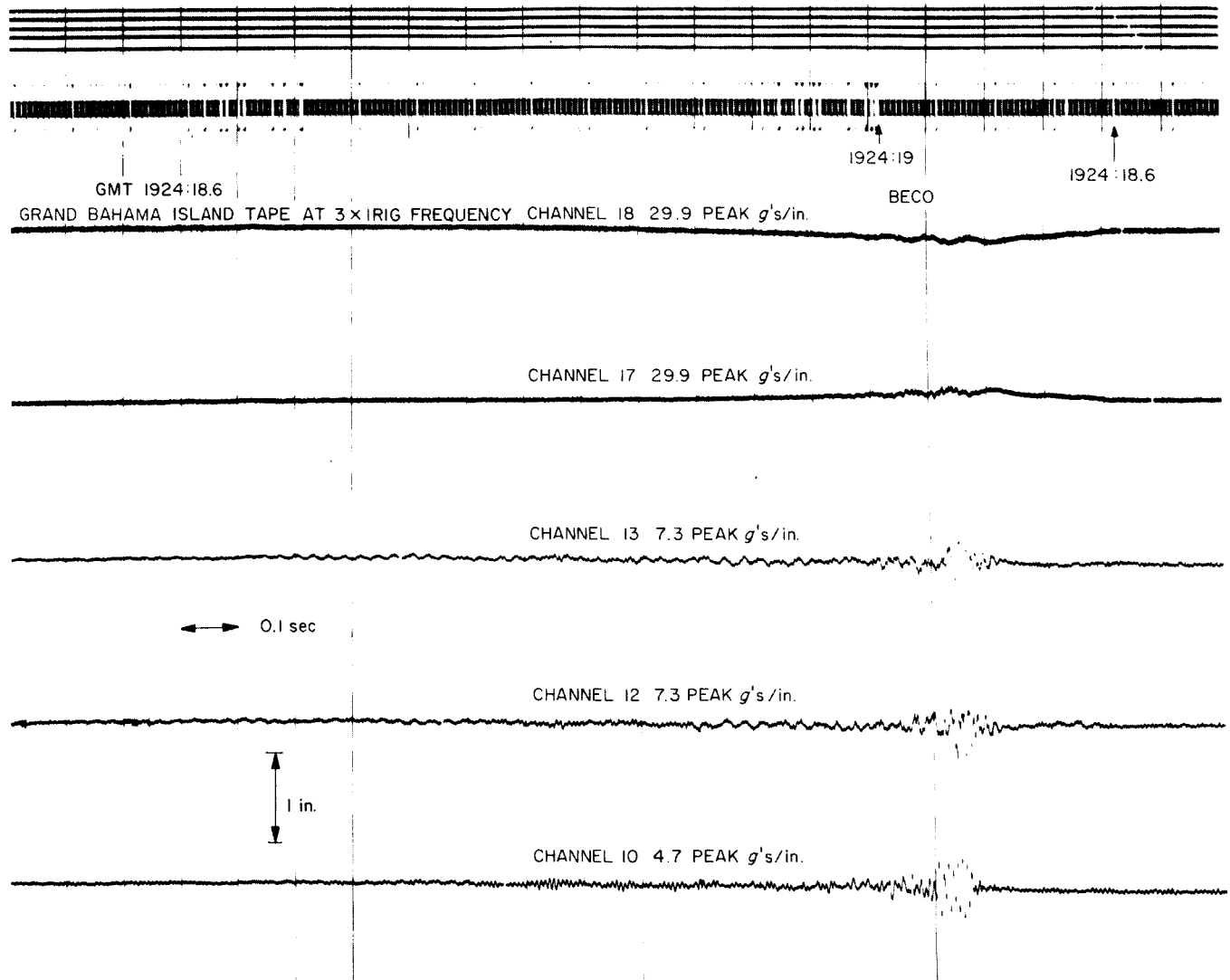


Fig. 59a. Oscillogram, *Mariner III*, BECO, all channels

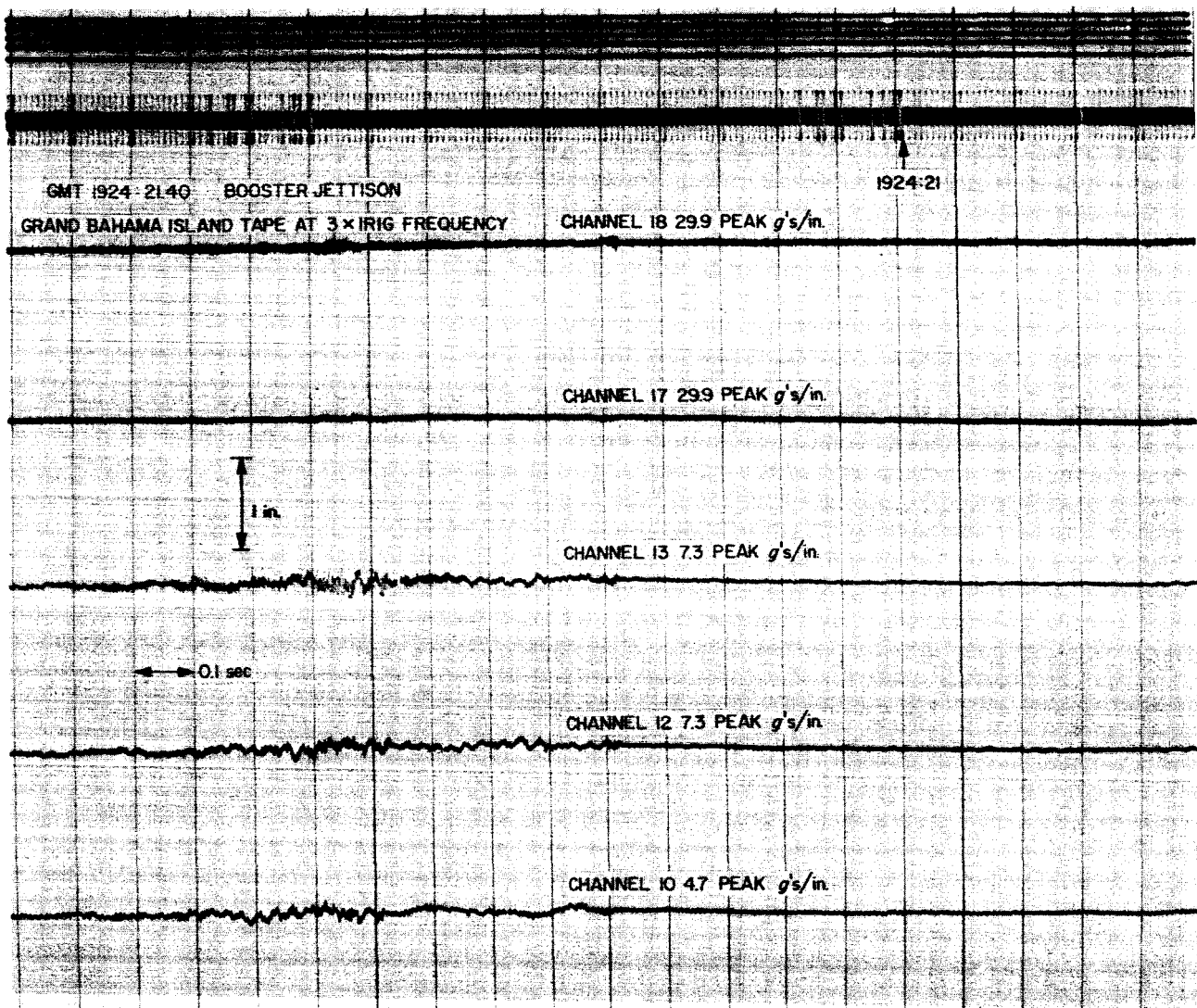


Fig. 59b. Oscillogram, Mariner III, booster jettison, all channels

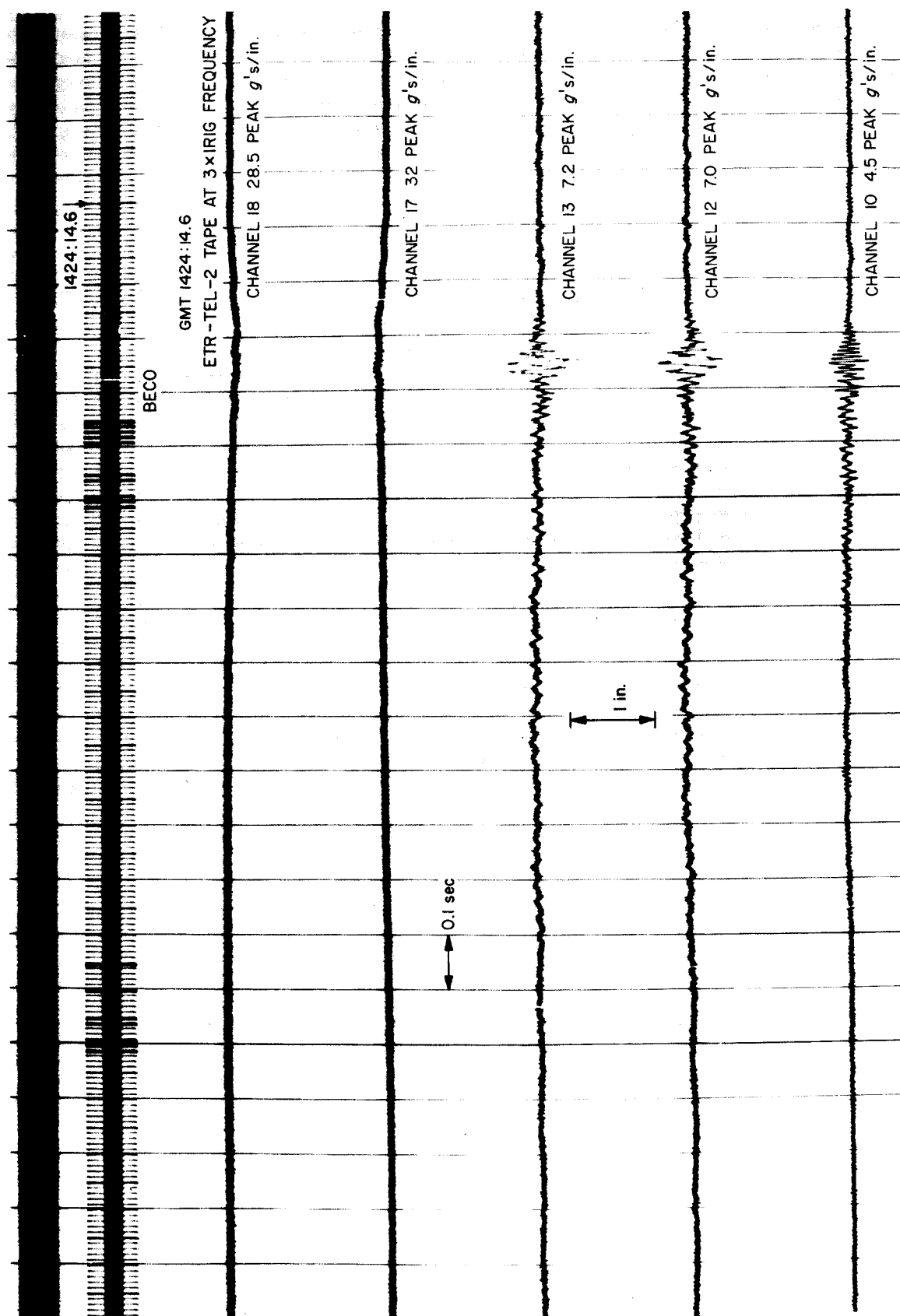


Fig. 60a. Oscillogram, Mariner IV, BECO, all channels

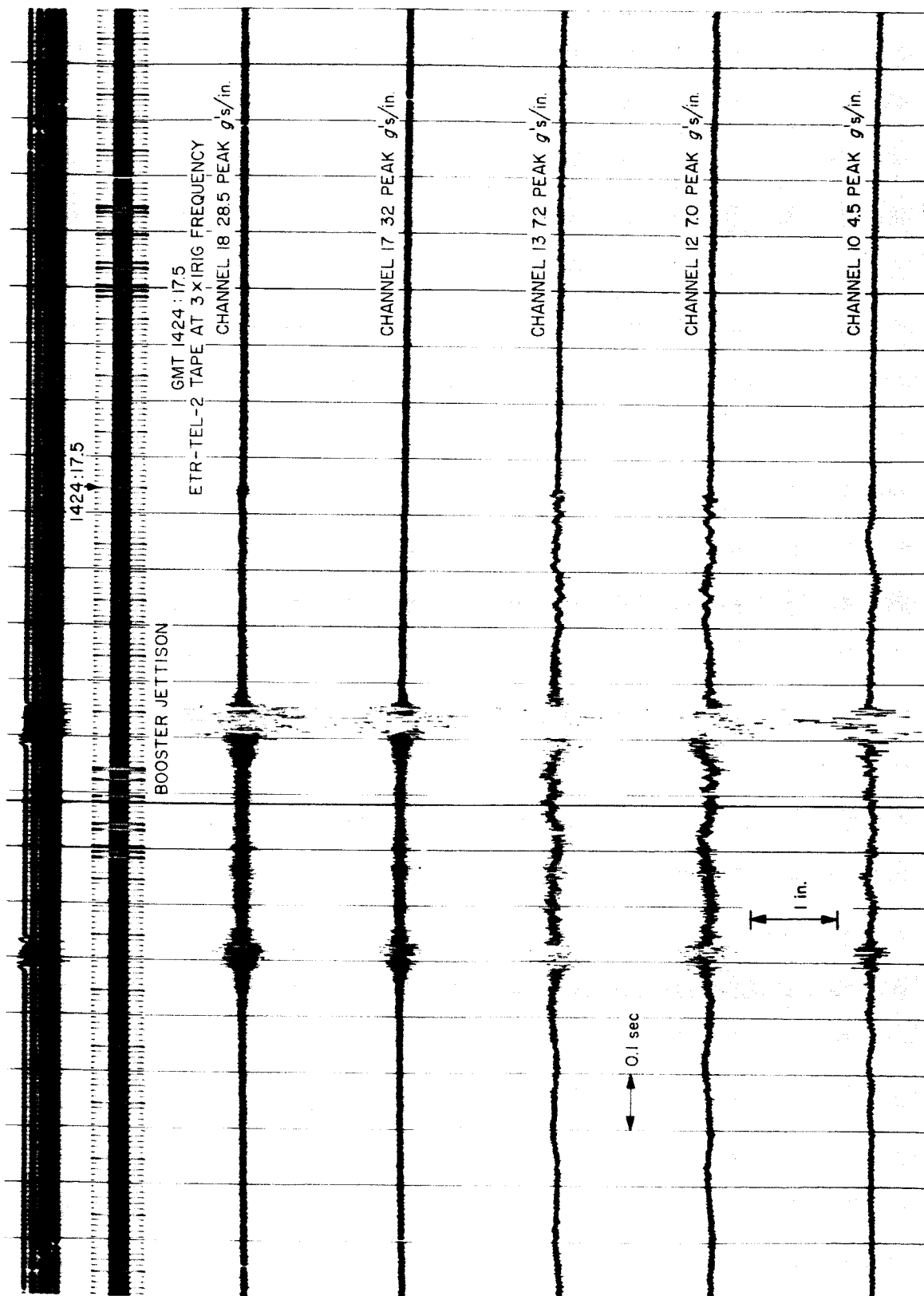


Fig. 60b. Oscillogram, Mariner IV, booster jettison, all channels

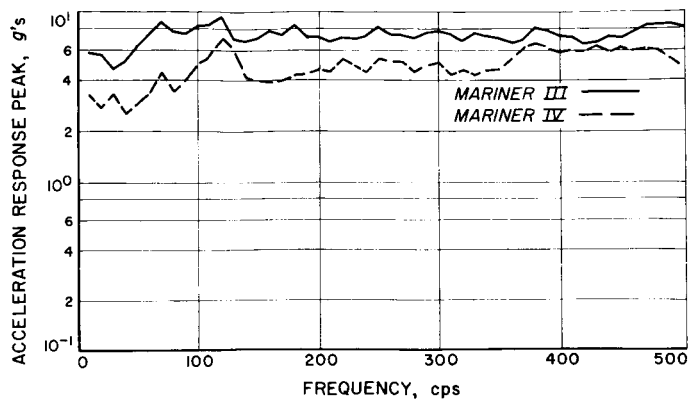


Fig. 61. Shock spectra, Mariner III, IV, BECO, B3

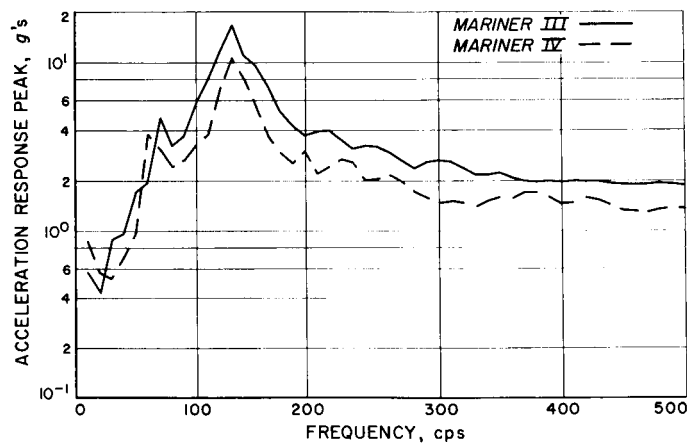


Fig. 62. Shock spectra, Mariner III, IV, BECO, F1

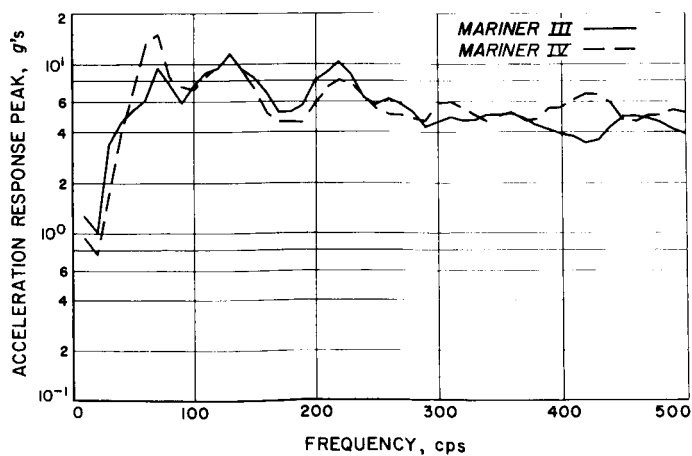


Fig. 63. Shock spectra, Mariner III, IV, BECO, F3

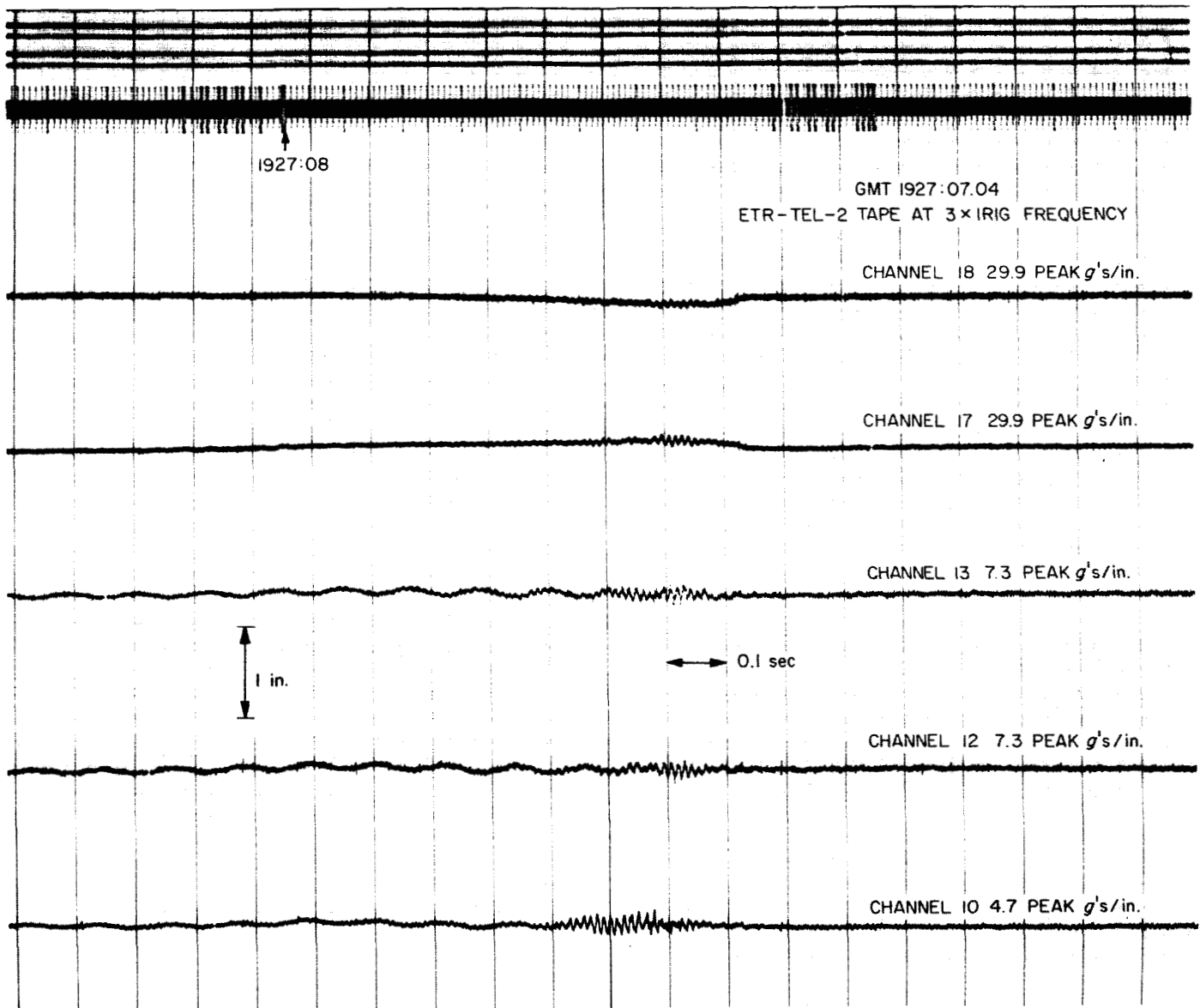


Fig. 64. Oscillogram, Mariner III, SECO, all channels

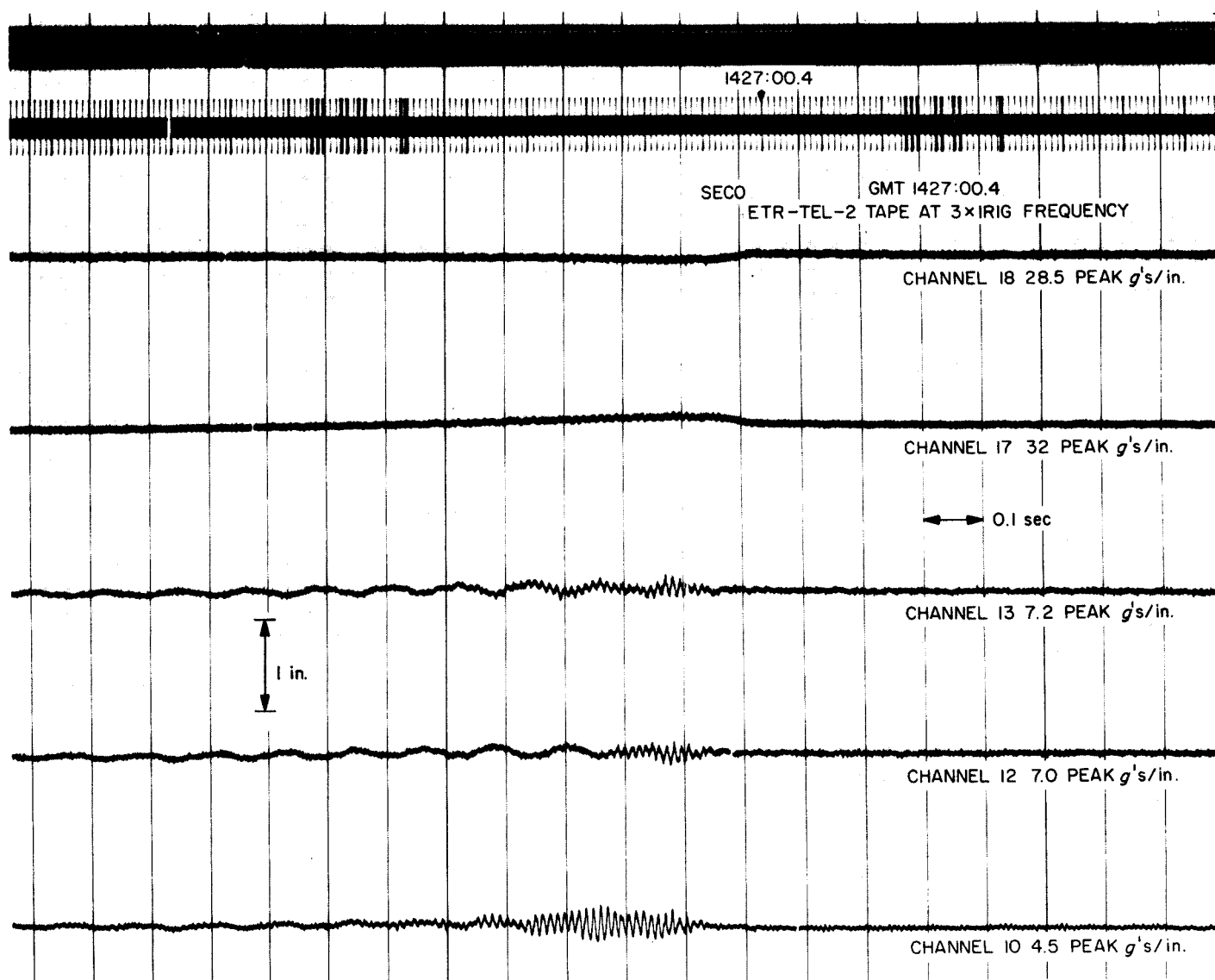
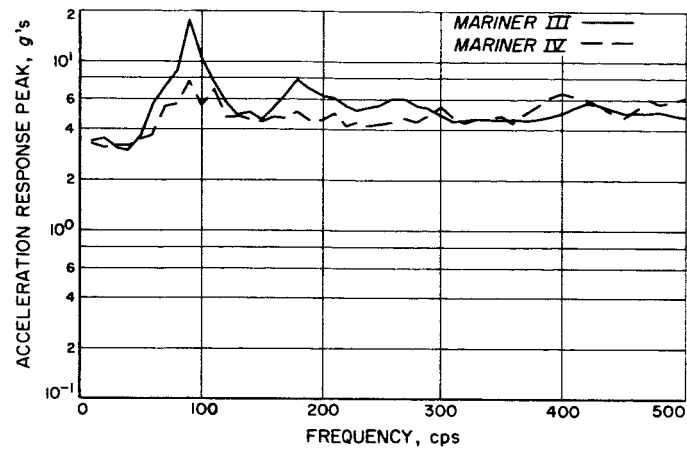
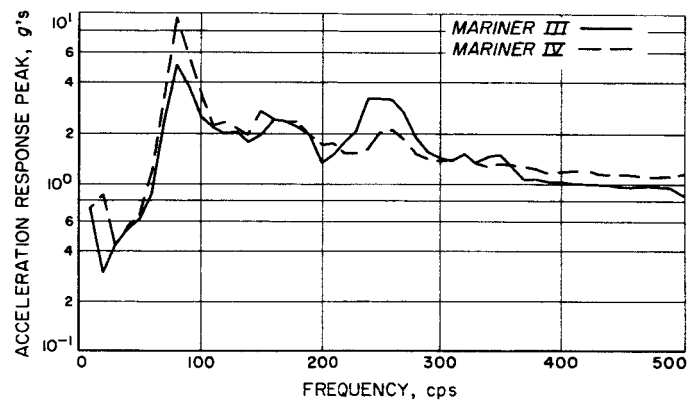
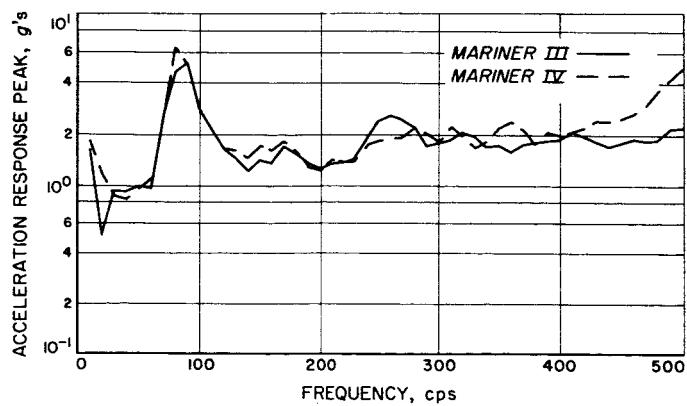


Fig. 65. Oscillogram, Mariner IV, SECO, all channels

**Fig. 66. Shock spectra, Mariner III, IV, SECO, B3****Fig. 67. Shock spectra, Mariner III, IV, SECO, F1****Fig. 68. Shock spectra, Mariner III, IV, SECO, F3**

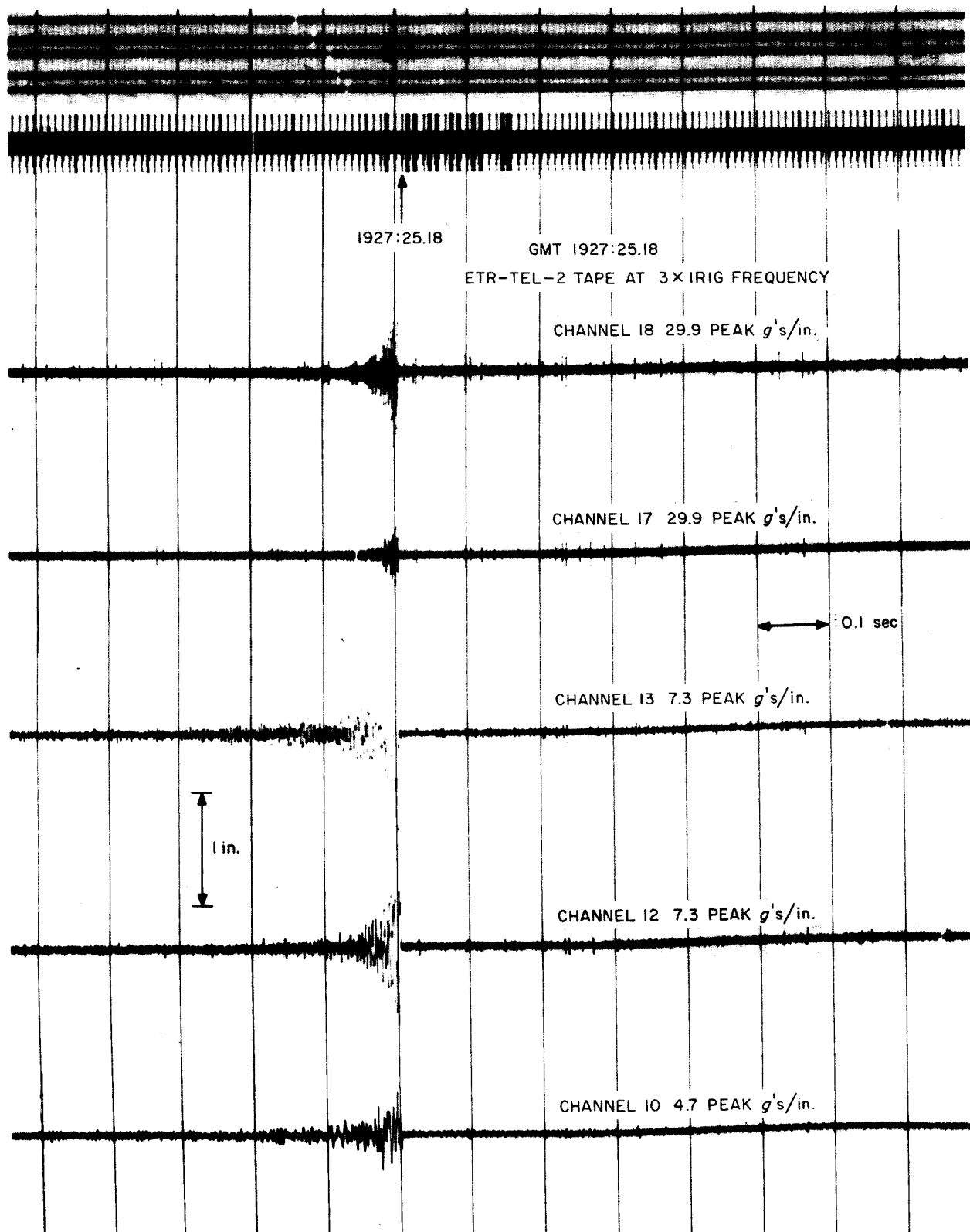


Fig. 69. Oscillogram, *Mariner III*, H/S fairing jettison, all channels

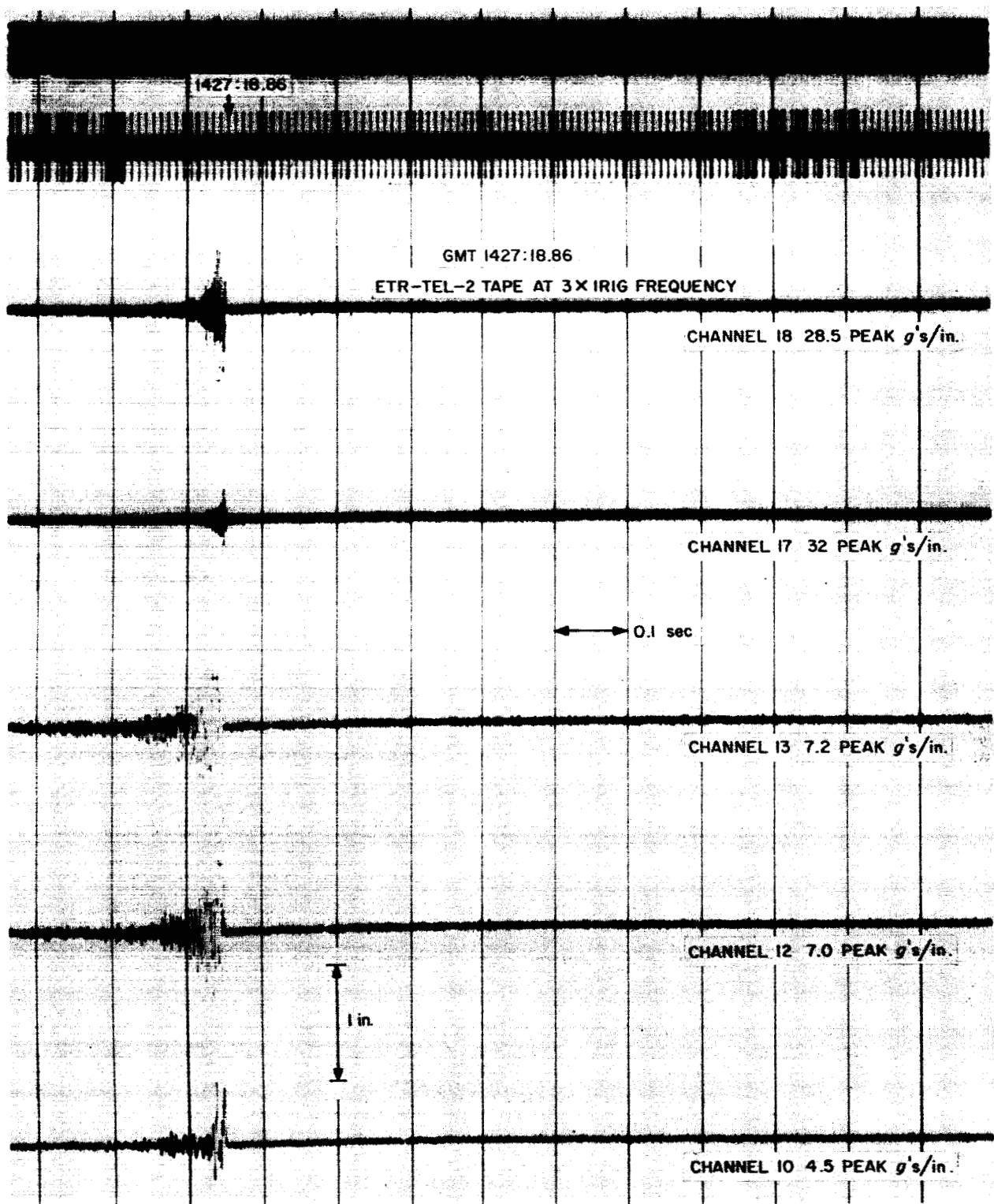


Fig. 70. Oscillogram, Mariner IV, H/S fairing jettison, all channels

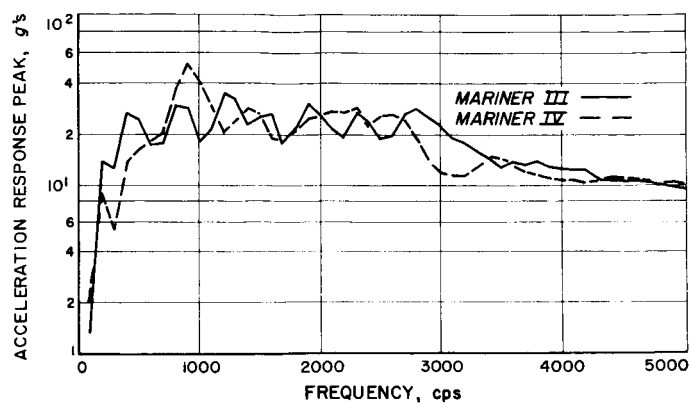


Fig. 71. Shock spectra, Mariner III, IV, H/S
fairing jettison, B3

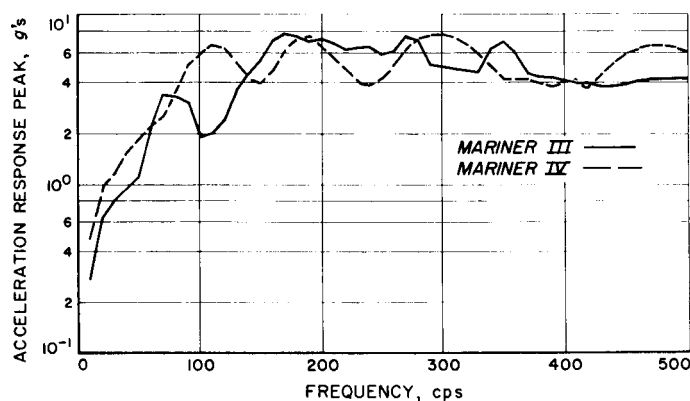


Fig. 72. Shock spectra, Mariner III, IV, H/S
fairing jettison, F1

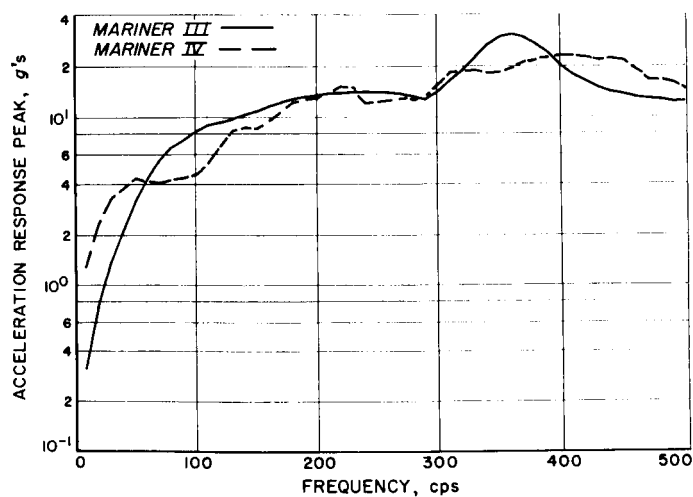
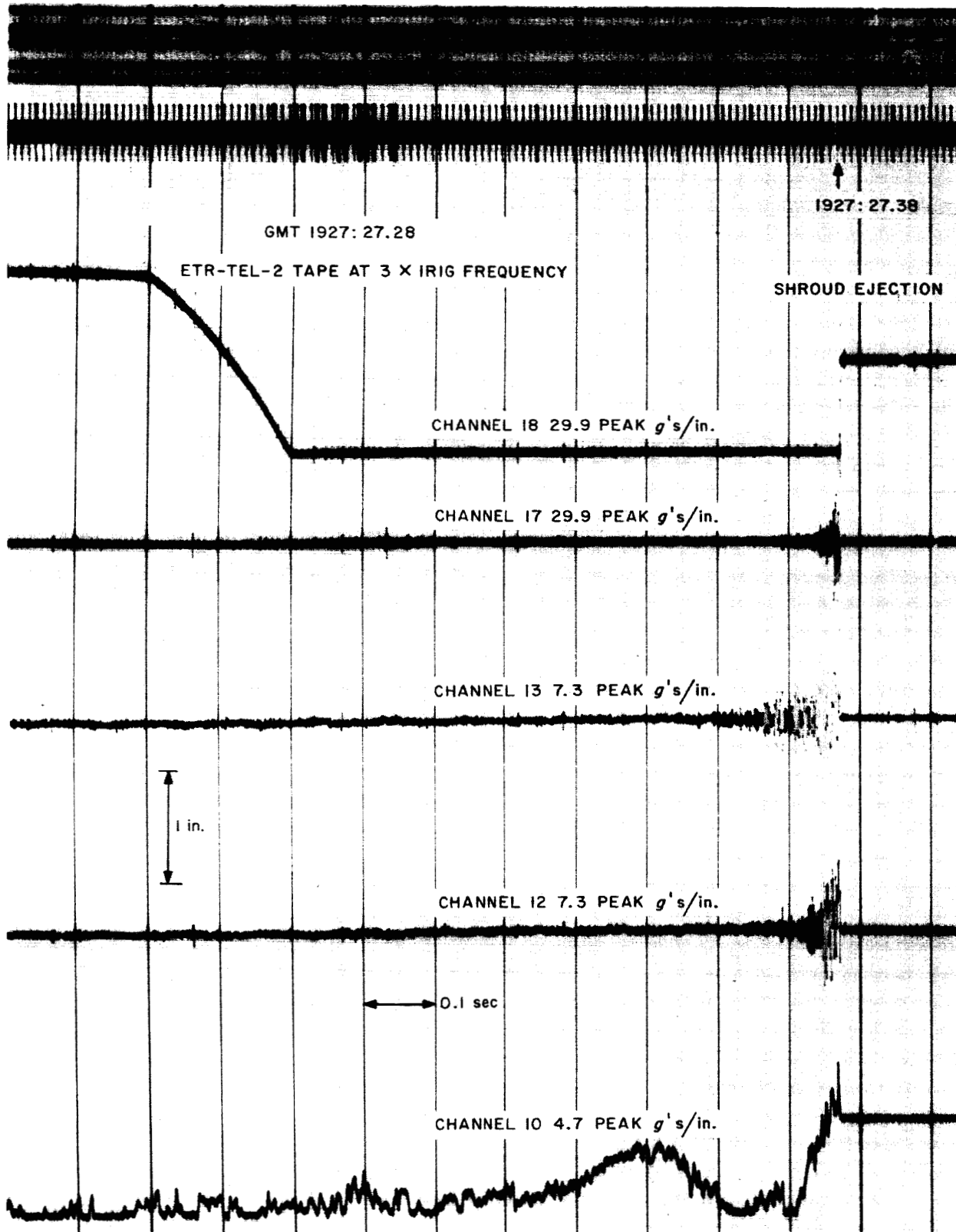


Fig. 73. Shock spectra, Mariner III, IV, H/S
fairing jettison, F3

Fig. 74. Oscillogram, *Mariner III*, shroud ejection, all channels

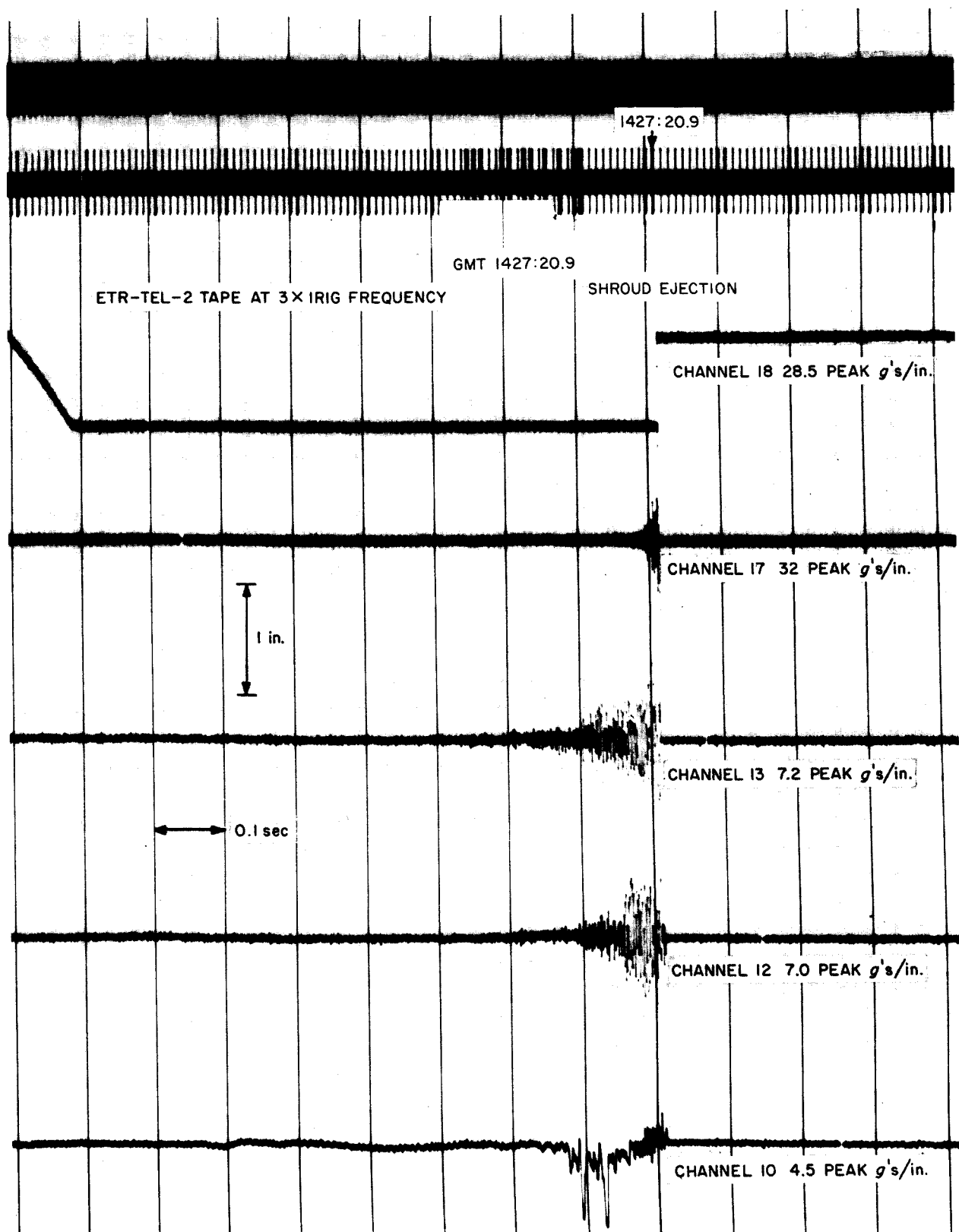


Fig. 75. Oscillogram, *Mariner IV*, shroud ejection, all channels

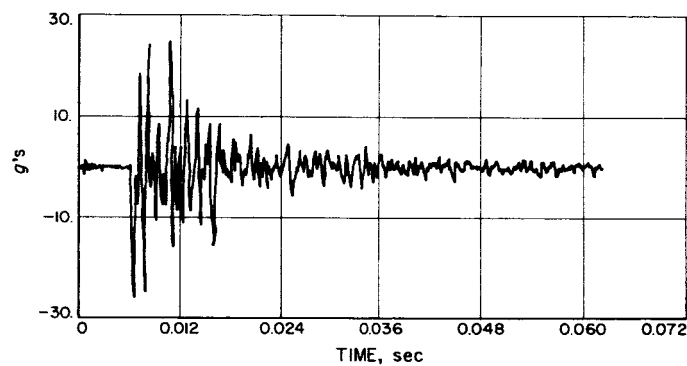


Fig. 76. Transient, *Mariner III*, shroud ejection, B3

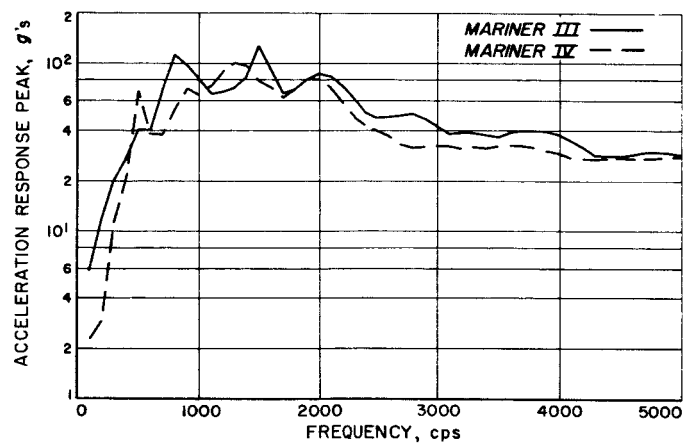


Fig. 77. Shock spectra, *Mariner III, IV*; shroud ejection, B3

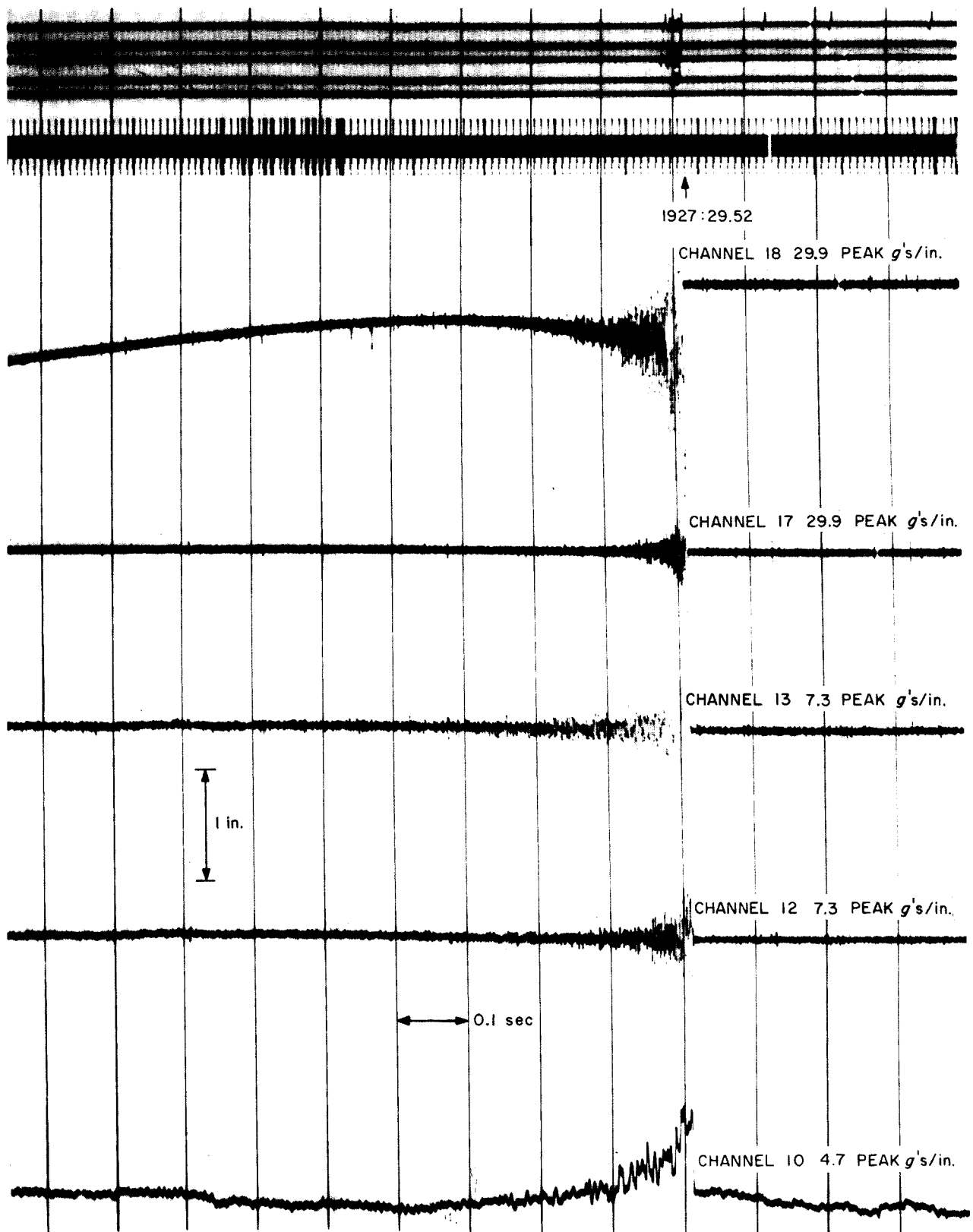


Fig. 78. Oscillogram, Mariner III, Atlas-Agena separation, all channels

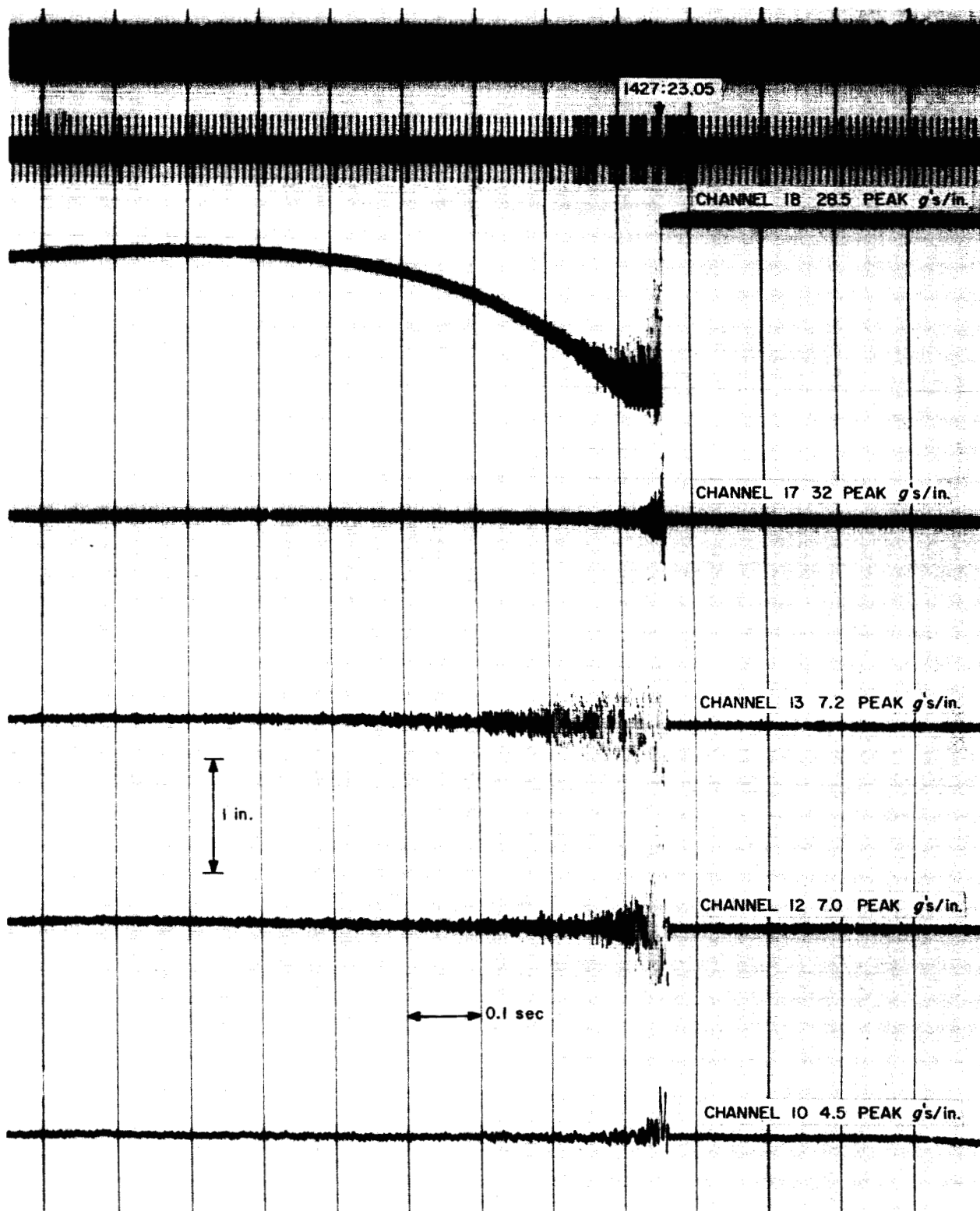


Fig. 79. Oscillogram, Mariner IV, Atlas-Agena separation, all channels

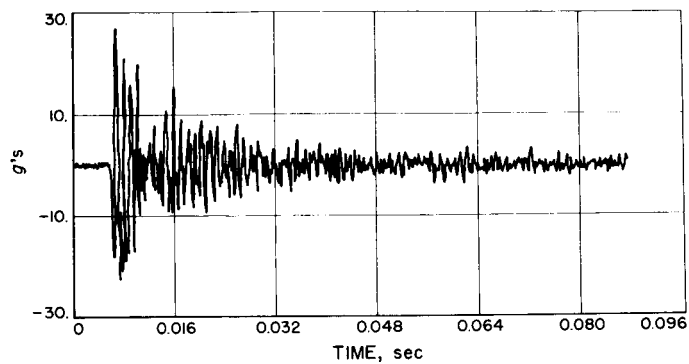


Fig. 80. Transient, Mariner III, Atlas-Agena separation, B3

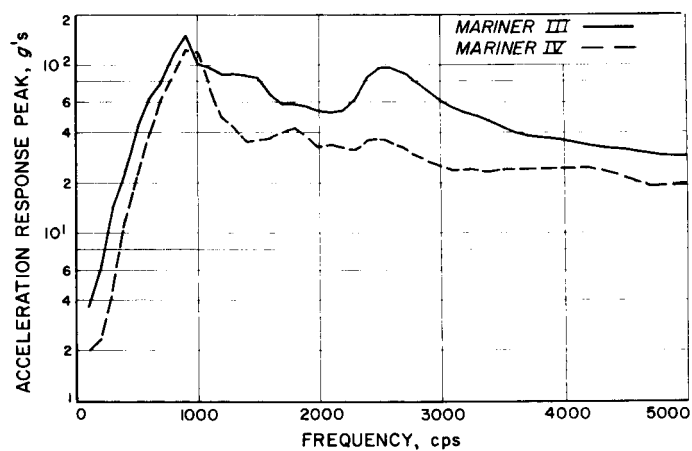


Fig. 81. Shock spectra, Mariner III, IV, Atlas-Agena separation, B3

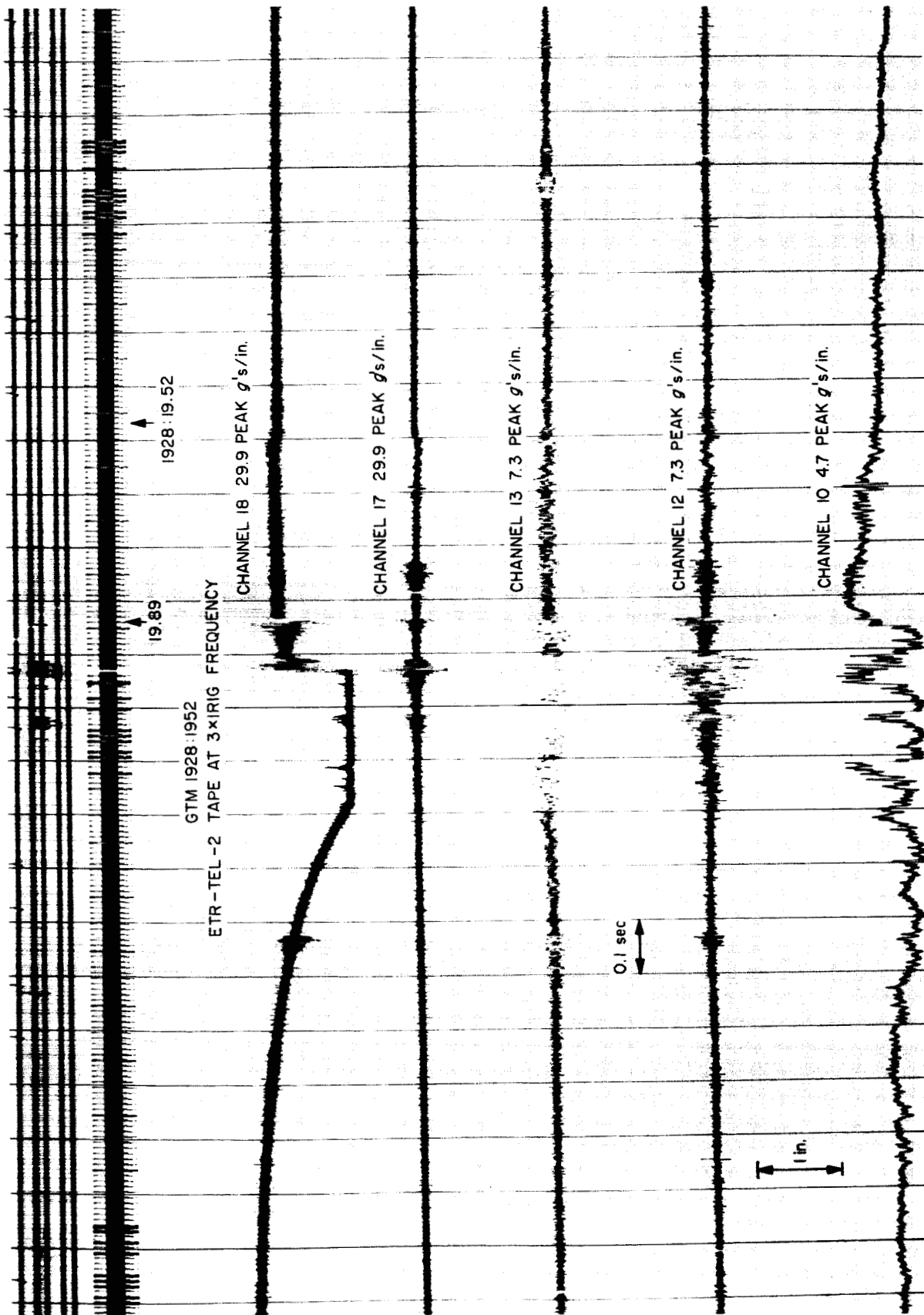


Fig. 82. Oscillogram, Mariner III, Agena first ignition, all channels

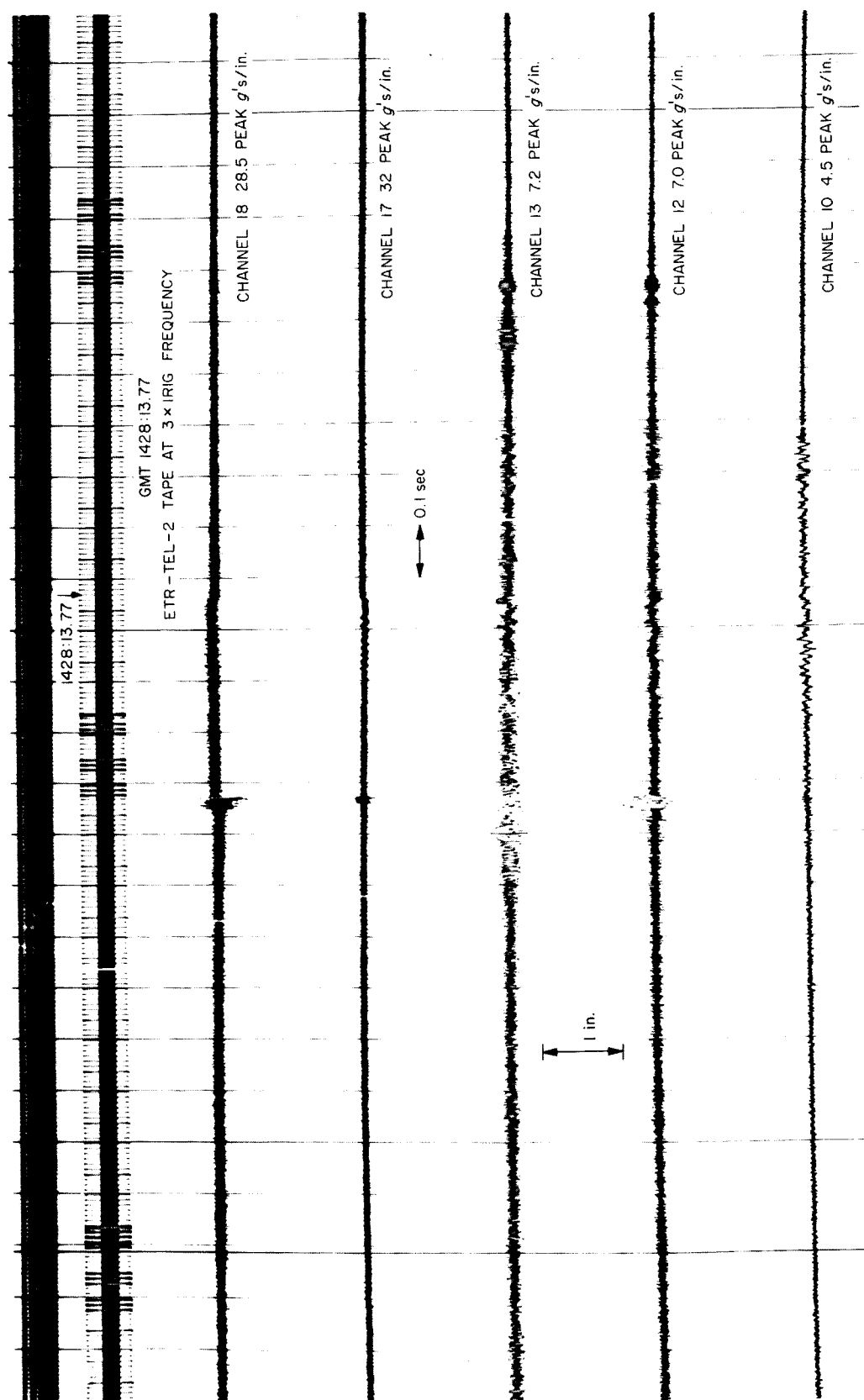


Fig. 83. Oscillogram, Mariner IV, Agena first ignition, all channels

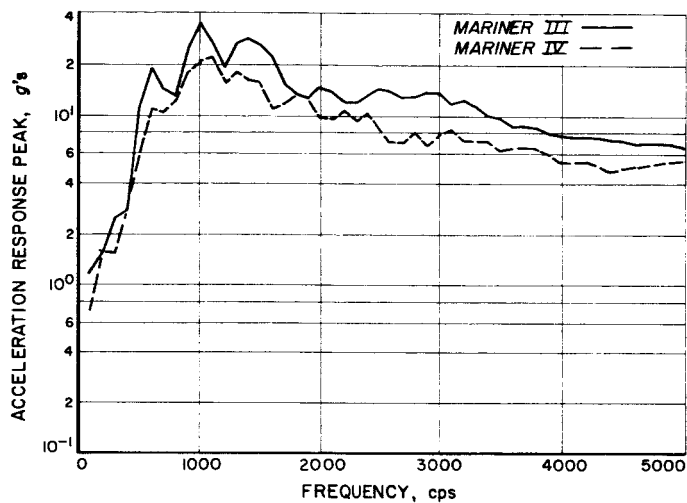


Fig. 84. Shock spectra, Mariner III, IV, Agena first ignition, B3

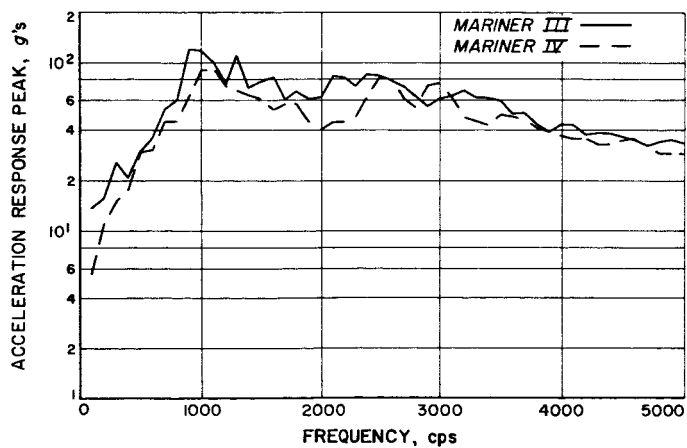


Fig. 85. Shock spectra, Mariner III, IV, Agena first ignition, F4

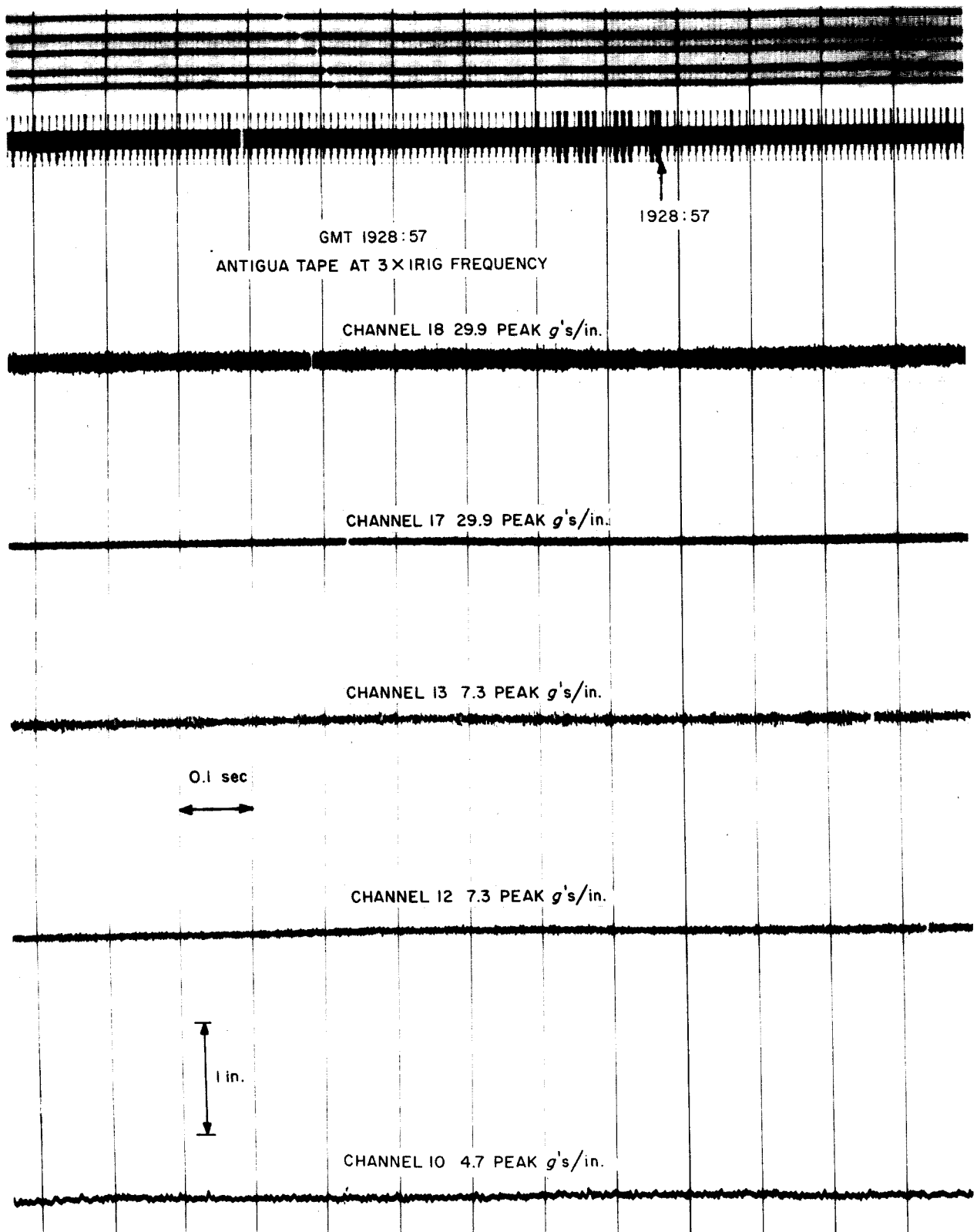


Fig. 86. Oscillogram, *Mariner III*, typical *Agena* first burn, all channels

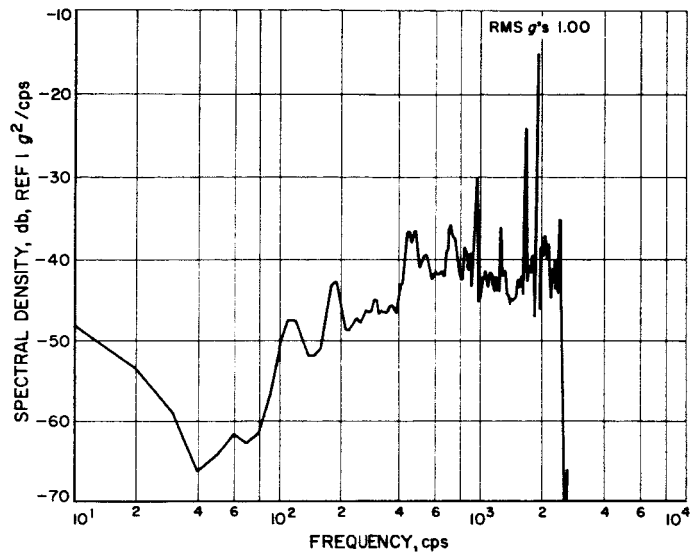


Fig. 87. Acceleration spectral density, Mariner III, Agena first burn, F4

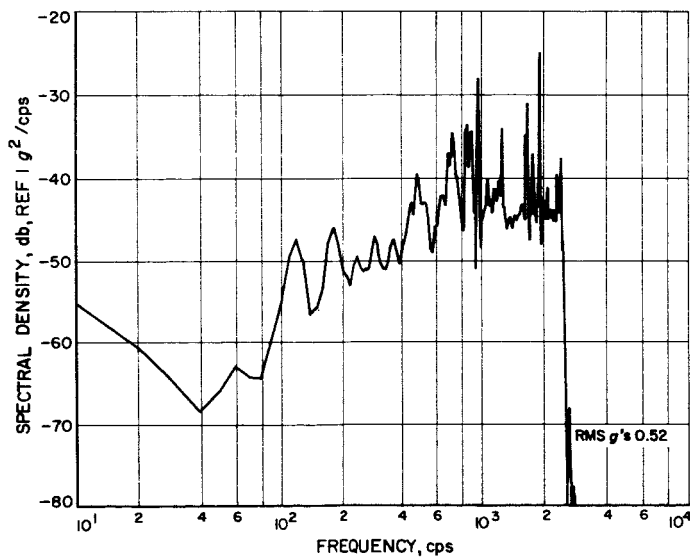


Fig. 88. Acceleration spectral density, Mariner IV, Agena first burn, F4

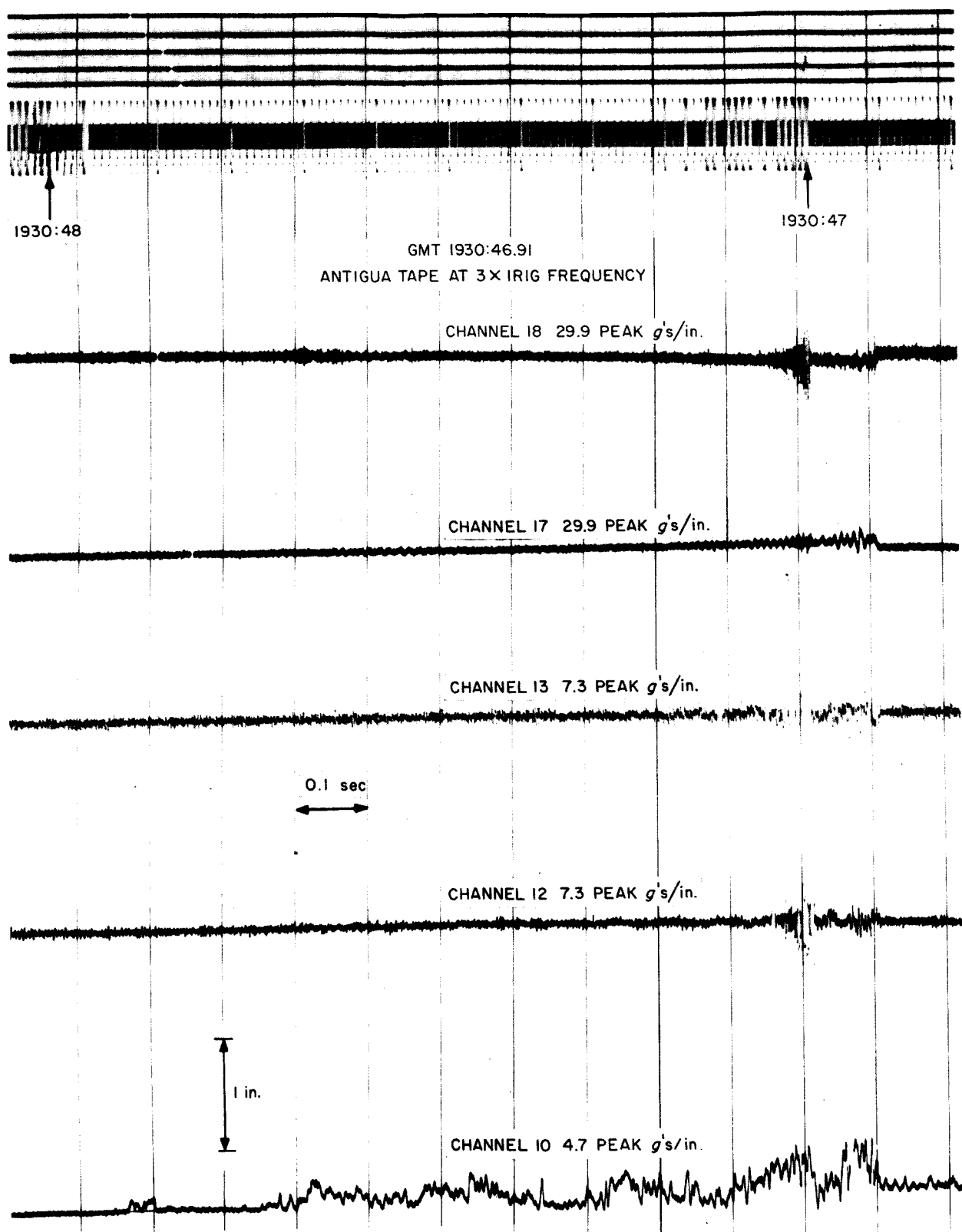


Fig. 89. Oscillogram, Mariner III, Agena first cutoff, all channels

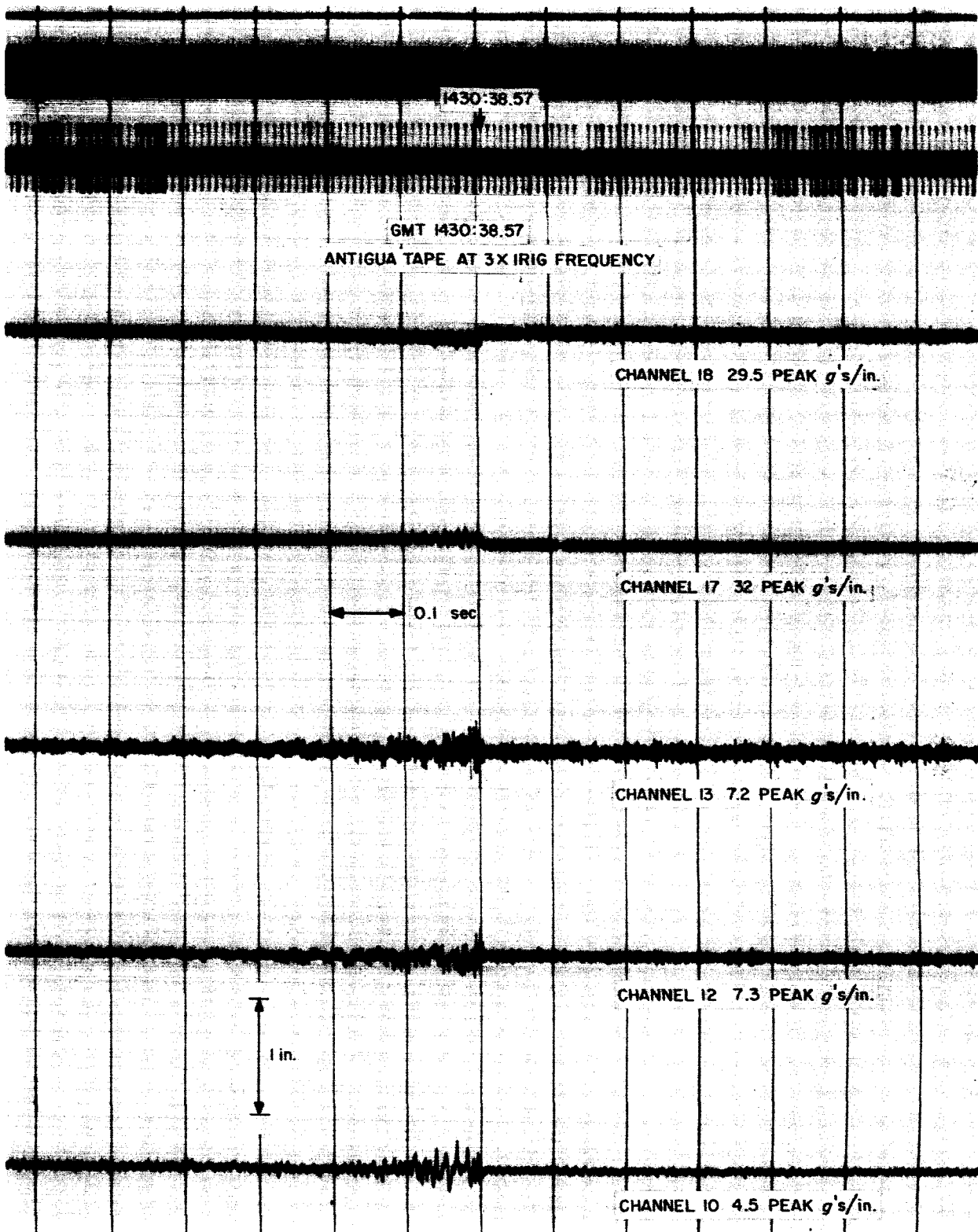


Fig. 90. Oscillogram, Mariner IV, Agena first cutoff, all channels

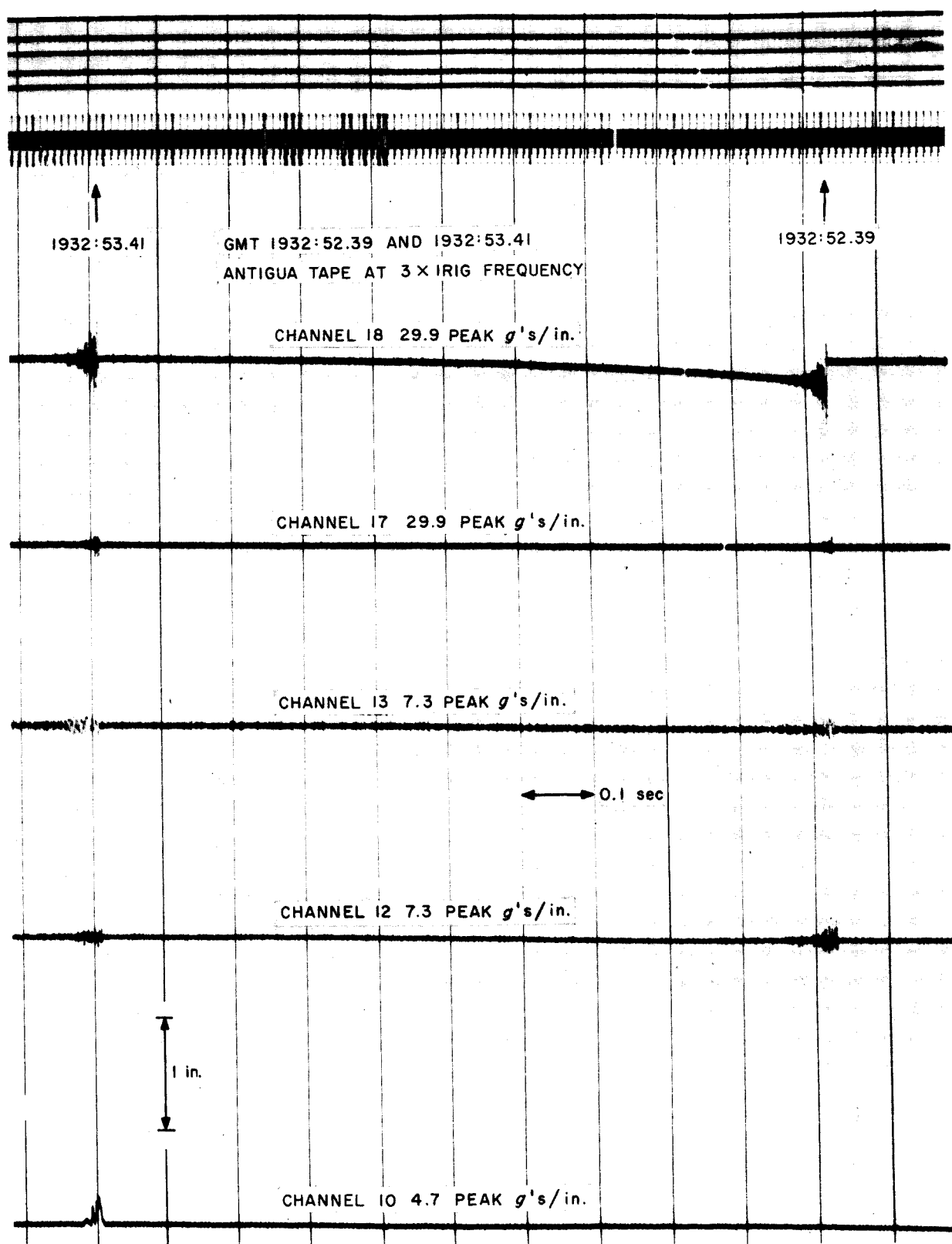


Fig. 91. Oscillogram, *Mariner III*, Agena pyro events, all channels

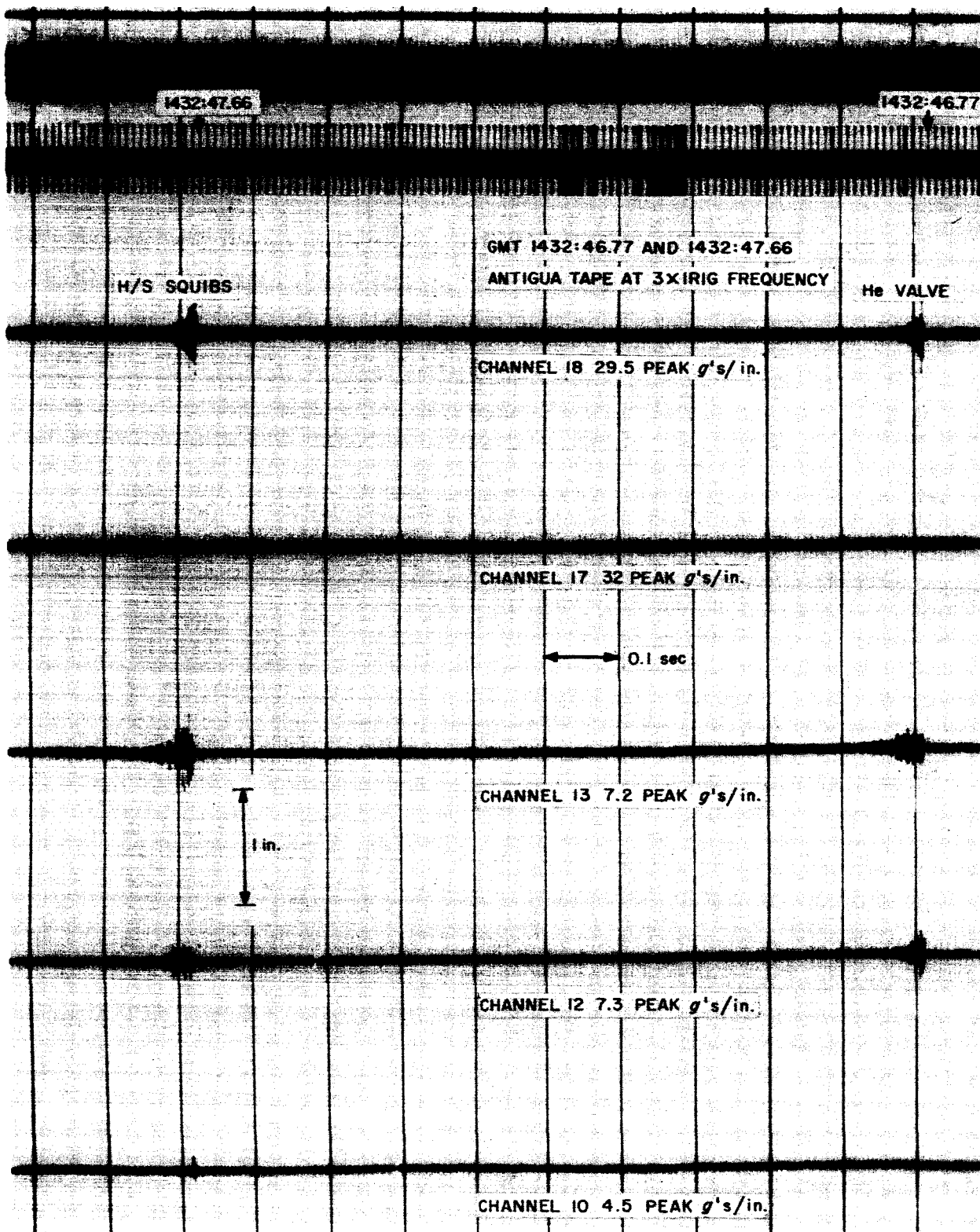


Fig. 92. Oscillogram, Mariner IV, Agona pyro events, all channels

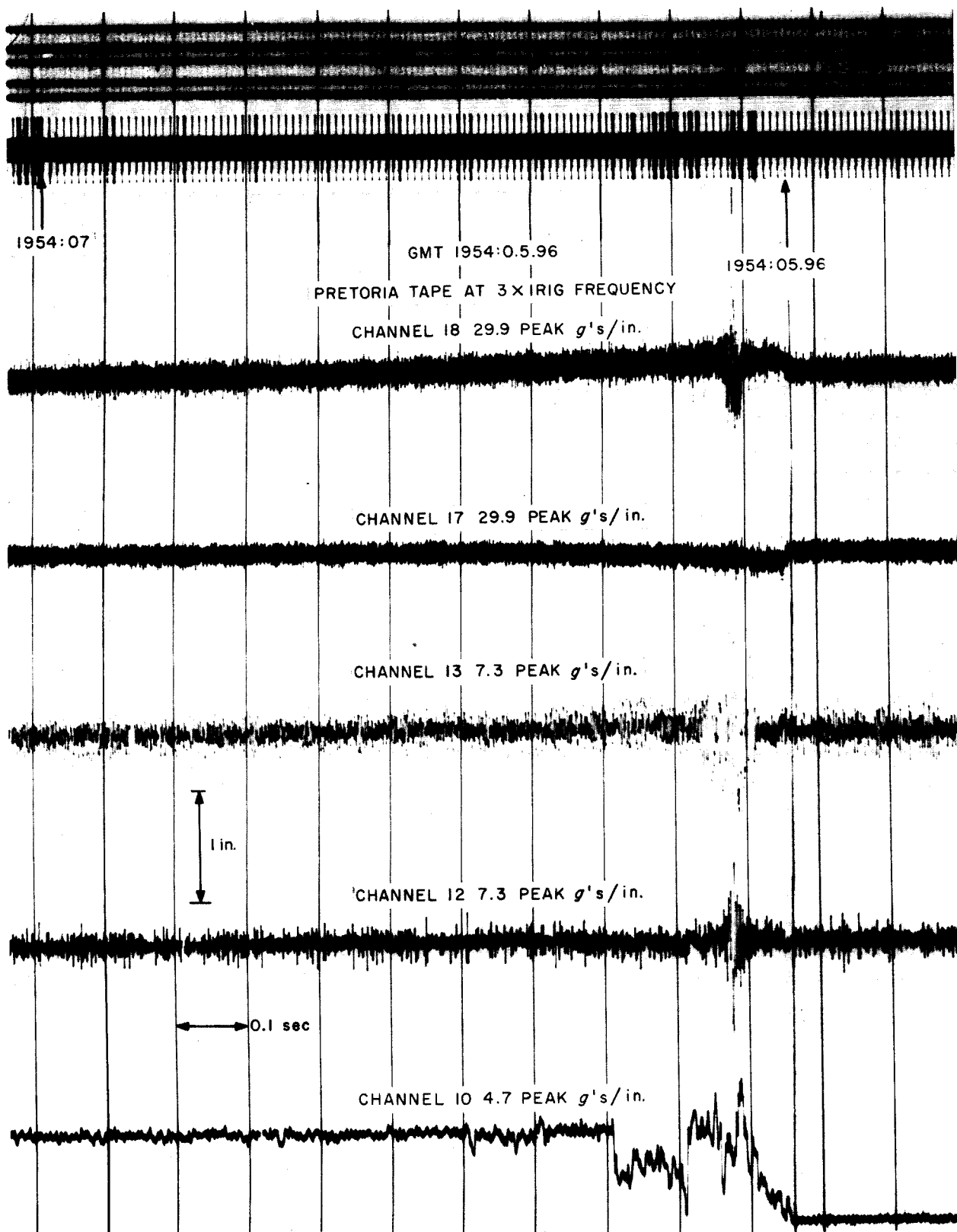


Fig. 93. Oscillogram, *Mariner III*, Agena second ignition, all channels

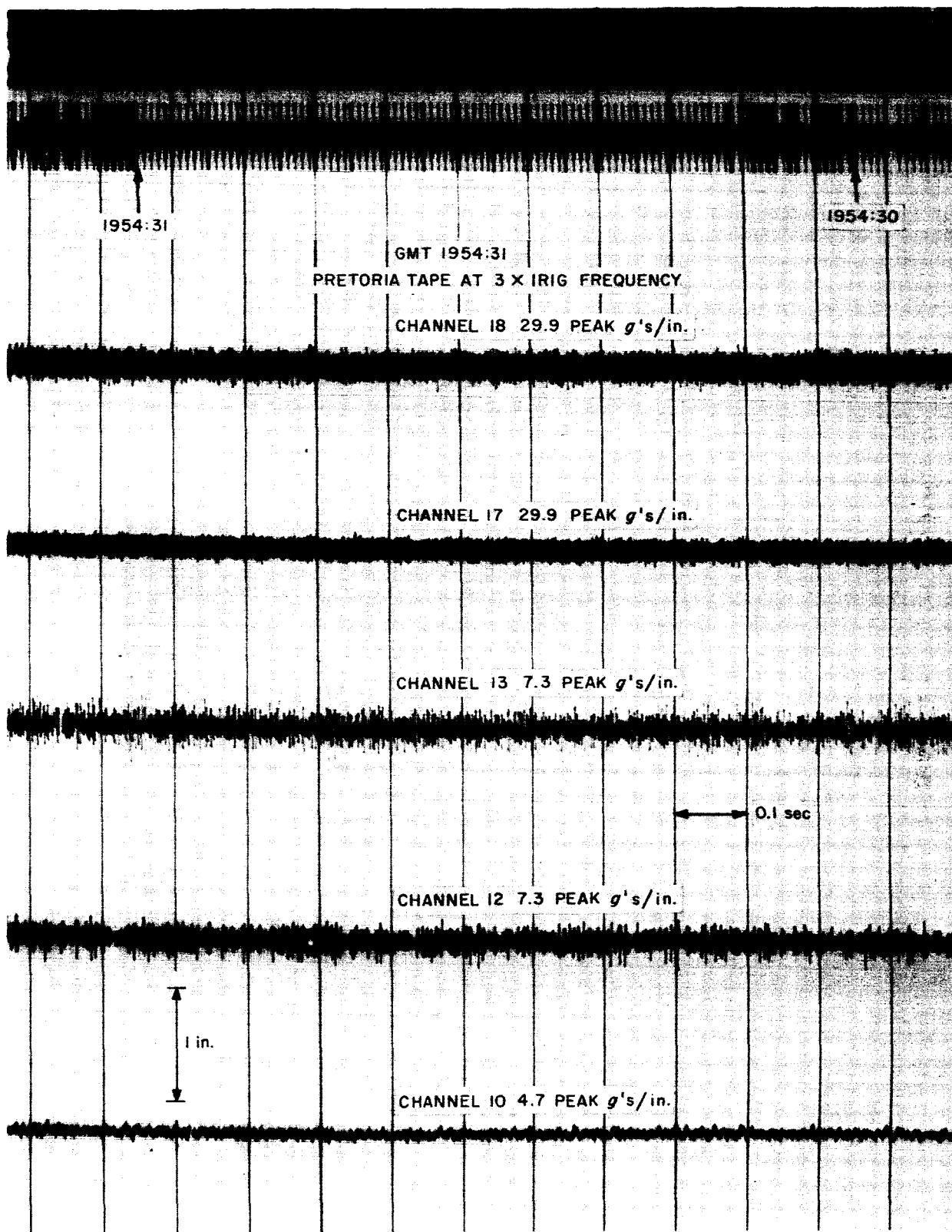


Fig. 94. Oscillogram, Mariner III, Agena second burn, all channels

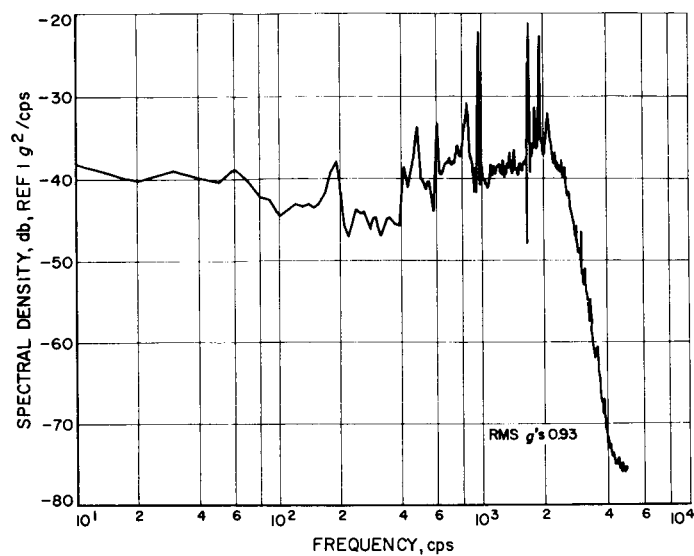


Fig. 95. Acceleration spectral density, Mariner III, Agena second burn, F4

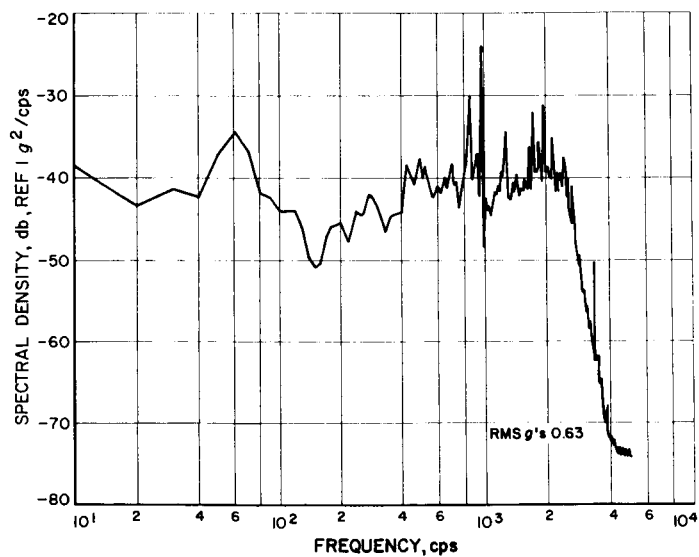


Fig. 96. Acceleration spectral density, Mariner IV, Agena second burn, F4

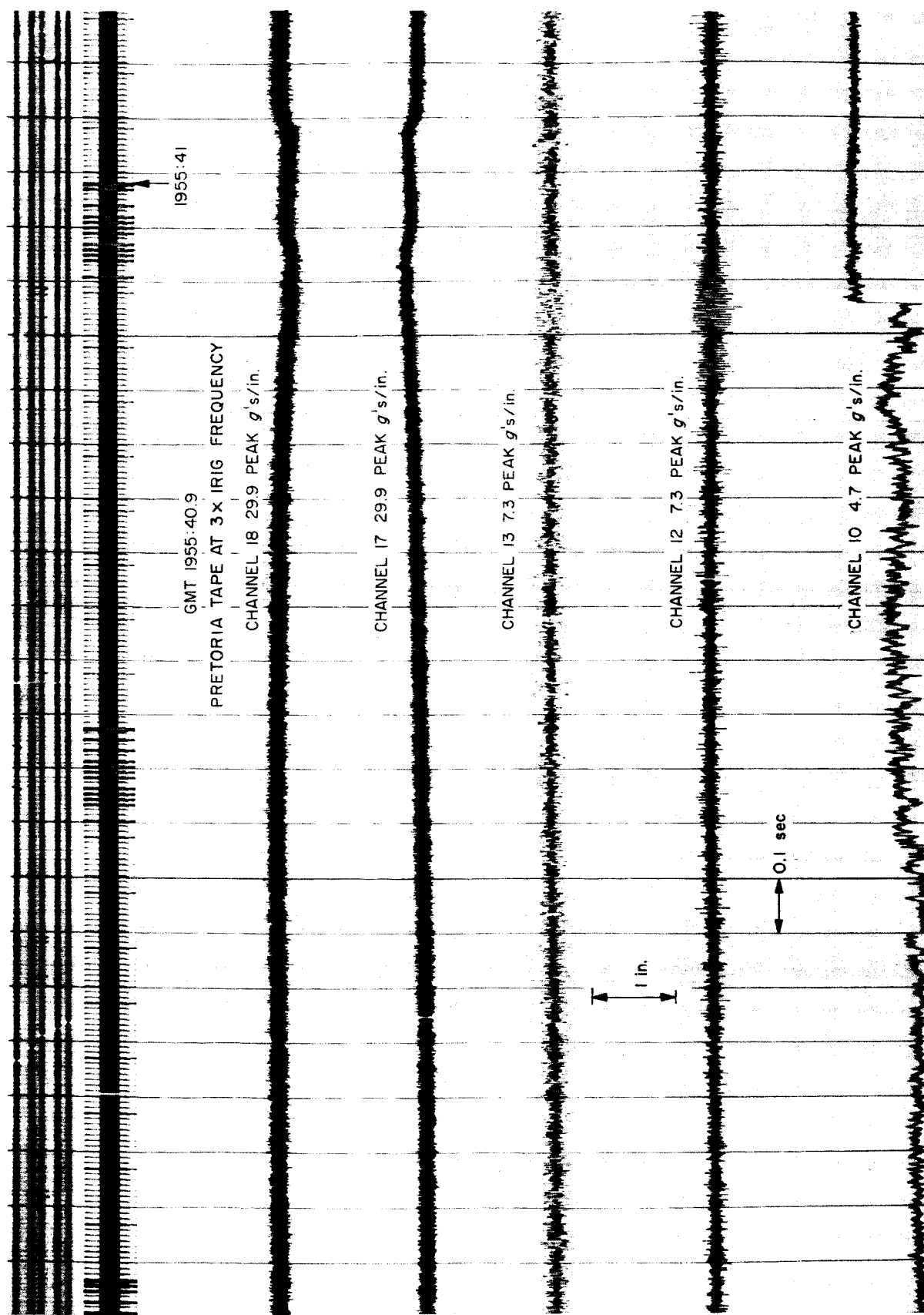


Fig. 97. Oscillogram, Mariner III, Agena second cutoff, all channels

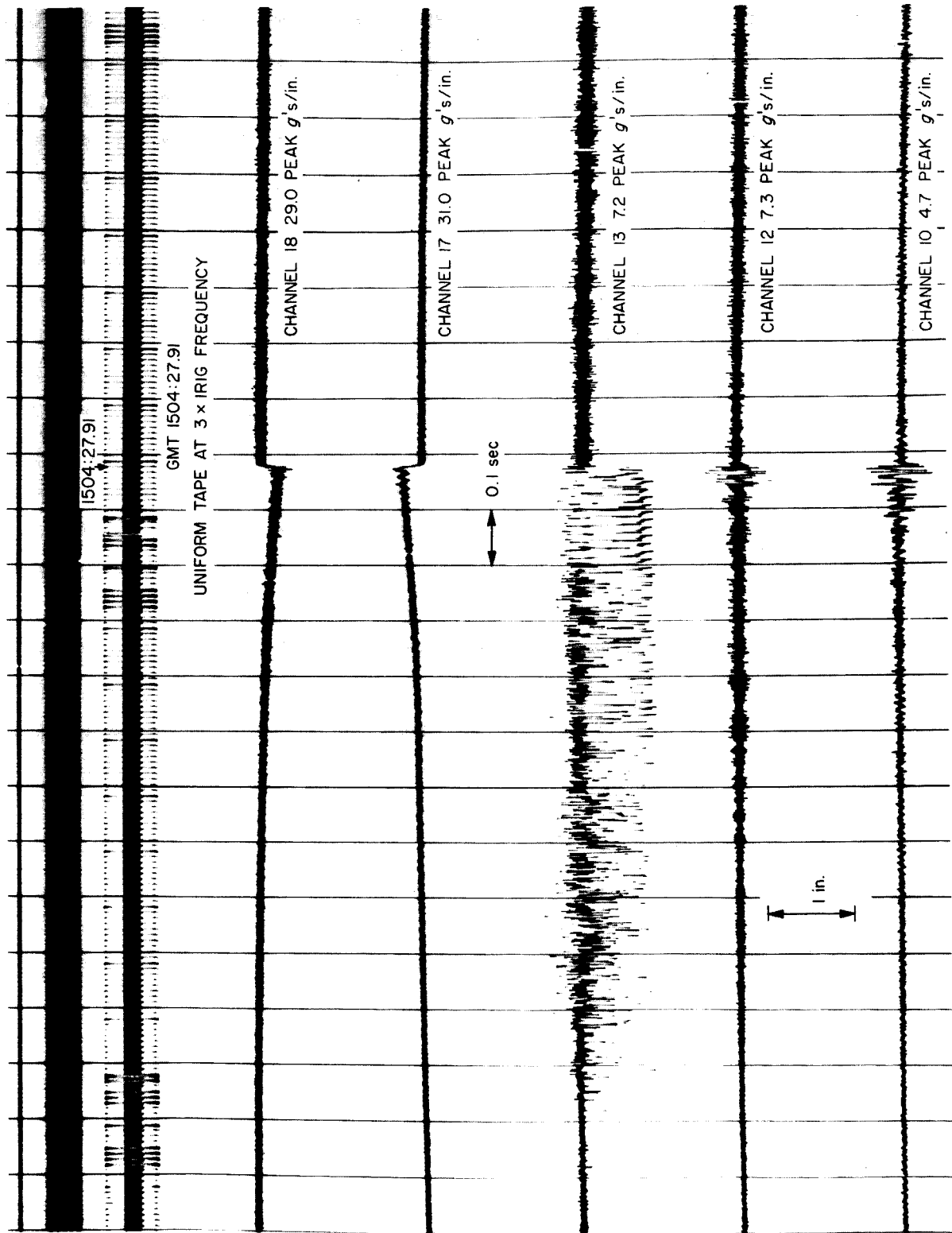
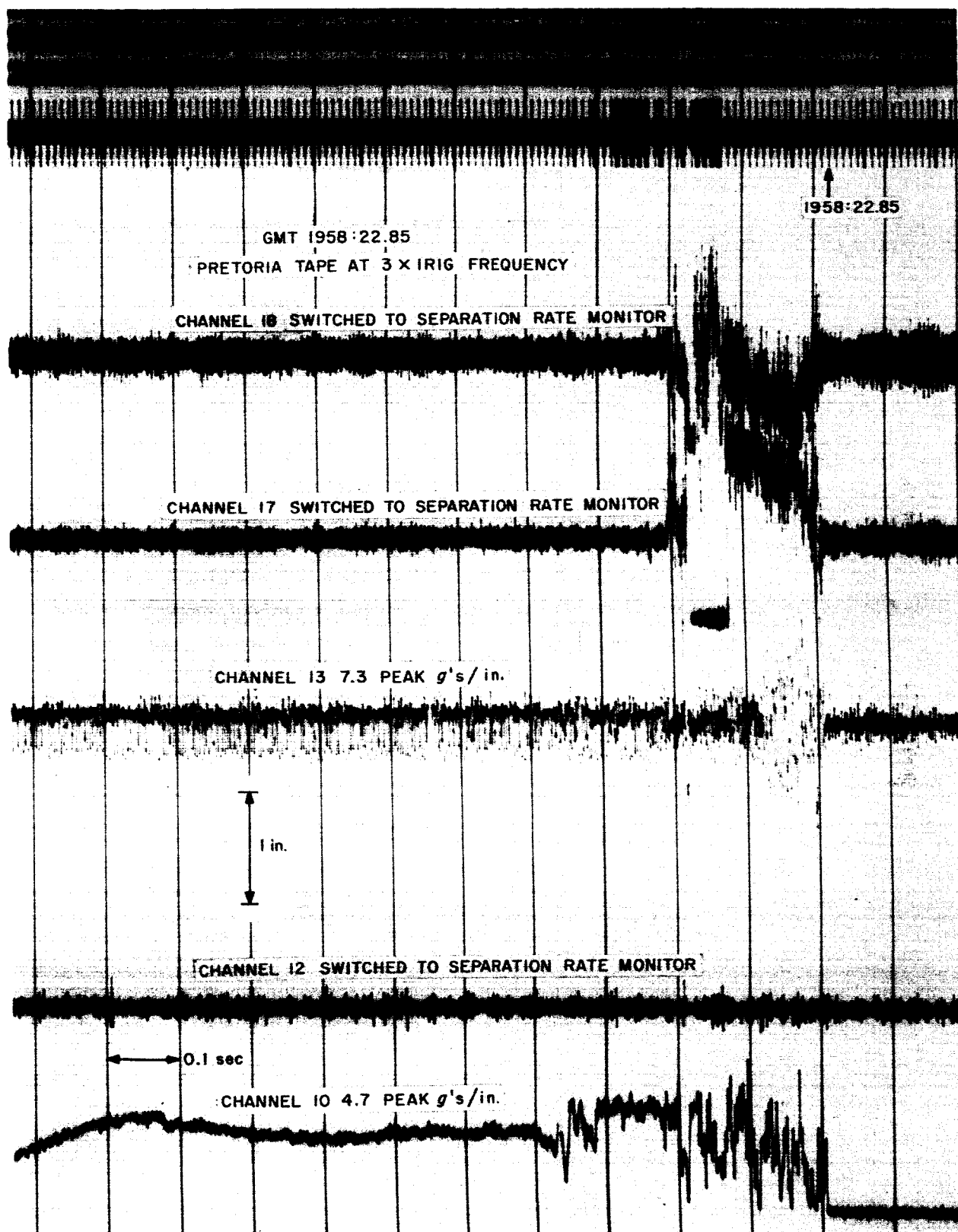
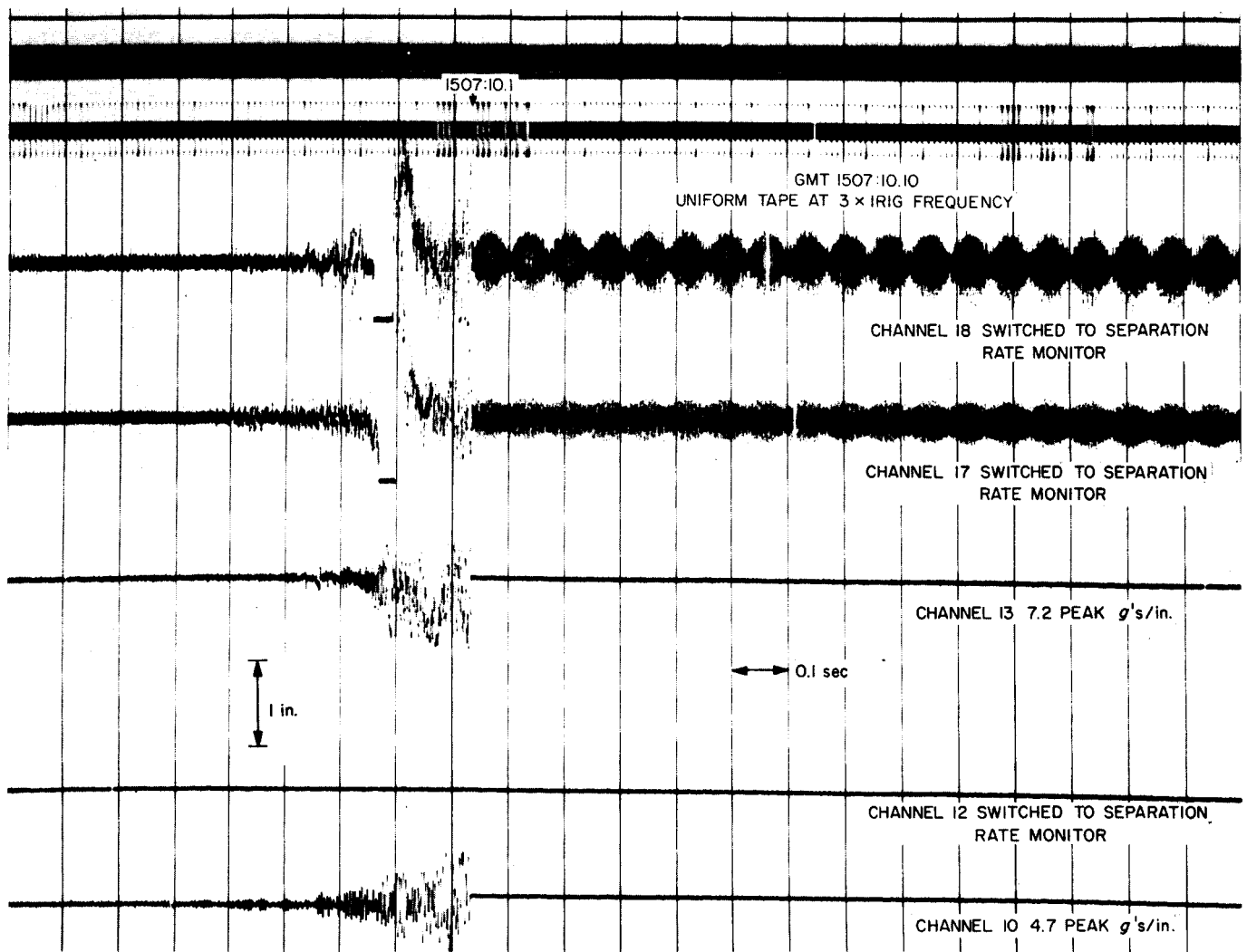
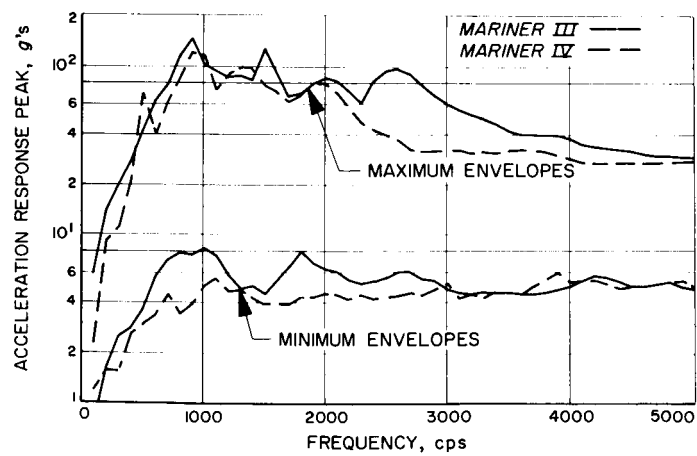


Fig. 98. Oscillogram, Mariner IV, Agena second cutoff, all channels

Fig. 99. Oscillogram, *Mariner III*, spacecraft separation, all channels

Fig. 100. Oscillogram, *Mariner IV*, spacecraft separation, all channelsFig. 101. Shock spectra, *Mariner III, IV*, maxima, minima, B3

VI. CONCLUSIONS

An effort has been made here to present the total dynamic environment of the *Mariner* Mars 1964 flights from the few telemetry measurements that were available. Because of the high confidence in the spacecraft instrumentation within the ranges presented here, these data are considered adequate for future test specifications and comparisons. In any specification taken from these data, the possibility must be considered that some of these responses may be very localized phenomena (e.g., at high frequencies) and not a true indication of the total spacecraft response to the environment.

Future instrumentation capabilities could be improved by including more general measurements and increasing the range of existing measurements. The inclusion of a flight microphone would be a desirable measurement. An increase in the frequency response and amplitude deviation would also improve telemetry data.

The maximum dynamic environments have been defined for random and shock excitation periods. *Mariner*

III at liftoff (Fig. 23) was the maximum overall random vibration observed on either flight on the spacecraft. There were, however, some higher power spectrum levels at high frequencies during the transonic period of *Mariner IV* (Fig. 56). The maximum recorded shock environment on the spacecraft occurred at the *Atlas-Agena* separation event on *Mariner III* (Fig. 81). The shroud ejection event (Fig. 77) also contained high levels in higher frequency ranges. The maximum shock level probably occurred at the spacecraft separation event but telemetry was lost before this.

Any interpretation of this type of data is limited by the analysis techniques. The techniques utilized in processing the data presented in this Memorandum are a significant improvement over those used only a few years ago. Some techniques under consideration and on trial at this time may further improve our capability to interpret this type of information. Such items as cross power and variable resolution spectra may result in more valuable analyses and predictions of this dynamic environment.

REFERENCES

1. LMSC-Mariner Mars 1964 Agena Vehicle Instrumentation Handbook, Lockheed Missile and Space Center, A708354, October 26, 1964.
2. Wiksten, David B., *Dynamic Environment of the Ranger Spacecraft: I through IX (Final Report)*, Jet Propulsion Laboratory, Pasadena, California, Technical Report No. 32-909, May 1, 1966.
3. Blackman, R. B., and Tukey, J. W., *The Measurement of Power Spectra*, New York: Dover Publications, 1958.
4. Schiffer, R. A., and Hyde, J. R., "The Mariner Mars 1964 Acoustically Induced Vibration Environment," *The Shock and Vibration Bulletin*, No. 35, Part 7, April 1966, pp. 31-53, U. S. Naval Research Laboratory, Washington, D. C.

ACKNOWLEDGMENT

The reduced data included here were a result of the efforts of many people, too numerous to list here. Special thanks are expressed to the personnel of the Data Analysis Facility at JPL. An acknowledgment is due to R. A. Schiffer and J. R. Hyde for providing comments and criticism included in this Memorandum.